Technical Report No. 226

004860-4-T

INVESTIGATION OF THE PROPAGATION STABILITY OF A

TIME SPREAD UNDERWATER ACOUSTIC CHANNEL

by

Raymond L. Veenkant

Approved by _Theodore G. Birdsall_

COOLEY ELECTRONICS LABORATORY

Department of Electrical and Computer Engineering
The University of Michigan
Ann Arbor, Michigan

for

May 1974

ABSTRACT

An experimental investigation of analysis and display tech-
niques for extracting stability information from underwater acoustic
propagation data has shown the feasibility and usefulness of a specific
display format, called the Channel Digit Response. All of the com-
plex nature of the channel reception is retained in the display, but
the format compresses the data and enhances the extraction of quali-
tative stability information. The investigation and conclusions are
limited to propagation tests using periodic transmissions, as periodic
transmissions are the usual type used for studying varying multi-
path propagation.

The investigation data base spanned 133 hours, from a 43 n.
mile range across the Straits of Florida. The effective time resolu-
tion of the data was .02 seconds. Crosscorrelation, autocorrelation,
and power spectrum analysis, and several threshold techniques based
on time-lag crosscorrelation were investigated, and their effective-
ness compared to the Channel Digit Response.

ACKNOWLEDGMENTS

TABLE OF CONTENTS

TABLE OF CONTENTS (Cont.)

LIST OF ILLUSTRATIONS

LIST OF ILLUSTRATIONS (Cont.)

LIST OF SYMBOLS AND ABBREVIATIONS

A(t)   The received carrier signal phase angle

B   The channel frequency spread extent

BL   Kailath's doubly spread channel factor

C(t)   The received carrier signal power

cdr(t, λ)   The time spread channel digit response, also
                       $\hat{h}(t, \lambda)$, $\hat{h}_t(\lambda)$

CDR   Channel digit response

CDS   Channel digit spectrum

CM   Complementary-phase modulation

COVH   Covariance of $\hat{h}_t(\lambda)$

$Covh_t(\mu)$ The covariance of $h_t(\lambda)$ at time t

CW   Carrier wave

CZT   The Chirp-Z-Transform

FFT   The fast Fourier transform algorithm

f, Δf   The discrete frequency index and discrete
                       frequency increment

g_i Processing gaps in the data

$H_C(f)$ The carrier processing filter transfer function

$H_N(f)$ The noise process filter transfer function

$H_R(f)$ The reverberation filter transfer function

$H_S(f)$	The pulse signal filter transfer function
$\hat{h}(t, \lambda)$, $\hat{h}_t(\lambda)$	The channel digit response (complex envelope)
$hs_t(\lambda)$	The channel sequence response
L	The channel time spread extent
m_t	The binary signal sequence
$N(t)$	The measured noise power process
$n(t, \lambda)$	The instantaneous noise process of the time spread channel
$pof(\lambda)$	The phase-only matched filter for $hs_t(\lambda)$
$R(t)$	The measured reverberation power process
RBR	Refracted-Bottom-Refracted propagation
$S(t)$	The measured pulse power process
$S_t(f)$	The channel digit magnitude spectrum
SRS	Surface-Reflected-Surface propagation
$s(t)_{bp}$	The bandpass signal reception
$\hat{s}(t)$	The complex envelope of $s(t)_{bp}$
T_d	The signal (sequence) digit duration
T_p	The signal (sequence) period
$T_\zeta^+(t)$	The measured forward decorrelation time of the channel's normalized cross-correlation coefficient, measured with respect to criterion ξ
$t, \Delta t$	The discrete time index and the discrete time increment

t_i The starting time of data file i

UWAP   Underwater acoustic propagation

λ , $\Delta\lambda$ The discrete time-delay index and the time-delay increment

p_{t_1, t_2} The channel's normalized cross-correlation coefficient

CHAPTER I

INTRODUCTION

The goal of this thesis is to discover signal processing concepts and methods that can be used in channel modeling and measurements of underwater acoustic propagation. This work is based on a firm foundation. There are two major aspects of this foundation: first are the theoretical materials of various authors on characterization, modeling and measurement of channels, and, second is the very well planned MIMI propagation experiment which has existed for approximately ten years, and which has been conducting virtually continuous field measurements since 1970.

The theoretical efforts mentioned provide a basis for this work for several reasons. Although many ideas come from intuition, it is always reassuring to be able to put the intuitive situation in theoretical context, adding legitimacy to the results. The particular case is described in theoretical terminology of a general case and makes possible ready communication and education of ideas and results to others. Finally, intuition gets the credit for many ideas but it is the theory that breeds, extends and perpetuates that intuition for other and later co-workers.

The MIMI design consists of three very interactive and interdependent parts: (1) signal design, (2) receiver design and

(3) transmitter and receiver implementation. The MIMI experiment has most recently consisted of a processing program called DUAL together with all the required support. DUAL has been collecting and measuring propagation data in many sites for several years. Very briefly, DUAL is an experiment to continuously measure and record for long periods of time, several propagation parameters:

1. Broadband noise power,

2. Broadband signal power,

3. Narrowband signal power and phase angle, and

4. Forward scattered surface reverberation power.

DUAL also obtains an approximate instantaneous measurement of the channel impulse response, most accurately called the channel pulse or digit response, but often simply referred to as the channel multipath response.

All of these data, which represent a tremendous reduction of information from the raw unprocessed propagation data, are the input data for this thesis. More specifically, the data used in this thesis is from a DUAL experiment conducted in November 1970 in the Straits of Florida and reported by Dr. R. H. Heitmeyer [1]. Therefore, in the context of the MIMI experiment, this thesis is to be an extension of DUAL. In particular, the channel digit response, CDR, will be concentrated on as the starting

point for developing methods to extract more information from the channel.

The UWAP channel is clearly stochastic so that the basic questions that immediately arise are:

1. Is a stationary model satisfactory,

2. Can an uncorrelated model be used,

3. To what extent is the channel spread,

4. What are the channel's statistics (can it be modeled as Gaussian)?

The answers to these questions are a major objective of this thesis; or at least to obtain methods which may be used to answer such questions. Conclusive answers to each of the above general questions concerning characterization of the UWAP channels may be hard to come by, that is, conclusions drawn here may be somewhat on the subjective side, however, the methods used will be objective. Thus, if the reader and later experimenters disagree with the conclusions here, they will certainly be free and able to draw their own conclusions from the results presented here or obtained later using methods presented here.

Considerable literature concerning the theoretical aspects of channel modeling and measurements exists. VanTree's Detection, Estimation, and Modulation, Part III is a comprehensive, easily read text largely concerned with detection and estimation

(and, therefore, modeling) in singly and doubly spread stochastic channels [25]. This text also contains a very extensive and recent bibliography of theoretical and empirical work in this area. A classic article by Kailath addresses the problems of noise-free measurements in doubly spread channels [3]. The important result of this work is that if the channel spreading area (BL product) is less than 1, the channel is called underspread, and instantaneous (impulse response) channel measurements are meaningful. Otherwise, (BL > 1) the channel is overspread and average (e.g., autocorrelation of the impulse response) measurements must be relied on to obtain unambiguous measurements. Bello [32] discusses at length variations of fundamental models of spread random channels. Although the UWAP channel turns out to be an underspread channel, so that Kailath's results guarantee that instantaneous measurements are meaningful here, our measurement techniques will be more physically motivated and are complicated by the presence of noise.

The UWAP channel is well known to be a doubly spread channel, where frequency or Doppler spreading is largely attributed to interaction of the random moving surface with propagation (the formal terminology for the frequency spreading phenomenon is "forward scattered surface reverberation") and the time spreading (usually referred to as "multipath") is due to the transmission

of sound between two points via multiple paths.

The primary emphasis of this thesis will be the study and characterization of the time-spread channel. The limitation of noise contaminated measurements and the impracticality of two-dimensional processing preclude the use of instantaneous measurements of the doubly spread channel. However, because the channel is underspread, proper signal design provides a decomposition of the general doubly spread UWAP channel into two singly spread channels, which can readily be investigated either simultaneously or separately. Although the multipath channel is emphasized, the frequency spread channel is still of interest. As this thesis proceeds, another very natural and convenient decomposition results in the identification of two UWAP channels which may each be considered as a general channel to be characterized. Indeed, these two channels are quite different and therefore, each is interesting in its own right.

CHAPTER 2

MIMI: THE EXPERIMENT AND THE CHANNEL

2.1 Introduction

Since the early 1960's cooperative efforts to study under-

water acoustic propagation (UWAP) have been conducted by The

University of Michigan and the University of Miami. The primary

site of these studies has been the 43-mile range in the Straits of

Florida from a fixed transmitter off the Miami shore to various

hydrophones in the waters of Bimini Island in the Bahamas. The

major features of the MIMI experiments are: (1) fixed transmit-

ters and receivers and (2) the interest in very long time series of

data. The fixed sites greatly simplify the experimental setup,

provide a relatively permanent facility necessary for long time

operation, and avoid the introduction of Doppler effects due to mov-

ing platforms. Long time series data are believed necessary for

understanding UWAP and for developing and testing UWAP models.

The Miami-Bimini range is illustrated in Figure 2.1(a) to-

gether with a bottom profile in Figure 2.1(b). A velocity profile,

obtained in November 1961, of the straits is illustrated in Figure

2.2. Although the velocity profile changes continuously, this

example can be considered reasonably typical for this time of year.

6
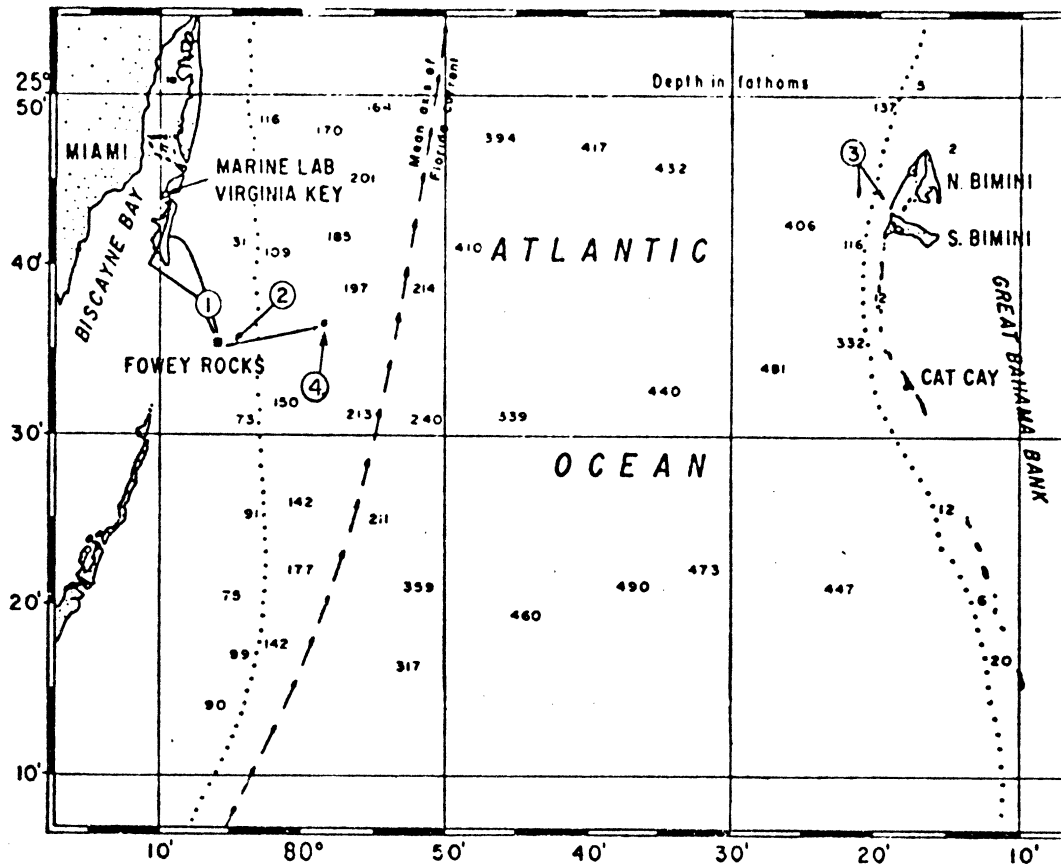
(a).
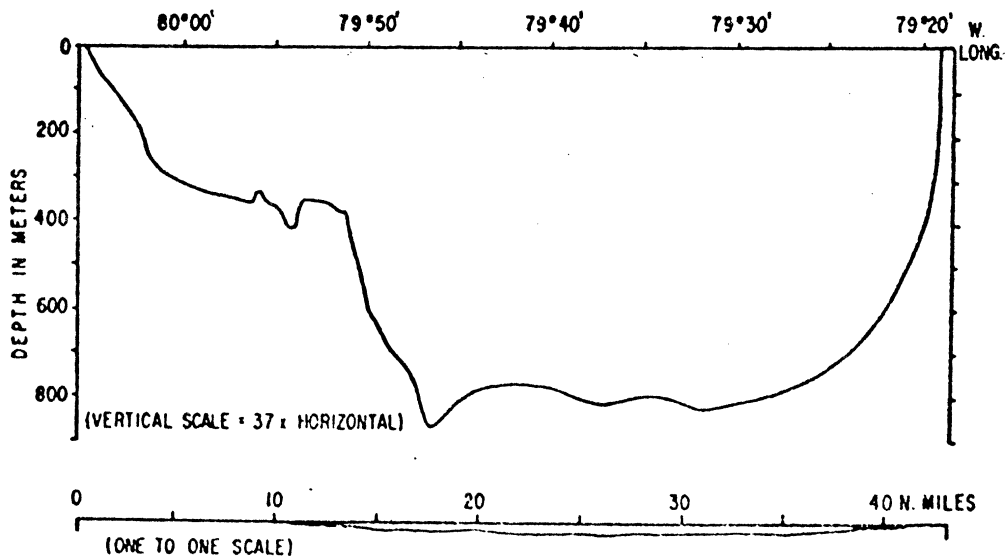
(b)

Fig. 2. 1.   The Miami-Bimini Range: (a) The Straits of Florida,
(b) Bottom Profile
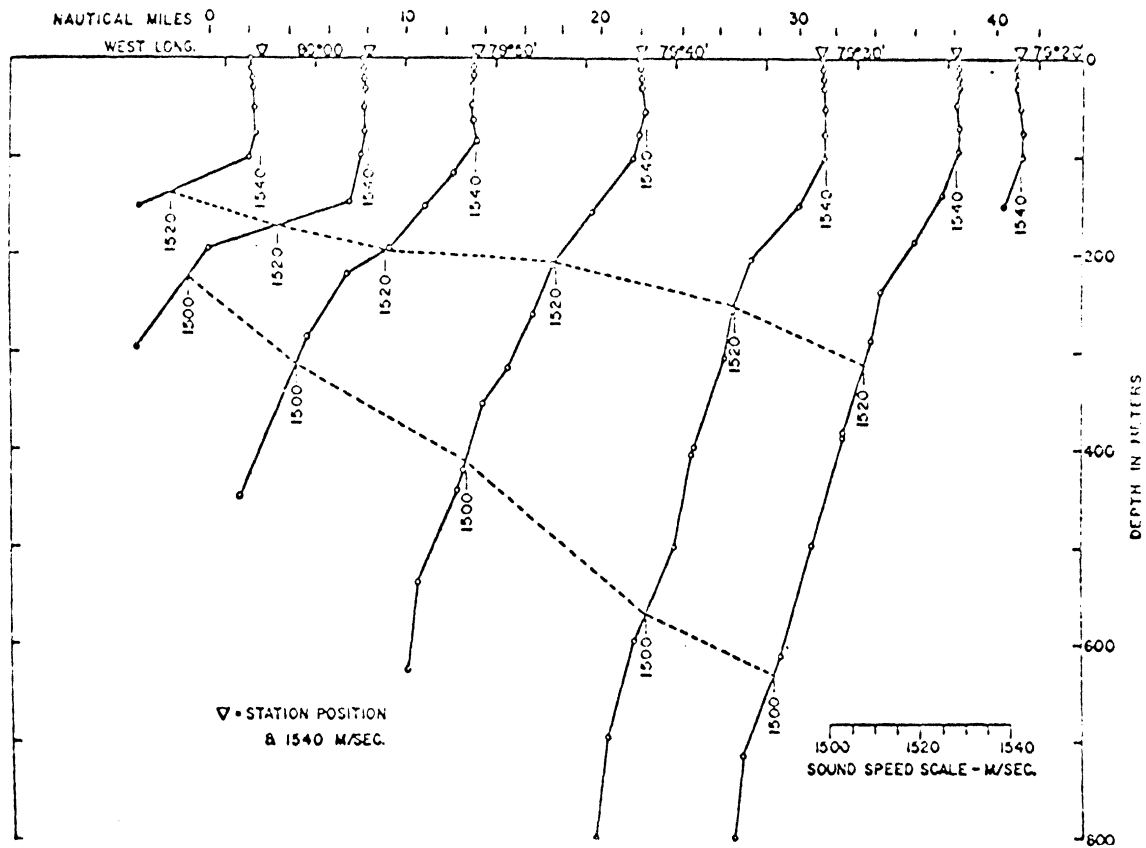
Fig. 2.2. Sound Speed vs. Depth

The point of interest is the velocity gradient, which is a function of

time and space. The velocity gradient, even as a function of depth,

leads to a very complex propagation structure. The propagation

ray trace corresponding to this velocity profile is presented in

Figure 2.3. In this figure there are illustrated two basic types of

propagation. There are sound paths traveling along the surface

boundary undergoing reflection and refraction. This is called SRS
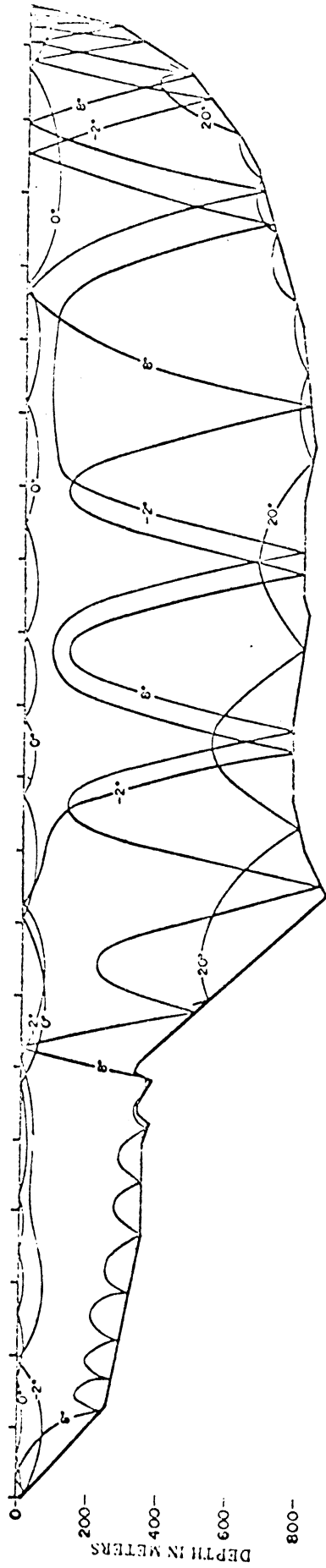
Fig. 2. 3. Sound Ray Paths Along 25° 44' on 28-29 Nov. 1961

propagation. Sound paths are similarly traveling along the bottom by reflection and refraction. This is called RBR propagation.

The data for the research in this thesis are selected from a two-week experiment conducted at this site in November of 1970. The data were conveniently available, are of good quality, and are representative of the Straits of Florida at this time of year. The data were organized into 19 files. File 1 to 8 are continuously recorded from the deep (1200 feet) bottom mounted hydrophone located at point 3 in Fig. 2. 1(a), starting at 17:16 hours on November 11, 1970, until 18:46 hours on November 17, 1970. Files 9 to 19 are from 10:20 hours on November 23 to 9:05 hours on November 29, 1970, and were recorded from the bottom mounted shallow (100 feet) hydrophone also located near point 3 in Fig. 2. 1(a). For more details of the experiment refer to Reference [1], a preliminary report on that experiment.

2. 1. 1 Signal and Receiver Designs. The signal and receiver designs of the MIMI experiment have evolved over a period of time, and are largely due to the efforts of Dr. T. G. Birdsall. Detailed discussions and analyses of the signals and receivers may be found in References [1], [15], and [16]. A brief discussion of the more important properties of the signals and the receivers is useful. The signal consists of a 63-digit binary maximal pseudo-random sequence complementary-phase modulated (CM) onto an ultra-stable 420 Hz

carrier wave (CW). The signal is transmitted continuously. Each

digit of the sequence corresponds to 8 carrier cycles (approximately

20 msec) and the period of the sequence is 1.2 seconds. The signal

may be expressed

$$s(t)_{bp} = A \cos (2\pi\ 420t + m_t\ \pi/4)$$

where $m_t = \pm 1$ the binary values of the sequence. Thus, the trans-

mitted signal is a continuously transmitted 420 Hz sinusoid with ± 45

degree phase shifts occurring at integer multiples of 20 milliseconds

with resulting spectrum sketched in Fig. 2.4. (There are actually 62

lines on each side of the carrier to the first nulls.)
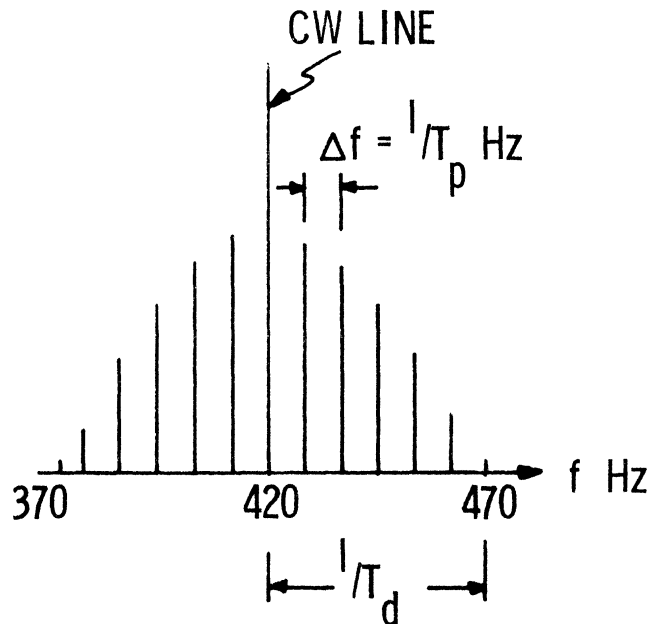
Fig. 2. 4. Magnitude Spectrum of the MIMI CM Signal

The carrier contains approximately half the total power.

The remainder of the signal magnitude spectrum is a line spectrum

with a $\dfrac{\sin \pi f\, T_d}{\pi f\ T_d}$ envelope. The line spacing is determined by the

signal period, T_p , so that $\Delta f = 1/T_p$. The zeros of the envelope

are determined by the duration, $T_d = 20$ msec , of the sequence

digits. The phase spectrum of the CM signal is a pseudo-random

function of frequency. It should be clear that since this phase

spectrum is known, by simple phase correction and adjustment of

the carrier line, multiply by $1/63$, the signal spectrum becomes

$\dfrac{\sin \pi f\, T_d}{\pi f\ T_d}$ with constant phase. This transformation can be accom-

plished by multiplying the complex signal spectrum by a spectrum

of the transmitted signal. The transformation can also be performed

in the time domain by cross-correlating the signal with the original

63-digit sequence of 1 and -1's. This technique has become known

as phase-only matched filtering. Obviously, the resulting spectrum

is that of a T_p second periodic pulse with duration, T_d .

Thus, the CM-CW signal provides continuous and simultan-

eous CW and pulse experiments with high average power in both

experiments at low peak transmitted power. Although simultan-

eous CW and pulse experiments are performed, they will be treated

separately through the remainder of this work.

2. 1. 2 Low-Pass Processing of Bandpass Signals. In all

MIMI processing the received bandpass (100 Hz) signal centered

at 420 Hz is translated to DC (zero Hz). The result is that the

original real-valued bandpass signals become complex-valued low-

pass signals. The following relations between the bandpass and

low-pass signals are valid. *

$$s(t)_{bp} = |\hat{s}(t)| \cos(wt + \Theta) = \text{Re}\left\{\hat{s}(t) e^{iwt}\right\}$$

where $\hat{s}(t)$ is the complex-valued envelope of $s(t)_{bp}$

$$\hat{s}(t) = |\hat{s}(t)| e^{i\Theta(t)}$$

Hereafter, all discussions will be in terms of the process complex

envelopes and complex low-pass filters. Therefore, the CW ex-

periment becomes, in the receiver, a DC experiment. And, al-

though the multipath structure is denoted by $\hat{h}_t(\lambda)$ a low-pass

process, the real measurement is at 420 Hz. That is, the $\hat{h}_t(\lambda)$

discussed and presented is the complex envelope of the bandpass

channel

---

*See Reference [15] for the MIMI implementation and
Reference [25] for the proofs of these relations for both determin-
istic and stochastic signals.

$$h_t(\lambda)_{bp} = \mathrm{Re}\left\{ \hat{h}_t(\lambda)\, e^{i2\pi 420 t} \right\}$$

2.1.3 Independent Variables - Discrete Notation. Since all

of the signal processing discussed here is performed on a digital

computer following antialias filtering, sampling and analog-to-

digital conversion, the independent variables are integer-valued

discrete indices rather than continuous variables. The purpose of

this discussion is to eliminate subsequent questions about notation

or interpretation.

The three independent variables of interest are:

1. time $= t \cdot \Delta t$

2. frequency $= f \cdot \Delta f$

3. time-delay $= \lambda \cdot \Delta \lambda$

where f is the discrete Fourier transform index corresponding

to the λ index. This frequency index is not the frequency spread

variable corresponding to the Fourier transform with respect to

the time variable, t. This is a possible source of confusion, but

with this warning the distinction should be clear in the context.

The independent variables incremental values are fixed

throughout:

1. $\Delta t = 102$ seconds

2. $\Delta \lambda = 5$ milliseconds

3. $\Delta f \cong .833$ Hz

where Δf is determined by the transmission signal period, $\Delta f = 1/T_p$, $T_p = 1.2$ seconds and $\Delta \lambda$ is a more than adequate sampling interval for the 100 Hz transmission bandwidth.

The range of the indices are:

1. $t = 0, 1, \ldots$

2. $f = -63, \ldots, 0, \ldots, 62$ covering the ± 50 Hz transmission band

3. $\lambda \epsilon \Lambda$ where $\Lambda = \{0, \ldots, 251\}$

and the signal period, $T_p = 252\Delta\lambda$ and the signal pulse duration, $T_d = 4\Delta\lambda$.

The major functions involving these independent indices are:

1. The channel digit response, $cdr(t, \lambda) = \hat{h}(t, \lambda) \stackrel{\Delta}{=} \hat{h}_t(\lambda)$

2. Various DUAL scalar processes; e.g., $C(t)$

3. The channel digit spectrum,

$$S_t(f) = \sum_{\lambda \epsilon \Lambda} \hat{h}_t(\lambda)\, e^{i2\pi f\lambda/252}$$

A familiarity with discrete parameter representation has been assumed. Reference [28] is directed at the fundamentals of digital signal processing.

2.2 Characterization and Measurement of the MIMI Channel

2.2.1 General Characterization of the MIMI Channel. In general, the UWAP channel can be viewed as a linear, quasi-stationary doubly spread filter with an impulse response, $h(t,\lambda) \cong h_t(\lambda)$. The assumption of quasi-stationarity appears to be quite valid and will be justified in later development. This description of the UWAP channel is summarized in Figure 2.5.

$$n(t)$$

$$x(t) \longrightarrow \boxed{h(t,\lambda)} \longrightarrow \bigoplus \longrightarrow y(t)$$

$$y(t) = \int_0^\infty h(\lambda,t)\, x(t-\lambda)\, d\lambda + n(t)$$
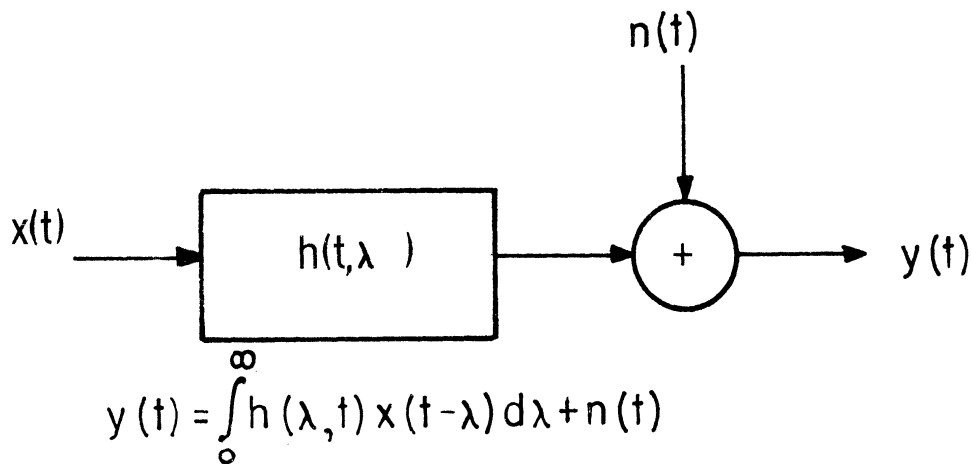
Fig. 2.5. The Linear, Quasi-Stationary UWAP Channel,
An Impulse Response Representation

The doubly spread description of the channel includes both frequency (or Doppler) spreading, which is caused by "short term" time fluctuation in the channel, and time-delay spreading, which in the UWAP channel is due to multiple path propagation. The concept

of spreading involves the influence of the channel upon a trans-

mitted signal, whereby the received signal is of greater bandwidth

or time duration than the transmitted signal [25]. Obviously, a

channel may be only time-delay spread, or only frequency spread

in which case the channel is called singly spread.

Frequency spreading is most clearly observed using a con-

stant amplitude continuous sinusoidal wave, CW, transmission.

In the UWAP channel the frequency spread phenomenon results in

a slight (on the order of tenths of millihertz) spreading in the CW

line and the introduction of sidebands of incoherent energy in the

approximate region from 0.1 to 0.3 Hz each side of the CW. This

is illustrated in Fig. 2.6. The slight spreading of the CW is attri-

buted to such long term phenomena as tides (12 and 24-hour periods)

and internal waves (1 to several hour periods) and is so insignifi-

cant that it is not considered in subsequent frequency spreading

discussion.
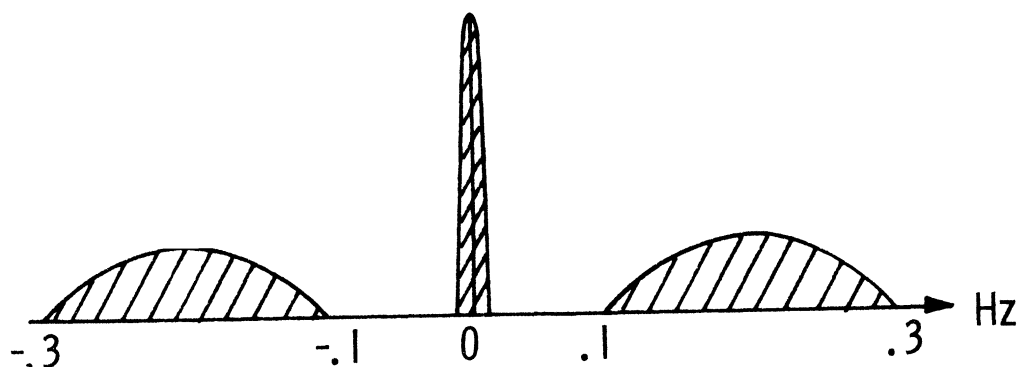
Fig. 2.6. Frequency Spreading of the UWAP Channel,
Observed Using a CW Transmission

The major frequency spreading has been adequately modeled to date as an amplitude modulation process of the CW transmission by a narrow band, 0.2 Hz, random process. Due to the high correlation of frequency spreading activity with the ocean's surface conditions and the modulation frequencies, 0.1 to 0.3 Hz, correspondence to common surface wave periods, 3 to 10 seconds, the frequency spreading in the UWAP channel is largely attributed to direct interaction of sound rays (or paths) with the randomly moving surface waves. This frequency spread energy is called forward scattered surface reverberation or just reverberation. Clearly, reverberation energy is dependent upon the presence of a surface mode of propagation as well as the surface conditions. However, given a surface propagation mode, the relation between the surface conditions and the reverberation energy is not known; however, total reverberation energy approaching 50 percent of the received CW energy is not uncommon.

The time-delay spread feature of the UWAP channel is often called multipath because the delay spreading is a result of the multiple propagation paths, each with its own attenuation, arrival (delay) time, etc. The multipath structure of the channel is best observed using a short pulse (approximate impulse) transmission. Figure 2.7 illustrates the delay spread created by an all pass, three path structure. The delay spread of the MIMI channel can

vary from approximately 20 milliseconds (msec) to 500 or 600 msec.
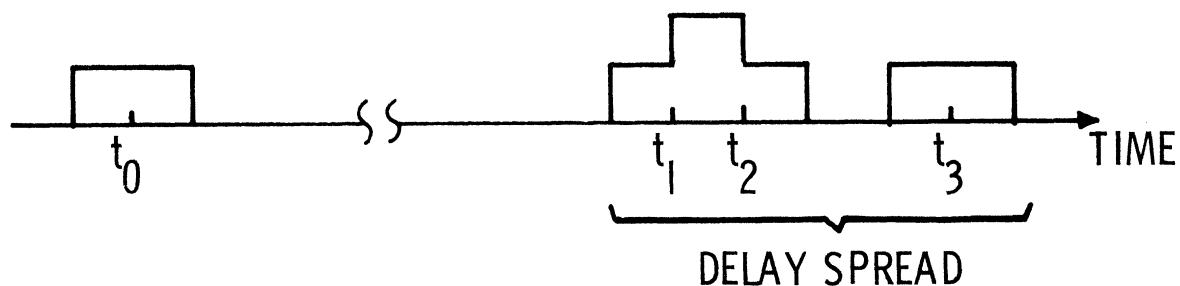
Fig. 2.7. Arrivals at t_1 , t_2 , and t_3 from a Single Pulse Transmission at t_0 Illustrate the Multipath Structure (Delay Spread) of the Channel

2.2.2. Noise Free Measurements of a Doubly Spread Channel.

Kailath [3] shows that, even in the noise free case, unambiguous measurements of a doubly spread channel are only possible under certain restrictions. A doubly spread channel based upon the severity of spread is classified as either underspread or overspread. The severity of channel spread is measured by the channel spread factor, BL , where B is a measure of the channel frequency spread and L is a measure of the channel's delay spread. The parameters B and L are defined in terms of the channel's impulse response, $h(t,\lambda)$.

$$B = \max_{\lambda} \{ \text{Bandwidth of } h(t, \lambda) \}$$

$$= \max_{\lambda} \{\text{smallest } f_0 \ni H(f, \lambda) = 0, \ f > f_0 \}$$

and

$$L = \max_{t} \{\text{Duration of } h(t, \lambda)\}$$

$$= \max_{t} \{\text{smallest } \lambda_0 \ni h(t, \lambda) = 0, \ \lambda > \lambda_0 \}$$

where bandwidth is measured in terms of frequency variable in the Fourier transform of $h(t, \lambda)$ with respect to the time variable, t , and the duration of $h(t, \lambda)$ is measured with respect to the delay variable, λ . For practical reasons, looser definitions of bandwidth and duration are assumed in the data interpretation of this thesis.

If $BL > 1$, the channel is called overspread and only unambiguous average, e. g. , mean and auto-correlation, measurements are possible. Kailath [3] and Bello [19], and [20], discuss in length measurement techniques for the overspread, noise-free channel. These techniques generally made statistical assumptions about the channel and often are limited to the case $BL < 2$.

For $BL < 1$, the underspread channel, unambiguous instantaneous measurements of $h(t, \lambda)$ can be made. From previous discussion $B \cong 0.6$ and $L \cong 0.6$ in the MIMI channel so that $BL \cong 0.36$ and the channel is clearly underspread [15], [16], and [17]. Thus, "instantaneous" $h(t, \lambda)$ measurements can be made on the MIMI channel. In general, the UWAP channel will be less complex than the MIMI channel so that it may be safely generalized that the UWAP channel is underspread.

2.2.3. "Instantaneous" $h(t, \lambda)$ Measurements of the UWAP Channel in the Presence of Noise. Since the ocean contains considerable environmental (ambient, biological, surface, etc.) and

man-made (shipping) noise, measurements of $h(t, \lambda)$ must include

signalling and filtering techniques designed to obtain reliable, high

signal-to-noise ratio measurements of $h(t, \lambda)$ which can still be

considered instantaneous. Fortunately, the UWAP channel is

"time-invariant" for intervals of 5 to 15 or more minutes, so that

by using periodic, low peak power but high average power, signal

transmission techniques and long term, approximately one minute,

coherent "matched" filtering techniques high signal-to-noise ratio,

instantaneous channel measurements are obtained.*

2.2.4. Decomposition of the Doubly Spread Channel Into

Two Singly Spread Channels. A practical solution to the measure-

ment of a doubly spread channel under the constraint of additive

channel noise is to decompose the problem into the measurement

of two singly spread channels. In general, this would be a compro-

mise forced by the measurement noise. However, due to the nature

of the UWAP channel, this approach is a natural decomposition of

the coherent component (delay spread) from the incoherent (frequency-

spread) component, which is very simply accomplished, because

these components are orthogonal (occupy disjoint regions of the

---

*Coherent processing is obtained by use of very coherent
frequency and phase references at the transmitter and receiver,
and filtering is implemented digitally in a computer [15].

frequency axis), by appropriate signal design and linear filtering. Whenever, due to the lack of a surface mode, reverberation is not present, the channel is naturally and conveniently singly spread.

The means of this decomposition is quite simple and is briefly described. The basic idea is to transmit periodic signals with spectral lines spaced far enough apart so that the reverberation sidebands fall between these lines.

In the noise free case $h(t, \lambda)$ can be measured using an impulse input $x(t) = \delta(t)$ so that the output $y(t, \lambda) = h(t, \lambda)$. With additive noise this measurement becomes a highly contaminated one, $y(t, \lambda) = h(t, \lambda) + n(t, \lambda)$. The peak signal-to-noise ratio of this measurement is estimated at approximately -10 to 0 dB in the MIMI channel. By making $x(t)$ a periodic train of impulses,

$$x(t) = \sum_{m=0}^{M-1} \delta(t - mT_p)$$ and using the time invariance of the channel

over $t \epsilon[\, 0,\ MT_p\,]$, the multipath structure (delay spread) of $h(t, \lambda)$ is estimated by

$$\hat{h}_t(\lambda) \cong \sum_{m=0}^{M-1} h(t - mT_p, \lambda) + n(t - mT_p, \lambda)$$

In practice for values of $M = 85$ and $MT_p \cong 102$ seconds high (+10 to 20 dB) signal-to-noise ratio estimates of $h_t(\lambda)$ are obtained. Note that $MT_p = 102$ seconds is well within the time invariance limit of 5 to 15 minutes and that for $M \geq 8$ with $T_p = 1.2$

seconds the frequency spread energy is filtered out of the $\hat{h}_t(\lambda)$

measurement.

A description of the reverberation measurement is included

in the next section which briefly describes the DUAL experiment.

2.3 The DUAL Experiment

With minor variations, DUAL is the basic MIMI experiment

currently in the field obtaining long time series acoustical data

on the UWAP channel at various locations. The DUAL experiment

consists of three subexperiments simultaneously measuring various

aspects of the channel behavior. The first of these is the CW ex-

periment, which measures the CW power, $C(t)$, phase angle, $A(t)$,

and the reverberation power in the CW reception, $R(t)$. The mag-

nitude spectrum of the filters, $H_C(f)$ and $H_R(f)$, used to measure

CW and reverberation parameters, respectively, are illustrated

in Fig. 2.8. Second, the multipath experiment obtains an estimate

of the channel digit response, $\hat{h}_t(\lambda)$, measures the total received

broadband-signal power, $S(t)$, and measures the decorrelation

time, $T_\zeta^+(t)$, of the channel's normalized cross-correlation co-

efficient. Third, a total noise power measurement, $N(t)$, in the

transmission band is made. The filters $H_S(f)$ and $H_N(f)$ for the

multipath and noise measurements, respectively, are illustrated

in Fig. 2.8. Each of these three experiments are discussed in
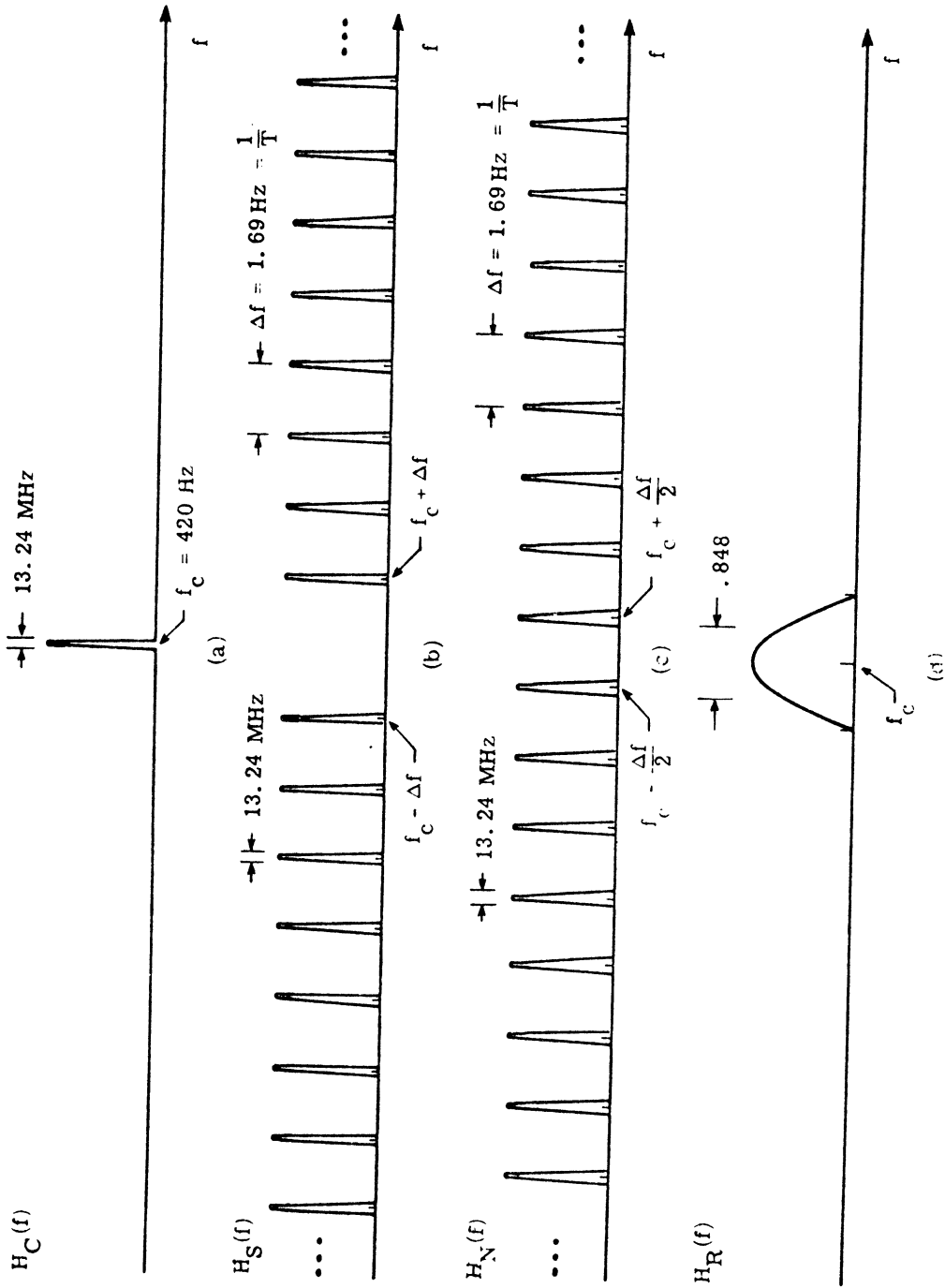
Fig. 2.8. The Frequency Responses of the DUAL Processing Filters

brief detail.

2.3.1. The CW Experiment. The CW experiment is used to obtain continuous narrowband power and phase angle measurements as well as the reverberation measurements. The CW power process is denoted by $C(t)$ and the CW phase process is $A(t)$. The reverberation measurement is a total power measurement, $R(t)$. The $R(t)$ measurement is only made on the CW sidebands because it is the only line in the signal spectrum providing sufficient reverberation to noise power ratio for meaningful $R(t)$ measurements. The CW and reverberation filters, $H_C(f)$ and $H_R(f)$, respectively, are illustrated in Fig. 2.8.

2.3.2. The Multipath Experiment. In the multipath experiment $\hat{h}_t(\lambda)$ is measured using

$$\hat{h}_t(\lambda) = \sum_{k=0}^{M-1} h(t - kT_p, \lambda) + n(t - kT_p, \lambda)$$

where $T_p = 1.2$ seconds and $M = 85$ so that each $\hat{h}_t(\lambda)$ represents the multipath structure of the channel for 102 seconds. Every 102 seconds a new $\hat{h}_t(\lambda)$ is measured. DUAL measures $\hat{h}_t(\lambda)$, computes some parameters of physical significance and saves $\hat{h}_t(\lambda)$ on digital tape, but does not display $\hat{h}_t(\lambda)$. The physical parameters computed are: (1) the total received broadband (pulse) power, $S(t)$, and (2) $T_\zeta^+(t)$, the decorrelation time of the

normalized cross-correlation coefficient of $\hat{h}_t(\lambda)$.

The $T_\zeta^+(t)$ analysis is discussed later in this section in the CANDOR experiment. $S(t)$ is related to $\hat{h}_t(\lambda)$ by

$$S(t) = \sum_{\lambda \in \Lambda} |\hat{h}_t(\lambda)|^2 = \sum_{\lambda \in \Lambda} |\hat{hs}_t(\lambda)|^2$$

where $\hat{h}_t(\lambda)$ is the phase-only match filtered form of $\hat{hs}_t(\lambda)$. This relationship is illustrated in Fig. 2.9.

$\hat{hs}_t(\lambda)$ → pof(λ) → $\hat{h}_t(\lambda)$
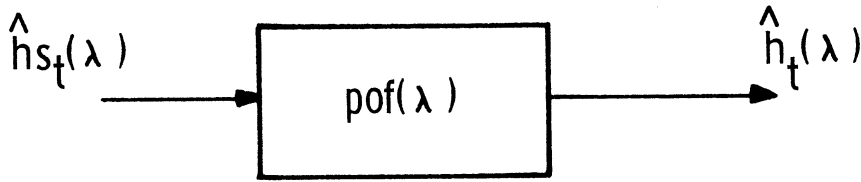
Fig. 2.9. The Phase-Only Matched Filter

This is the transformation in the receiver which provides the channel equivalent pulse response $h_t(\lambda)$ from the binary sequence response $\hat{hs}_t(\lambda)$. For this reason, the multipath structure representation $\hat{h}_t(\lambda)$ is also called the channel digit response, CDR. As pointed out earlier, the phase-only matched filter has no effect on the magnitude spectrum of $\hat{hs}_t(\lambda)$ so that $S(t)$ can be computed from $\hat{hs}_t(\lambda)$ or $h_t(\lambda)$.* The transfer function ,

_____

*The CW signal is filtered out of $\hat{hs}_t(\lambda)$ before the phase-only filtering.

$H_s(f)$, of the multipath measurement filter, a comb filter on the signal lines, is illustrated in Fig. 2.8. For more details on the computation of $\hat{hs}_t(\lambda)$ and $\hat{h}_t(\lambda)$ see References [15] and [16].

2.3.3. Noise Measurement. By placing a comb filter, $H_N(f)$, between the passbands of $H_s(f)$ a total noise power measurement in the transmission band, 420 ± 50 Hz, is obtained. The noise power measurement is denoted $N(t)$. $H_N(f)$ is illustrated in Fig. 2.8.

2.3.4. The CANDOR Experiment. CANDOR is presented here as an extension and continuation of the experiment designed by T. G. Birdsall and performed in the MIMI experiments of July 1970. Results of that experiment are documented in Reference [2]. CANDOR is an acronym for Continuous Analysis with Decision Oriented Recording. As implied in the full title, the major goal of CANDOR is to represent the UWAP channel with a minimum, or at least reduced, quantity of recorded data. That is, the objective is to retain sufficient information about the channel while avoiding excessive redundancy in the data.

The motivation for this attempt at data reduction is the overwhelming task of data digestion necessary for understanding the UWAP channel. The storage of all the data from a continuous DUAL experiment is alone a great practical problem. An effective means for displaying and interpreting long time series of $\hat{h}_t(\lambda)$

is the major contribution of this thesis. But, off-line analysis of propagation experiments is necessary in developing new ideas and techniques, and the cost of such analysis in dollars, human resources, computer resources and simply time is at least proportional to the quantity of data involved. Thus, an order of magnitude reduction of data necessary for an adequate representation of the channel can be the difference that makes a post-processing task practical. That is, unless considerable data reduction techniques are developed, many post-processing efforts will never be started, which will greatly stunt the development of new MIMI experiments.

The premise of CANDOR is that a single $\hat{h}_t(\lambda)$ from each interval of channel time-invariance is a sufficient representation of the channel. Since a new $\hat{h}_t(\lambda)$ is measured every 102 seconds and the channel is time-invaiant for durations of typically five to fifteen minutes, an approximate order of magnitude reduction in data quantities is expected.

The criteria used to evaluate a representative $\hat{h}_t(\lambda)$ are all based upon the normalized cross-correlation coefficient of $\hat{h}_t(\lambda)$, ρ_{t_1, t_2} defined by

$$\rho_{t_1, t_2} \triangleq \frac{\sum_{\lambda=0}^{251} \hat{h}_{t_1}(\lambda) \hat{h}_{t_2}^*(\lambda)}{|| \hat{h}_{t_1}(\lambda) ||^{\frac{1}{2}} || \hat{h}_{t_2}(\lambda) ||^{\frac{1}{2}}}$$

where

$$\| \hat{h}_t(\lambda) \|^2 \triangleq \sum_{\lambda=0}^{251} \hat{h}_t(\lambda) \, \hat{h}_t^*(\lambda)$$

$\rho_{t_1,\,t_2}$ is the normalized cross-correlation function of $\hat{h}_t(\lambda)$ evaluated at zero delay. As will be seen in the CDR grams in Chapter 4 and as documented in Reference [2], the changes in the channel multipath structure are not manifested in arrival time changes, that is, the average propagation time of the multipaths are constant for hours, so that $\rho_{t_1,\,t_2}$ is as effective a measure of the similarity or dissimilarity of $h_t(\lambda)$ as the entire cross-correlation function and there is no reason to compute that function for these purposes.

The forward interval of time for which $\hat{h}_{t_1}(\lambda)$ is representative is the interval $t_2 - t_1 = T_\zeta^+(t_1)$ of time such that $\rho_{t_1,\,t_2}$ "satisfies ζ". Expressed in polar coordinates

$$\rho_{t_1,\,t_2} = |\rho_{t_1,\,t_2}| \, e^{i\Theta_{t_1,\,t_2}}$$

where

$$0 \le |\rho_{t_1,\,t_2}| \le 1 \quad \text{and} \quad -\Pi \le \Theta_{t_1,\,t_2} \le \Pi$$

where

$$\rho_{t, t} = 1$$

The three criteria investigated here are:

(1) $\quad \zeta_{-3 \text{ dB}} = \left\{ \rho_{t_1, t_2} \mid |\rho_{t_1, t_2}|^{\frac{1}{2}} \geq .7 \right\}$

(2) $\quad \zeta_{-6 \text{ dB}} = \left\{ \rho_{t_1, t_2} \mid |\rho_{t_1, t_2}|^{\frac{1}{2}} \geq .5 \right\}$

(3) $\quad \zeta_{\pm 45^\circ} = \left\{ \rho_{t_1, t_2} \mid -45^\circ < \Theta_{t_1, t_2} < 45^\circ \right\}$

The corresponding forward decorrelation times are $T^+_{-3 \text{ dB}}$,

$T^+_{-6 \text{ dB}}$ and $T^+_{\pm 45^\circ}$ respectively, where $T^+_\zeta(t) \overset{\Delta}{=} \max_{t_2} \{ t_2 - t \mid$

ρ_t, t_2 satisfies ζ for all t_2 in $\{t, T^+_\zeta(t)\}$.

Thus, CANDOR reduces the data set $\hat{h}_t(\lambda)$, $t_1 \leq t \leq T^+_\zeta(t_1)$

representing the channel from t_1 to $T^+_\zeta(t_1)$ to just $\hat{h}_{t_1}(\lambda)$. The

purpose in this thesis is not actual data reduction but investigation

of this technique. This is done by studying the parameter $T^+_\zeta(t)$

throughout the data set as a function of t and ζ . Therefore,

$T^+_\zeta(t)$ is computed and plotted with the DUAL parameters for each

$\hat{h}_t(\lambda)$ in the available data. Due to computer memory limitations,

values of T^+_ζ greater than 48 minutes were not computed so that

whenever $T^+_\zeta \geq 48$, $T^+_\zeta \overset{\Delta}{=} 48$.

$T_\zeta^+(t)$ as defined here is an arbitrary but reasonable measure of the duration of the channel's quasi-time-invariance at each t . A detailed discussion of the results of this analysis is in Chapter 3, Presentation and Discussion of DUAL Results. In general, the $T_\zeta^+(t)$ measurements reflect quite agreeably with the general rule that the MIMI channel is quasi-time-invariant for five to fifteen minutes.

One approach to data reduction has been investigated which promises to reduce recorded data in DUAL experiments by an order of magnitude. However, the approach is very strict in that the channel is essentially treated as deterministic and time-invariant, i.e., microscopic changes in the channel structure are retained even in the reduced data representation. Yet, the channel is admittedly stochastic and quasi-stationary. At this level, significant changes in the channel are much more macroscopic, e.g., the average propagation time of the channel changes significantly, a mode fades away or a new mode becomes apparent in the reception. This more general (statistical) viewpoint of data reduction appears feasible based upon observations of the CDR grams in Chapter 4, where the main structure of the multipath is "constant" for long periods of time, hours, while the microstructure is very complex, random and vague. Certainly this approach will not retain as much about the channel, but it will still represent the most significant

characteristics and will result in another order of magnitude of data reduction.

Candidates for statistical channel representations and evaluation criteria for those representations are not investigated or even proposed here. Obvious representation candidates include the auto-correlation function. However, later data analyses presented in Chapter 5, indicates that such a statistically classical represen-tation of the channel misses much of the channel's structure. The two approaches, deterministic and statistical, discussed here are extremes on opposite ends of the spectrum. Hopefully, study of the channel through the CDR gram presented in Chapter 4 will lead to a middle solution that sufficiently represents the channel and pro-vides more data reduction.

A DUAL experiment as has been described, performed in November 1970 in the Straits of Florida is the source of data for this thesis. Preliminary results on that experiment are reported in Reference [1]. However, no satisfactory means for displaying, interpreting or otherwise using $\hat{h}_t(\lambda)$ has previously existed. The solution to this problem of using $\hat{h}_t(\lambda)$ to understand and charac-terize the UWAP channel is the major contribution of this thesis. Many of the DUAL measurements from the November 1970 experi-ment will be presented here to assist in the interpretation of the UWAP channel developed. Before proceeding with the presentation

and interpretation of experimental results, the limitations of the
MIMI measurement techniques imposed by the channel's BL factor
and a comparison with the theoretical limitations discovered by
Kailath are investigated.

2.3.5. BL Effects on h(t, λ) Measurements.

Within the
constraints of the signal and receiver designs in the MIMI measure-
ments, there are limits on the ranges of B, L and BL for which the
measurements are undistorted. Kailath's results state that dis-
tortionless measurements of h(t, λ) are possible if and only if,
BL < 1 . However, it should be interesting and informative to
study in some detail the direct effects of B and L on the MIMI tech-
niques. It should be noted that Kailath's discussion was for noise-
free measurements which are not available in the MIMI experiments.

The periodic nature of all MIMI signals, whether carrier
(CW) or pulse, and the matched processing of those signals are
the fundamental properties of the MIMI signal and receiver designs.
Although the CW and pulse transmissions and measurements are
simultaneous, they may be discussed separately.

Consider the CW experiment first. The signal is a contin-
uous 420 Hz sinusoid. Thus, its spectrum is essentially a line at
420 Hz. However, the reception reflects much propagation phenom-
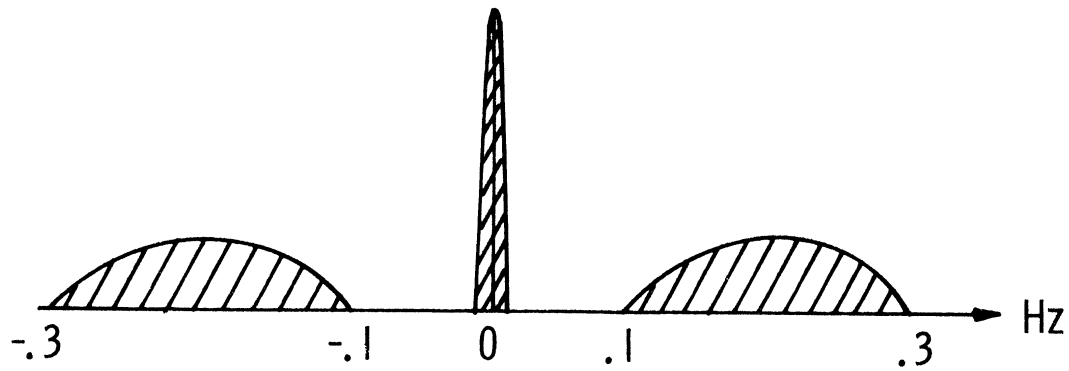ena. The received signal is essentially

Fig. 2. 10. CW Reception Magnitude Spectrum Demodulated
From 420 Hz to DC

a very narrowband process at 420 Hz with two significant sidebands

of incoherent energy. The narrowband carrier process has slight

frequency spreading due to long term (hours) effects such as tides

and internal waves. The two incoherent sidebands are attributed

to amplitude modulating effects of the surface upon the carrier.

Since the CW measurement is an average measurement over time-

delay (multipath), frequency selective fading of the carrier recep-

tion can occur relatively frequently. Typically, the fade is very

short (a minute or so) and fading often occurs at half-hour or hour

intervals.

Values of B and L have little direct effect upon the CW experi-

ment design except in the choice of filter bandwidths. However,

a large L implies excessive multipath presence setting the stage

for multipath interference effects, which are reflected as frequency

selective fading. That is, the rate of occurrence of carrier fading

is highly correlated with multipath activity.

The multipath measurements, $\hat{h}(t, \lambda)$ are based upon a periodic pulse signal, which has a line spectrum rather than a continuous spectrum. The channel impulse response is measured approximately by a train of short duration pulses rather than impulses. Thus, the signal line spectrum has a $\dfrac{\sin fT_d}{\pi fT_d}$ envelope with zeros determined by the pulse duration, T_d , and line spacing determined the signal period, T_p . The signal spectrum is illustrated in Fig. 2.11, The Multipath Measurement Signal Spectrum.
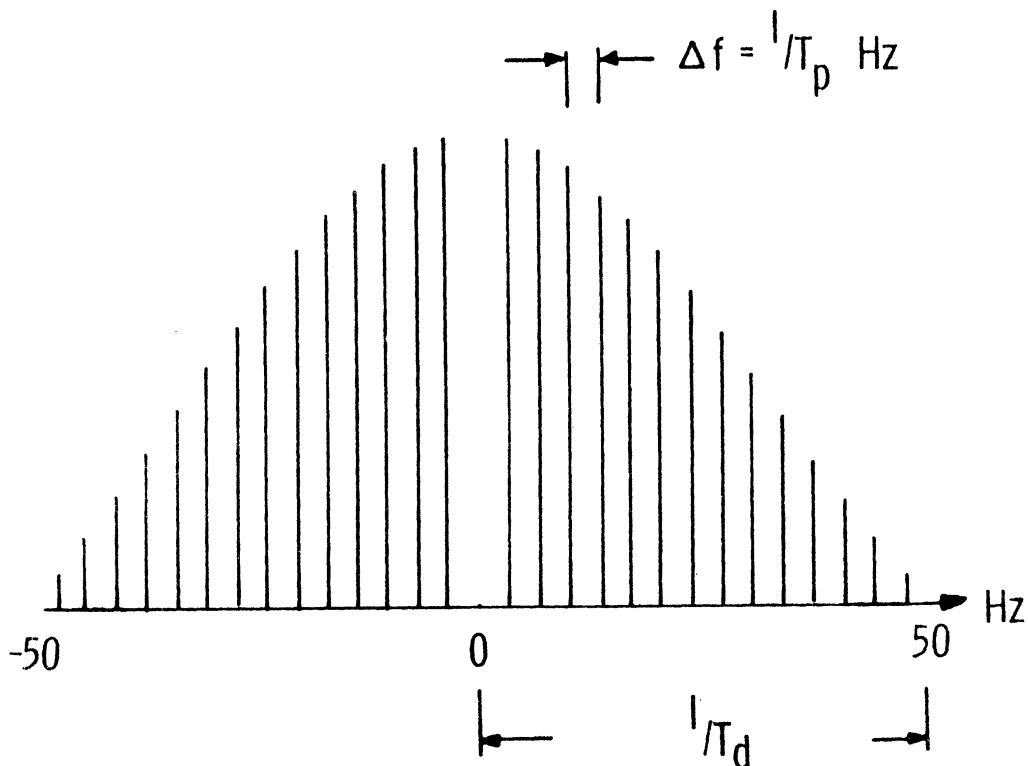
Fig. 2.11. The Multipath Measurement Signal Spectrum

The parameters of the pulse train are illustrated in Fig. 2.12.
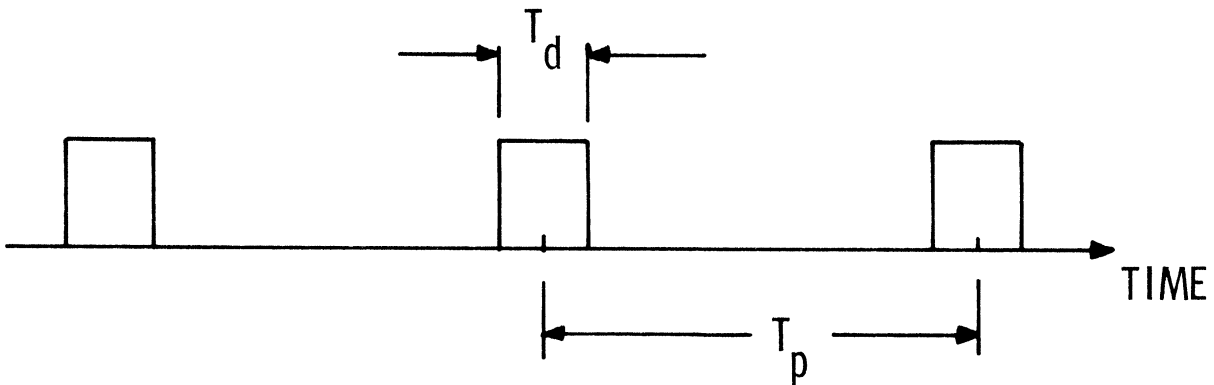
Fig. 2.12. Periodic Pulse Signal

The CW reception illustrated the frequency spreading effects on a line so that the spreading effects on the line spectrum of the pulse train signal are immediately clear. That is, each line undergoes a slight spreading and a pair of incoherent sidebands are associated with each line in the signal spectrum. This reception spectrum is illustrated in Fig. 2.13.

Fig. 2.13. Received Frequency Spread Line Spectrum

As can be seen from Fig. 2. 13, to prevent distortion $1/T_p$ must

place signal lines enough apart so that the frequency spread side-

bands fall between these lines rather than on the signal lines.

Thus, $1/T_p$ must be greater than .3 Hz . For the range of values

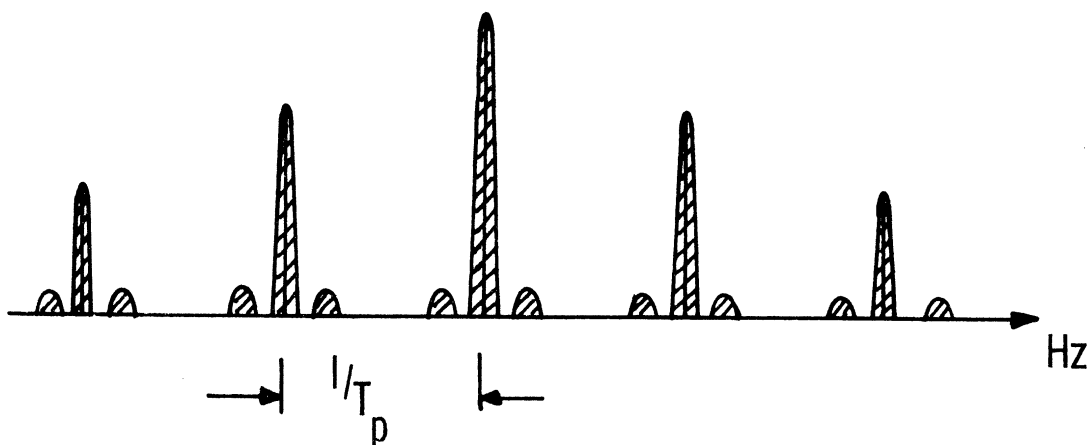of $1/T_p$ between .3 and .6 Hz sidebands from adjacent lines will

overlap. Since these sidebands are filtered out for the $\hat{h}(t, \lambda)$

measurements, the overlap is of no importance in $\hat{h}(t, \lambda)$ meas-

surements. Thus, an upper limit on the pulse train period of

$1/T_p > .3$ Hz has been established based on the frequency spread

characteristics of the channel.

A lower limit on T_p is determined by L , the delay-

spread parameter of the channel. The delay spread results from

the propagation of the transmitted signal over several routes

(multiple paths) each having a different distance. The result is

analogous to the reception of a pulse from a tapped delay line.

Each path corresponding to a tap on the delay with its own attenu-

ation, phase and propagation delay time. Figure 2. 14 illustrates

a typical multipath reception of delay-spread L , where a pulse

period of T_p seconds was used.

$(N-1)T_p$ NT_p $(N+1)T_p$
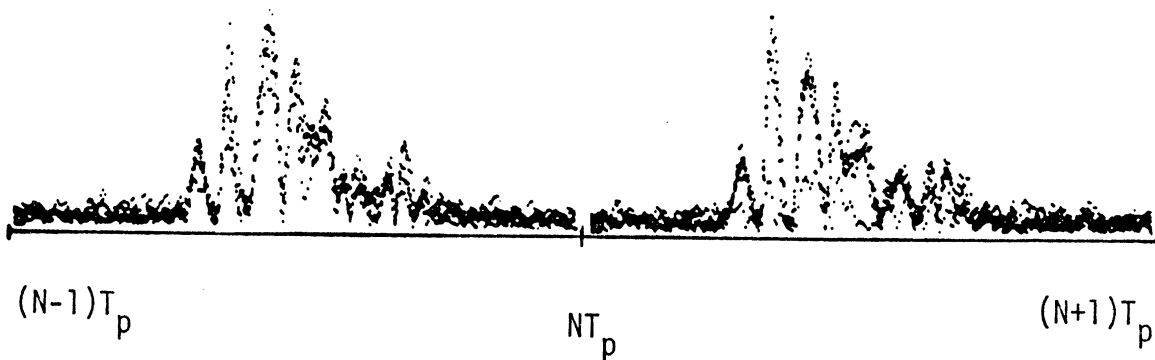
Fig. 2. 14.   Typical Multipath (Or Delay Spread) Reception

Clearly, the channel's maximum delay spread, L , must be less

than T_p . Otherwise, receptions from neighboring pulses will

overlap and the $\hat{h}(t, \lambda)$ measurement will be distorted. There-

fore, the channel delay spread factor, L , places a lower limit

on T_p in the signal design.

Summarizing, for distortionless $\hat{h}(t, \lambda)$ measurements

the relationships shown are $\dfrac{B}{2} < \dfrac{1}{T_p}$ (sideband distortion allowed)

and $T_p > L$. Combining these two equalities gives

$$\frac{BT_p}{2} < 1 \quad \text{or} \quad BL < 2$$

If sideband distortion is not allowed, then

$$B < \frac{1}{T_p} \quad , \quad T_p > L \quad \text{and} \quad BL < 1$$

Therefore, the MIMI measurement techniques for the doubly spread UWAP channel are effective in that they are limited only by the general theoretical limitations for instantaneous measurements of doubly spread channels.

Although noise considerations have been ignored in the discussion, all MIMI processing of transmitted signals is a modified form of matched filtering (with respect to the transmitted signals) that trades improved time resolution for snr. Generally, due to long coherent integration times and medium stability, high snr measurements are obtained.

CHAPTER 3

PRESENTATION AND DISCUSSION OF DUAL RESULTS

3.1 Results

The results presented here are the scalar parameter measurements of the MIMI channel from the November 1970 experiment. This data consists of a modified DUAL experiment. Some additional parameters are included, no spectral analysis of the surface reverberation is performed,[*] and the display of $\hat{h}_t(\lambda)$ is presented separately in Chapter 4, The CDR Gram.

The entire data set is organized into 19 files in chronological order, but not necessarily contiguous in time. Time and date information is summarized in Figure 3.1 and Table 3.1. The DUAL results of each data file are presented together in 5 different plots. In each of these plots the abscissa is the independent variable, time. Each parameter is measured and plotted every 102 seconds. Two hour intervals are marked on the abscissa. The plots were generated on a Hathaway Electronics 731 recorder, a raster scanning fiber optics device. The display format of a dependent variable plotted versus an independent variable is commonly known as an A-scan format. Such plots are most commonly generated on an X-Y device. However, Appendix A outlines a very

---

[*] For those results see Reference [1].

40

TABLE 3.1 DATA CHRONOLOGY

TABLE 3.1a. (DEEP HYDROPHONE)

$File_i$ extends from t_i through t_{i+1} with data obtained from the shaded intervals of time in Figure 3.1. During the non-shaded intervals, g_k, the time base was lost and data was either not recorded or not processed.	
t_i = Day (Hr:Min)	g_k = Day(Hr:Min) to Day(Hr:Min)
t_1 = 11(17:16)	
t_2 = 12(5:18)	
	g_1 = 12(9:27) to 13(16:53)
t_3 = 14(1:36)	
	g_2 = 14(9:29) to 14(10:55)
t_4 = 14(16:18)	g_3 = 14(15:29) to 14(16:18)
	g_4 = 15(3:06) to 15(5:38)
t_5 = 15(7:17)	
	g_5 = 15(10:13) to 15(19:13)
t_6 = 16(4:45)	
	g_6 = 16(10:55) to 16(12:52)
t_7 = 16(19:05)	
t_8 = 17(7:32)	
	g_7 = 17(12:06) to 17(12:33)
t_9 = 23(10:20)	g_8 = 17(18:46) to 23(10:20)

TABLE 3. 1b. (SHALLOW HYDROPHONE)

t_i = Day(Hr:Min)	g_k = Day(Hr:Min) to Day(Hr:Min)
t_9 = 23(10:20)	
t_{10} = 23(22:47)	
	g_9 = 24(10:49) to 24(18:42)
t_{11} = 24(18:42)	
t_{12} = 25(7:09)	
	g_{10} = 25(11:18:00) to 25(11:18:05)
t_{13} = 25(19:11)	
t_{14} = 26(7:38)	
t_{15} = 26(19:40)	
t_{16} = 27(8:07)	
t_{17} = 27(20:09)	
t_{18} = 28(8:36)	
t_{19} = 28(20:38)	
t_{20} = 29(9:05)	

simple procedure for generating on-line A scans with a raster scanning device.

The first plot contains the four power variables $C(t)$, $S(t)$, $R(t)$, and $N(t)$ in decibels (db) where unity is the arbitrary reference level. C, S, R, and N are plotted on a constant gain x band-
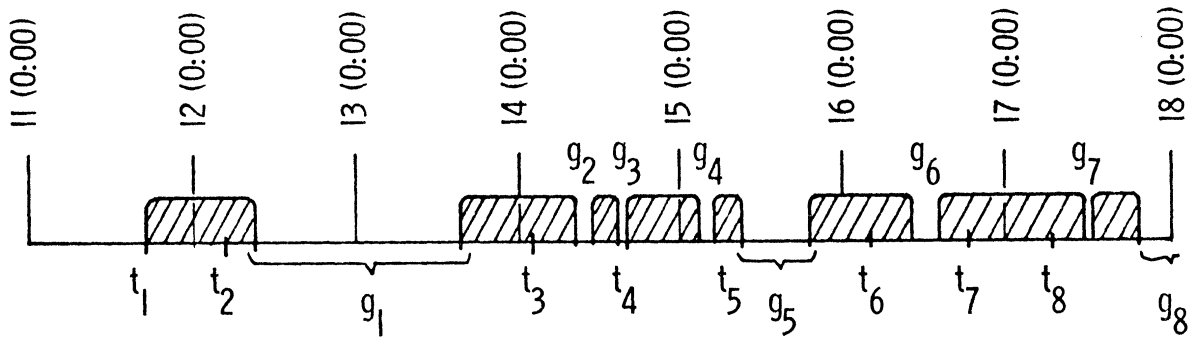
$\boxed{\mathit{7////7}}$ ≡ RECORDED, PROCESSED AND DISPLAYED DATA
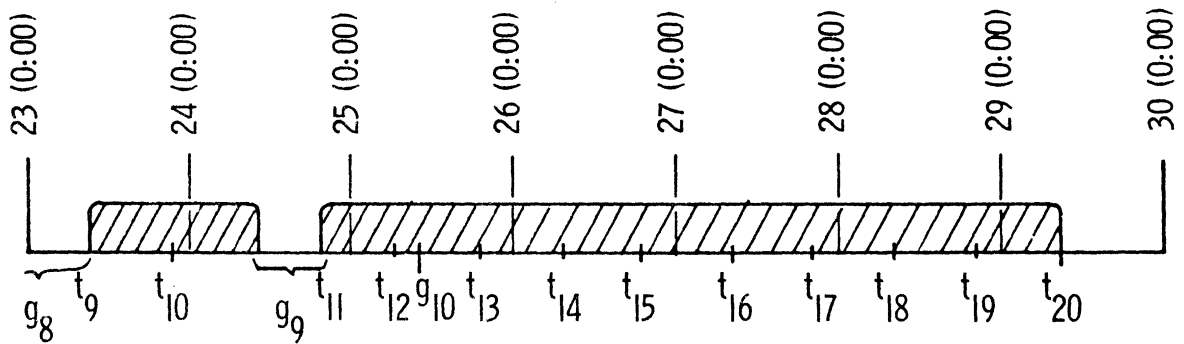
$\boxed{\mathit{7//////7}}$ ≡ RECORDED, PROCESSED AND DISPLAYED DATA

Fig. 3. 1. Chronology of November 1970 DUAL Experiment

width product basis so that signal-to-noise ratio is easily computed
from the plot by simply subtracting the indicated power levels.[*] The
power ordinate is marked in 12 dB increments.

Although the DUAL power measurements are time-spread
averaged measurements,

$$C(t) = \left| \sum_{\lambda \in \Lambda} \hat{h}_t(\lambda) \right|^2$$

$$S(t) = \sum_{\lambda \in \Lambda} |\hat{h}_t(\lambda)|^2$$

$$R(t) = \sum_{t' \in T_t} \left| \sum_{\lambda \in \Lambda} h(t', \lambda) \right|^2 \qquad T_t = (t, t+MT_p)$$

$$N(t) = \sum_{\lambda \in \Lambda} |\hat{h}_t(\lambda)|^2$$

they reveal much about the behavior of the UWAP channel. Most of
the time in the data here and typically in the past, a normal behav-
ior of these parameters has been observed. $C(t)$ is generally fluc-
tuating with rapid fading attributed to the narrowband frequency
selective fading due to highly interactive and interferring multipath
structure. $S(t)$ is normally steady in level indicating that the fre-
quency selective fading is narrowband. $S(t)$ and $C(t)$ are only
slightly correlated. $R(t)$ is low level, 3 to 6 dB above $N(t)$, and is
usually correlated with $N(t)$ rather than $S(t)$ or $C(t)$. Thus, $R(t)$

---

[*] For unity gain plots see Reference [1] where total power
measurement is readily available.

is generally noise driven indicating surface effects are definitely secondary phenomena under normal conditions in the 43 mile Straits of Florida channel. $N(t)$ is steady except for irregular increases due to shipping.

A second, more interesting channel behavior is exhibited when the channel surface effects become evident. $C(t)$ does not fade, $S(t)$ fluctuates, $R(t)$ drastically increases and $C(t)$, $S(t)$, and $R(t)$ are all highly correlated. This type of behavior is illustrated here in files 11, 12, 13, 14, and 15.

In the second plot an estimate of the phase-only matched filter gain is presented in decibels relative to 1. This matched filter gain measurement, denoted MFG is estimated by

$$MFG(t) \cong \text{peak } SNR(t)/\text{average } SNR(t)$$

$$= S_{PEAK}(t)/S(t)$$

where $S_{PEAK}(t)$ is measured from the threshold processed $\hat{h}_t(\lambda)$. The threshold processing is discussed in Section 4.2.3.

The theoretical value of MFG, where no decorrelation loss due to multipath is incurred and additive white Gaussian noise is assumed, is

$$MFG = 10 \log_{10} 2WT$$

$$= 10 \log_{10} 63 \simeq 18 \text{ dB}$$

A high MFG value indicates low decorrelation loss which in turn indicates relatively little multipath. Whereas low MFG implies high decorrelation loss and therefore high multipath activity. In this experiment, these observations are reflected where during the simplest multipath structure, files 11 and 13, MFG takes its highest values, +9 to +15 dB and MFG takes its lowest values, 3 to 6 dB, during periods of extensive multipath reception.

The CW phase angle in degrees, $A(t)$, is presented in the fourth plot. This plot substantiates the well-behaved nature of the CW phase, reveals any discontinuities in the phase and displays the short-term small variations.

The fourth and fifth plots are the channel's forward decorrelation times from the CANDOR analysis. $T^+_{-3}(t)$ and $T^+_{-6}(t)$ are in the fifth plot with $T^+_{-3}(t) \leq T^+_{-6}(t)$ for all t. $T^+_{\pm 45^\circ}(t)$ is in the last plot. Limited computer memory forced limiting values of $T^+_\zeta(t) \geq$ 48 minutes to $T^+_\zeta(t) = 48$ minutes. The ordinates are marked in 10 minute intervals from 0 to 50 minutes. The $T^+_\zeta(t)$ plots allow study of the channel's rate of time variation and evaluation of the data reduction potential of the deterministic, quasi-time-invariant CANDOR technique.

T^+_ζ values are large and often limited at 48 minutes during files 10 through 13.[*] That is, large T^+_ζ coincides with the occurrence

---

[*] $T^+_{\pm 45^\circ}(t)$ was inoperative in files 9, 10, 11, and 12 due to the Time Base Artifact, Section 3.2.

of high $R(t)$, smooth $C(t)$ and high $S(t)$ correlation with $C(t)$. The channel structure is surmised to be dominated by a surface mode, due to the high $R(t)$; and based upon past observations and reasoning the smooth $C(t)$ and high correlation of the three signal powers (C, S, and R) a very simple (non-interferring) multipath structure again dominated by a surface mode* is strongly implied.

Otherwise, T_ζ^+ values are between 5 and 15 minutes most of the time, reflecting the normal quasi-time-invariant behavior of the MIMI channel. During these times, the signal power measurements, C, S, R are behaving normally. $C(t)$ displays considerable rapid fading, caused by high multipath activity and interference. In contrast, $S(t)$ is very steady and only mildly correlated with $C(t)$. $R(t)$ is rather low, 3 to 6 dB above $N(t)$ and is generally correlated with $N(t)$ rather than $C(t)$ or $S(t)$. Thus, normal conditions definitely do not reflect any surface interaction and generally the narrowband frequency selective fading of complex multipath structure is clearly present.

Under normal conditions $T_{-6}^+ \simeq T_{-3}^+$ indicating that $|\rho_{t_1, t_2}|$ falls sharply so that the exact threshold value on $|\rho_{t_1, t_2}|$ is not critical.

$T_{\pm 45^\circ}^+(t)$ and $A(t)$ measure change in the multipath average

---

*These conclusions are supported further in the CDR gram presentations of $\hat{h}_t(t)$.

Fig. 3. 2. Dual Graph 1

Fig. 3.3. Dual Graph 2

Fig. 3.4. Dual Graph 3

Fig. 3.5. Dual Graph 4

Fig. 3.6. Dual Graph 5

Fig. 3.7. Dual Graph 6

Fig. 3.8. Dual Graph 7
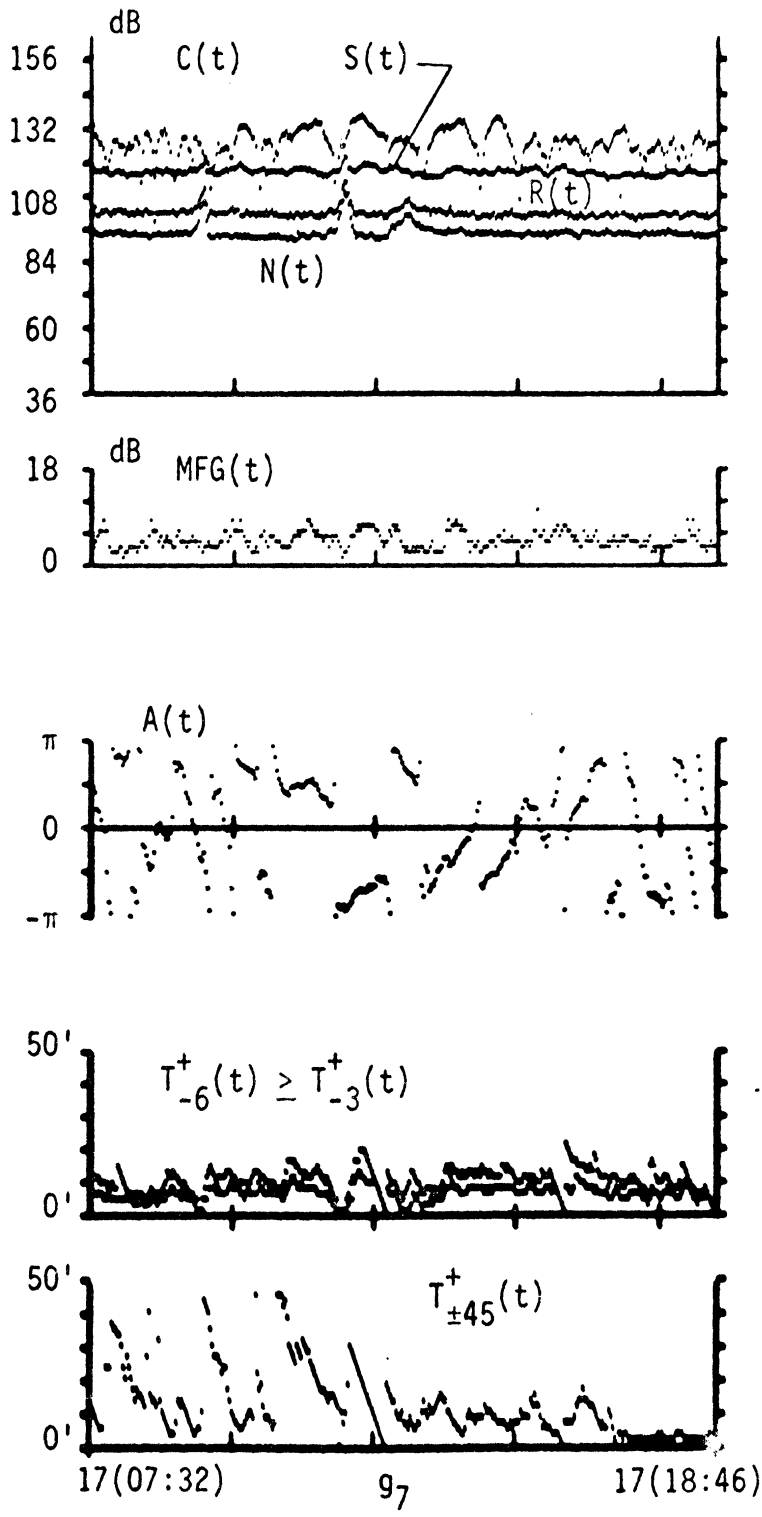
Fig. 3.9. Dual Graph 8
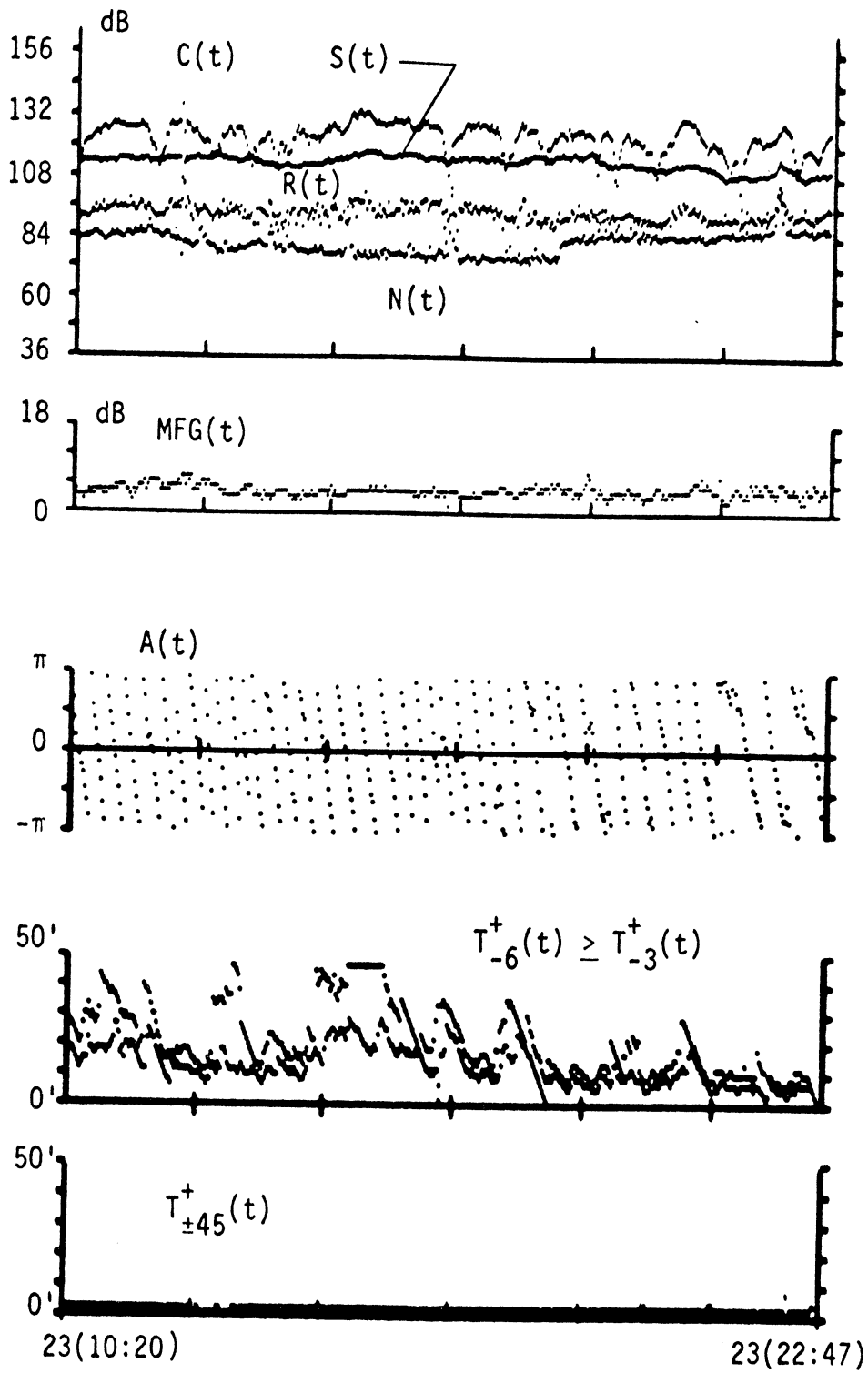
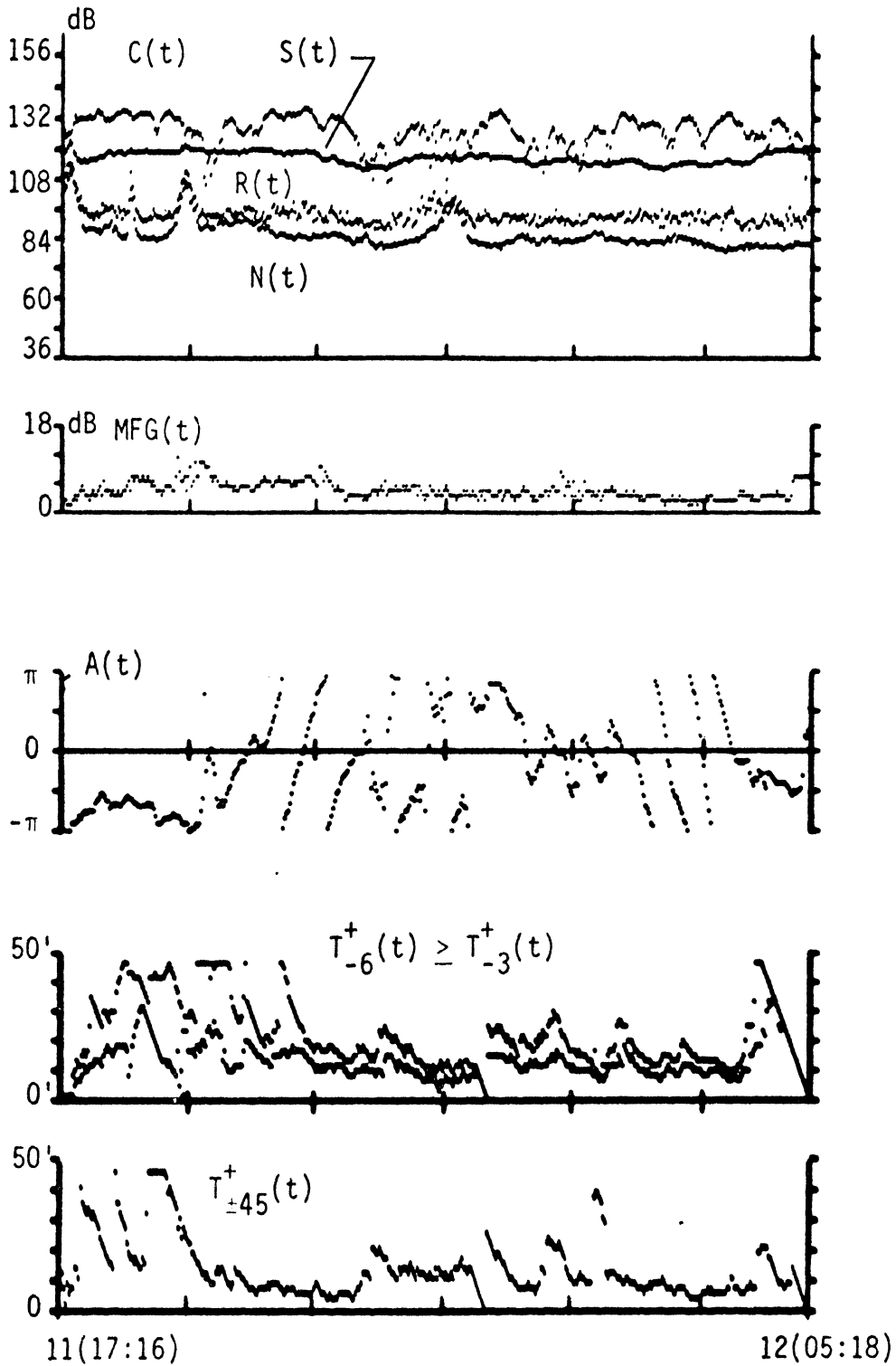Fig. 3.10. Dual Graph 9
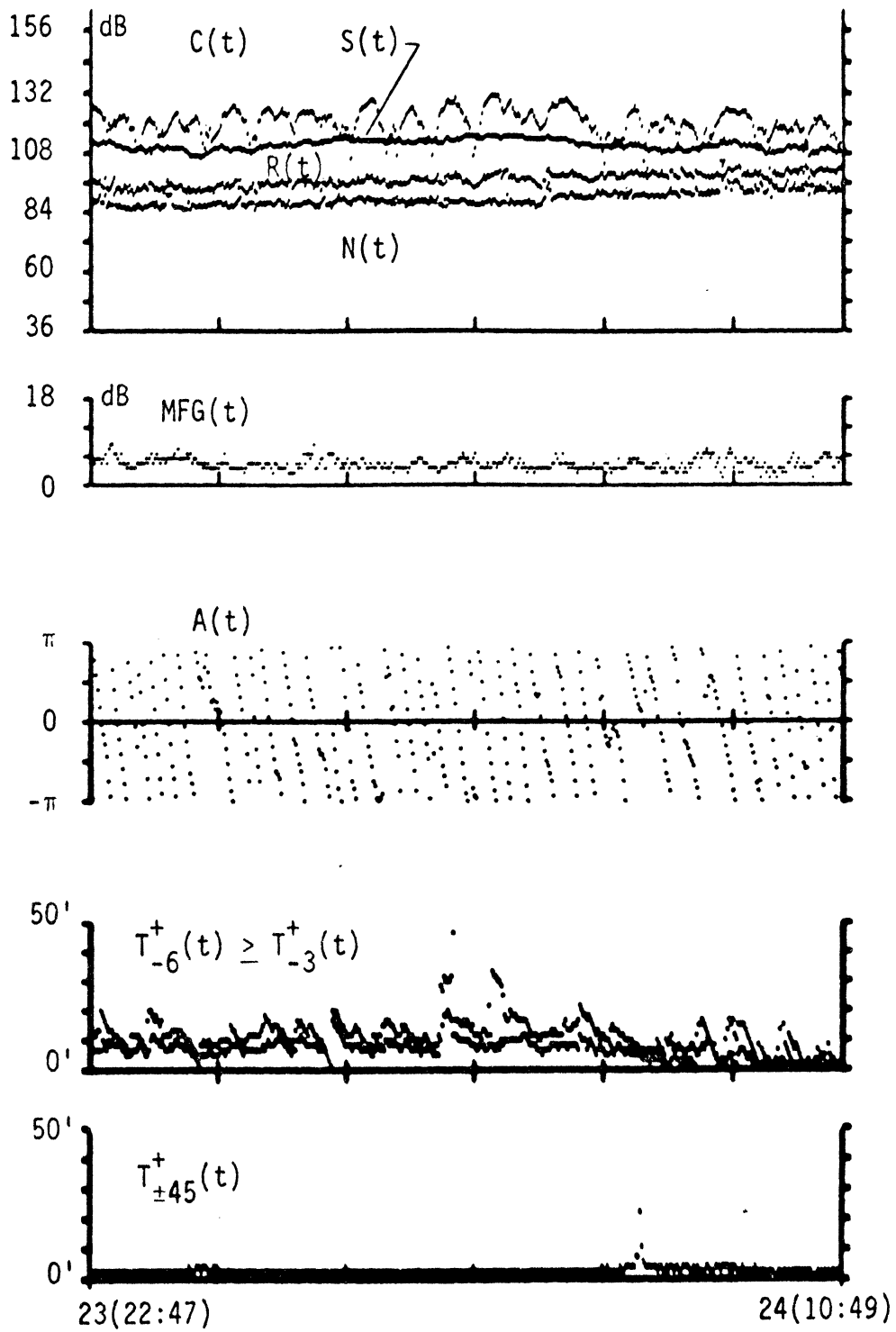
Fig. 3.11. Dual Graph 10
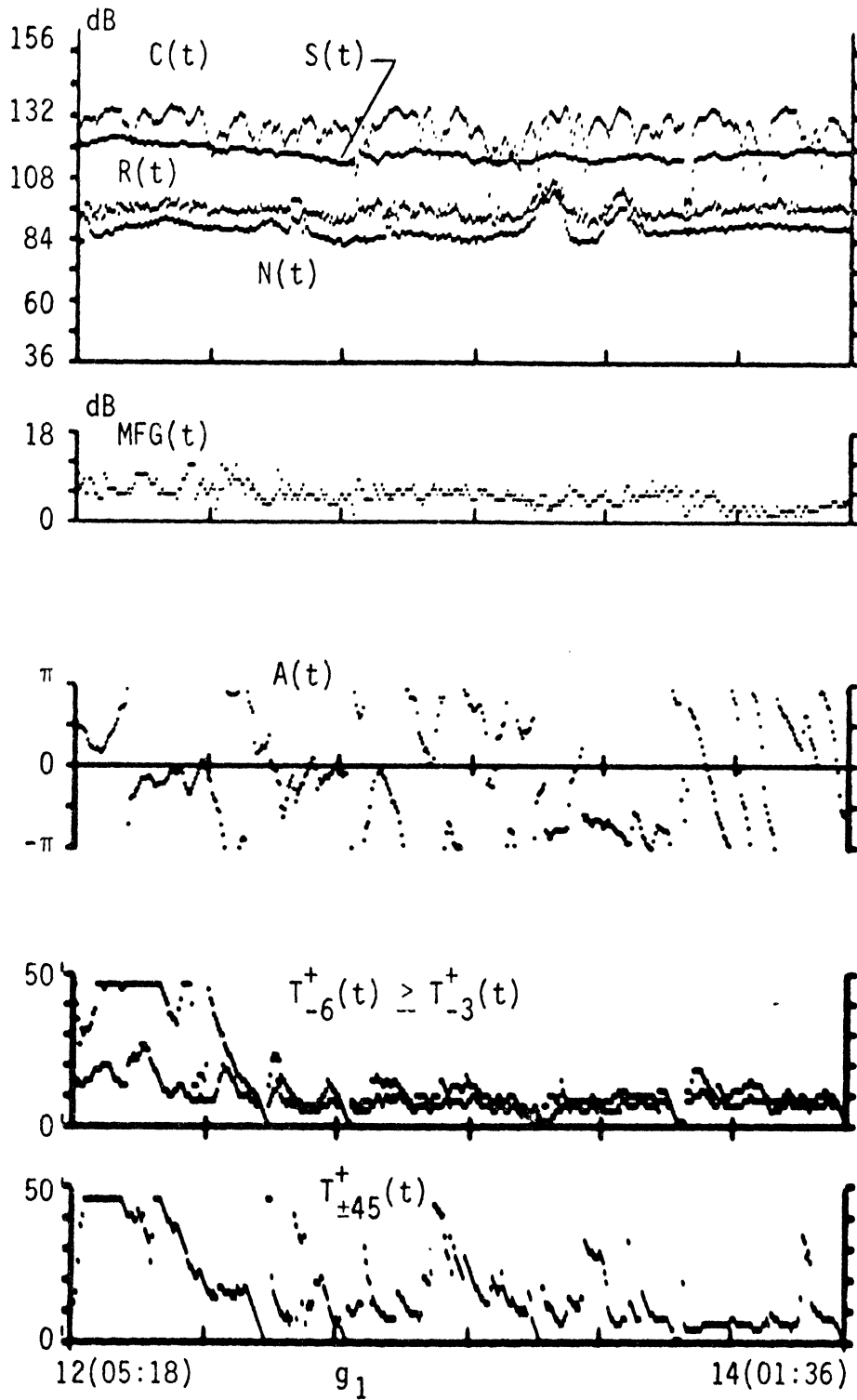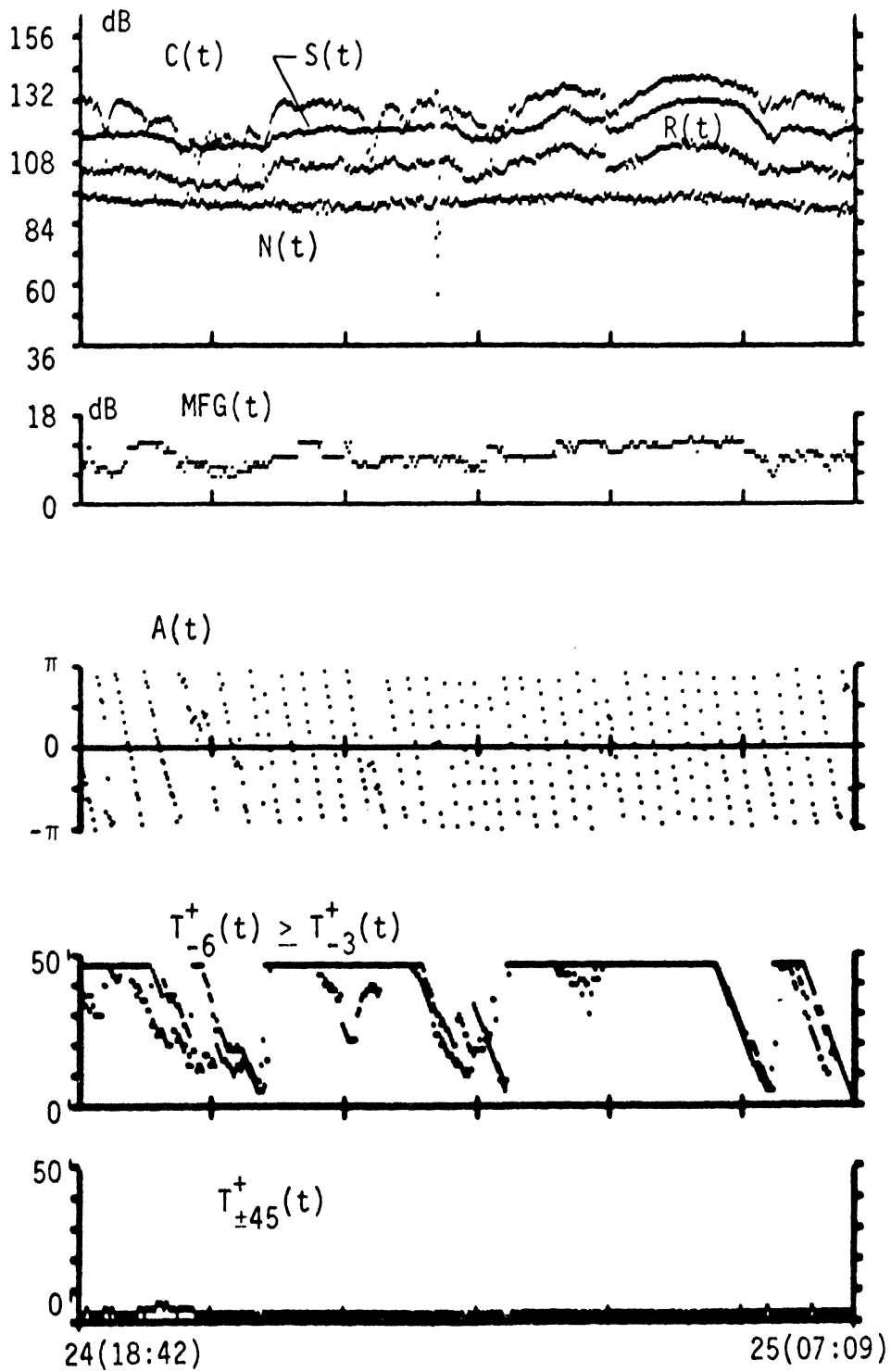
Fig. 3.12. Dual Graph 11
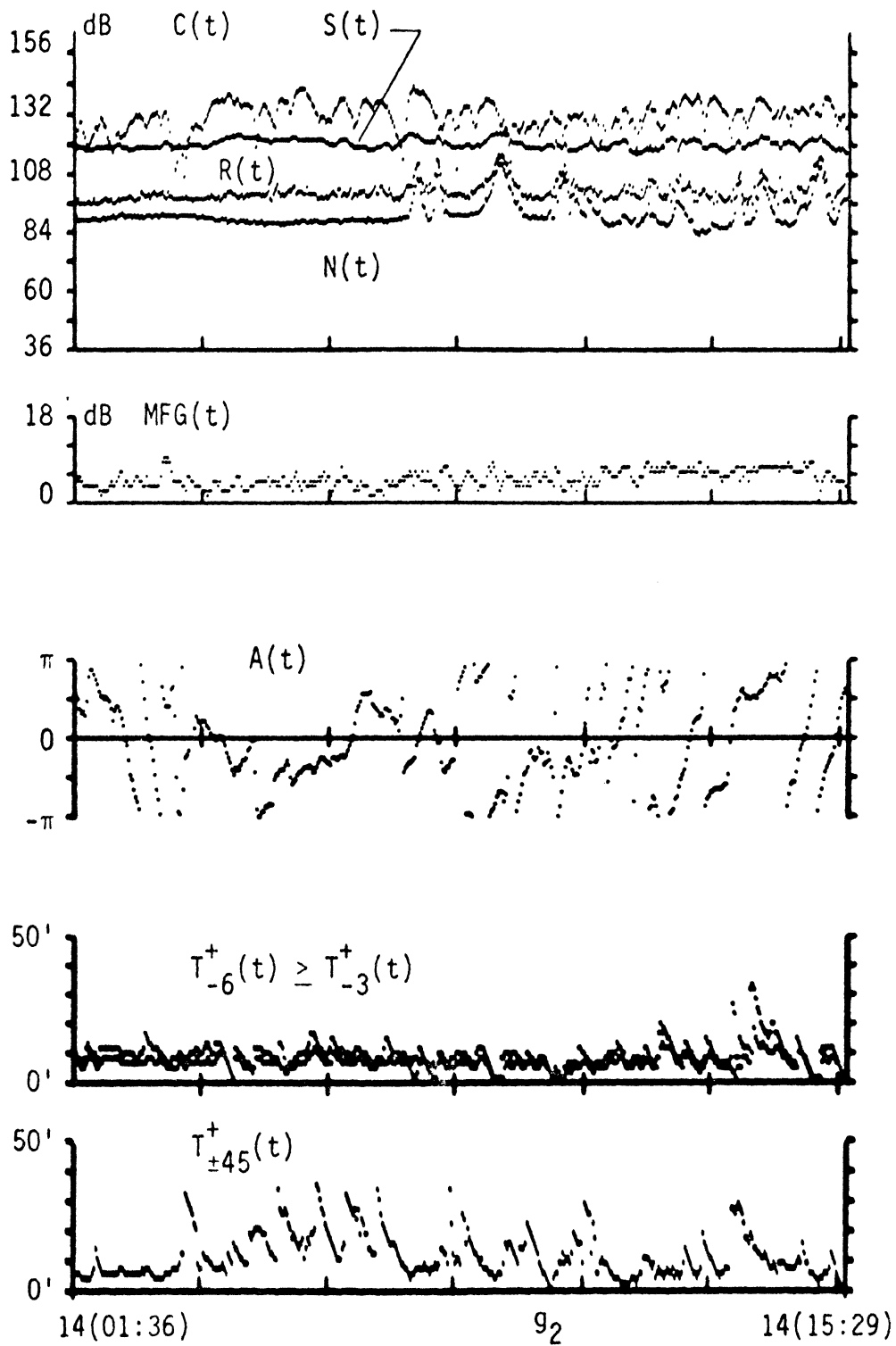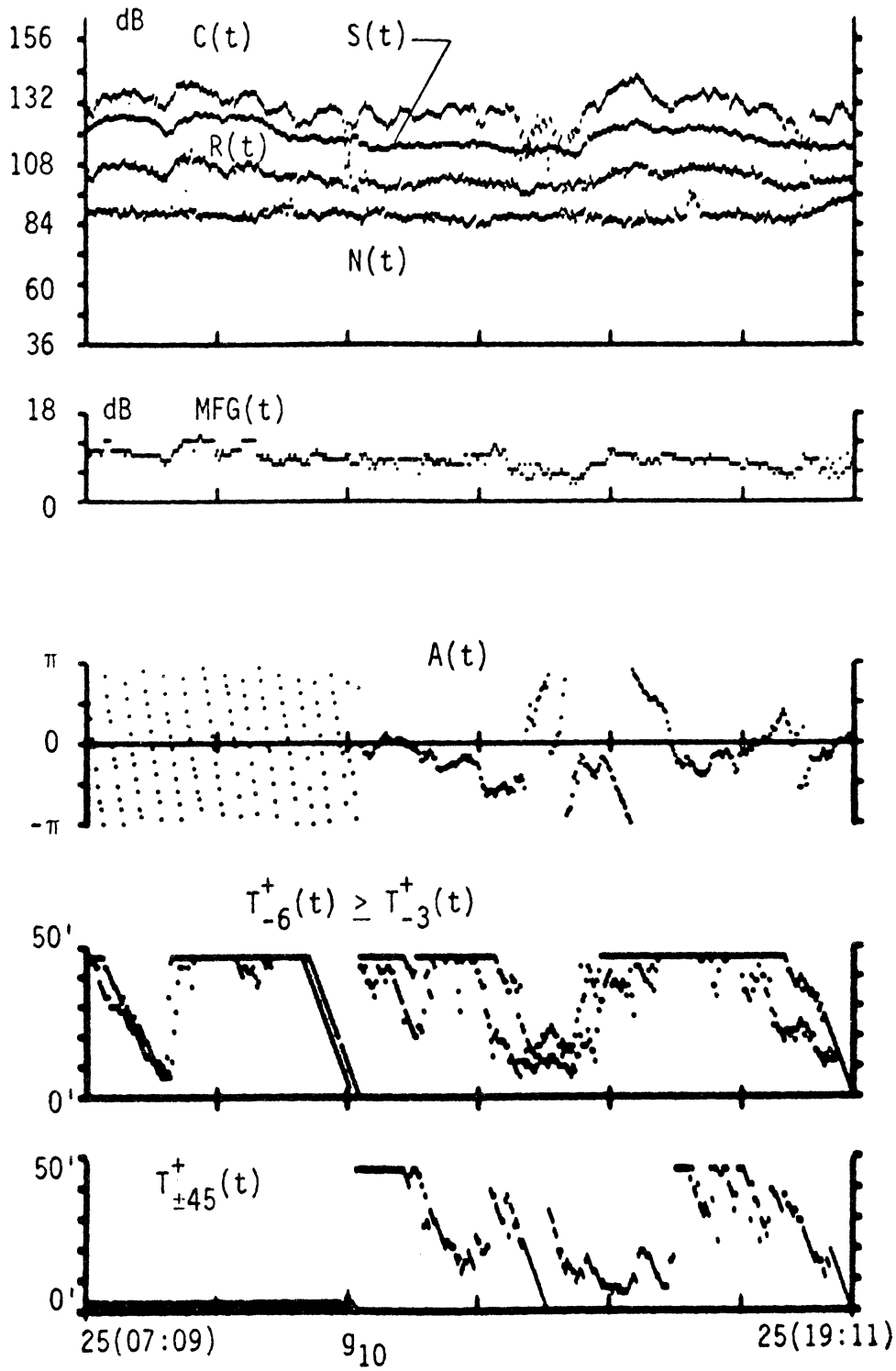
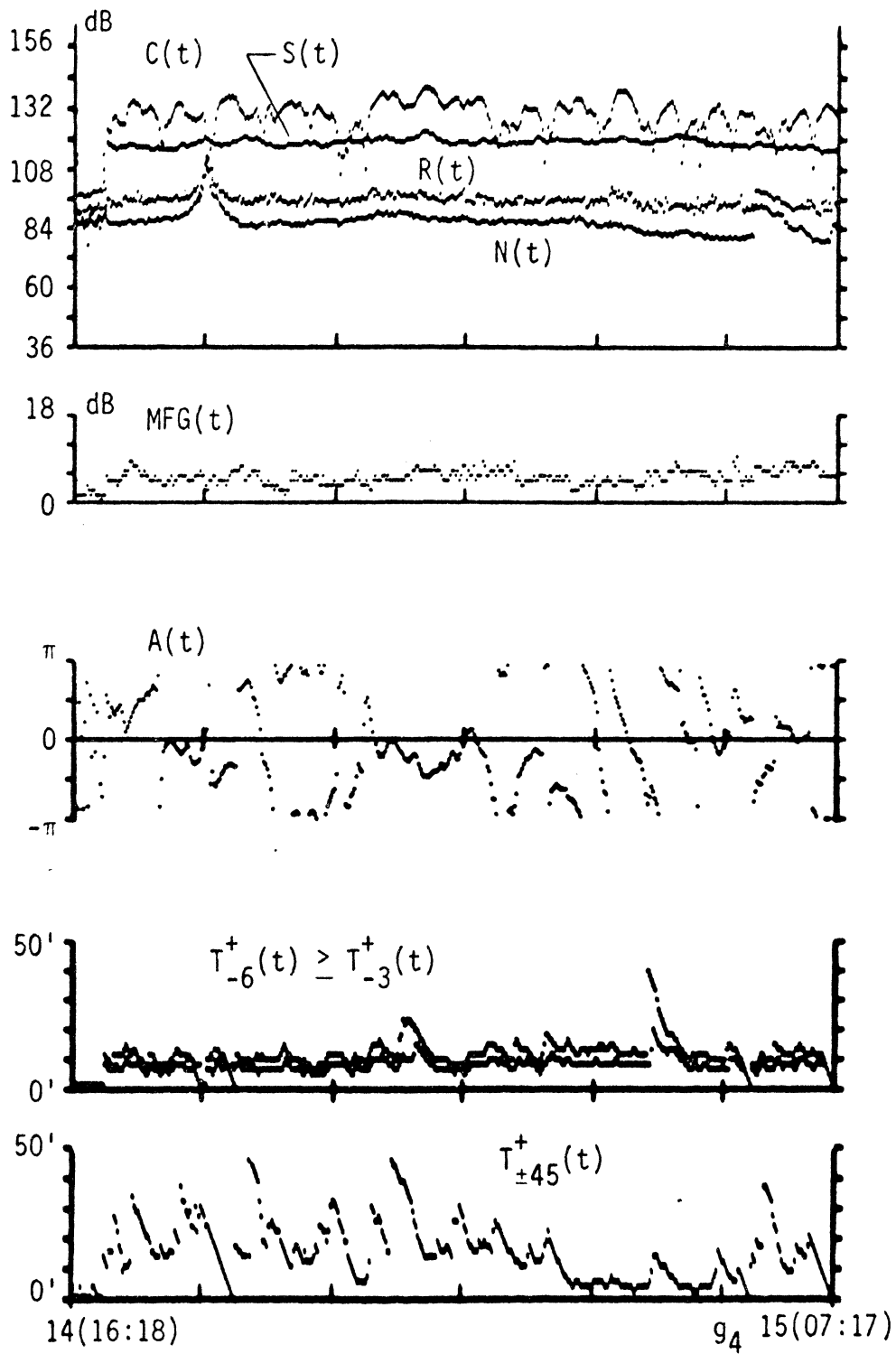Fig. 3.13. Dual Graph 12
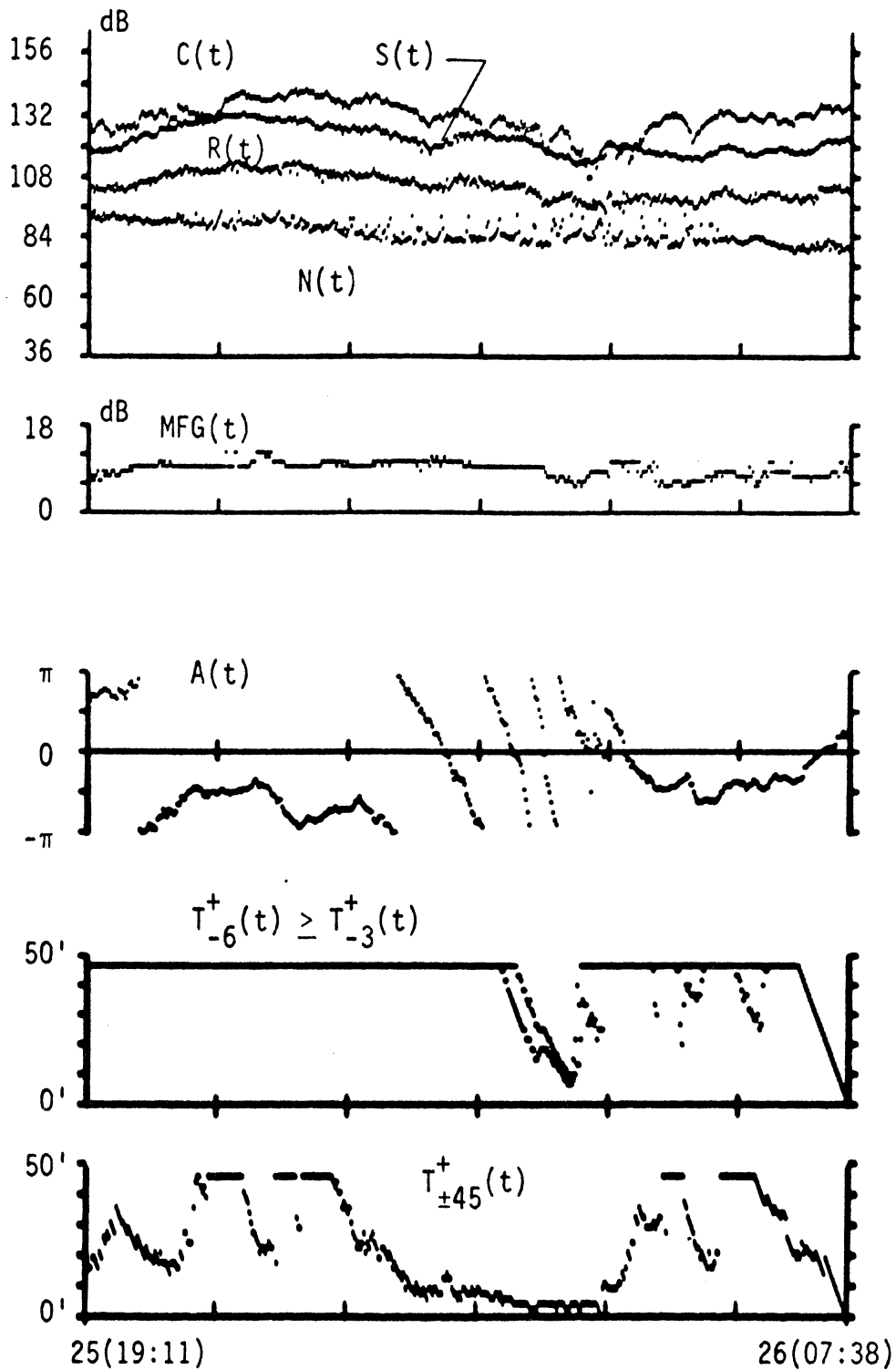
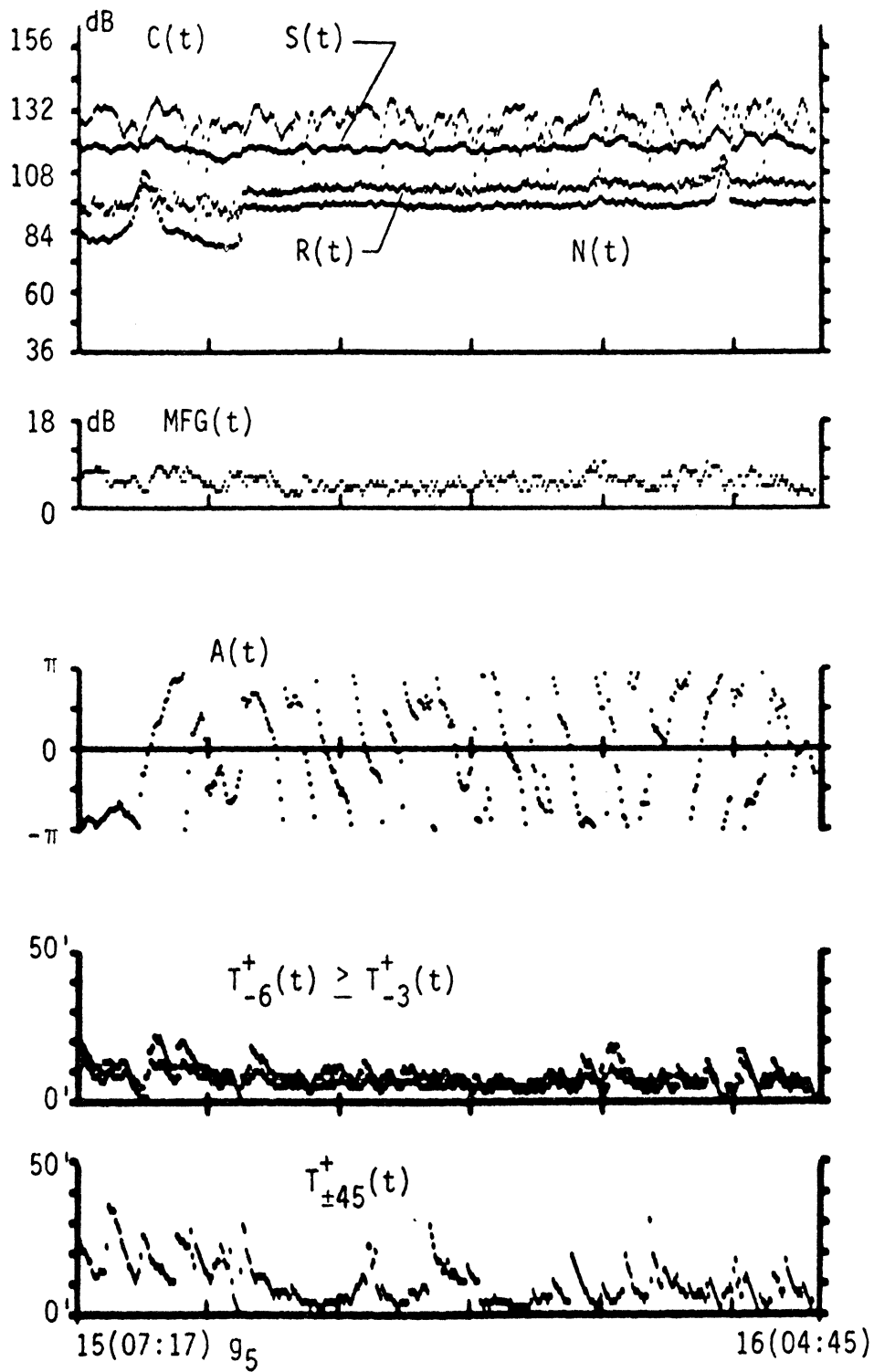Fig. 3. 14. Dual Graph 13
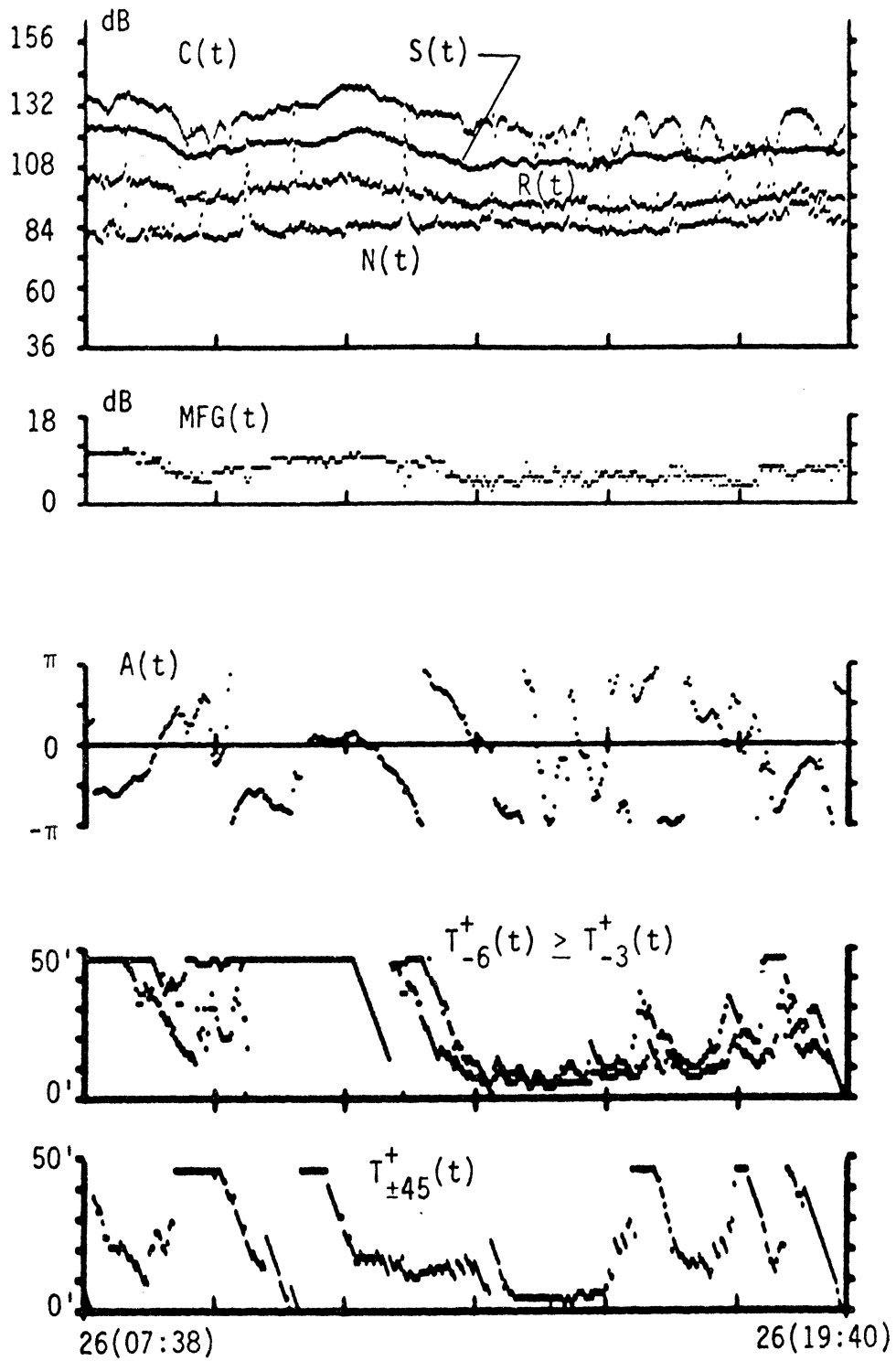
Fig. 3.15. Dual Graph 14
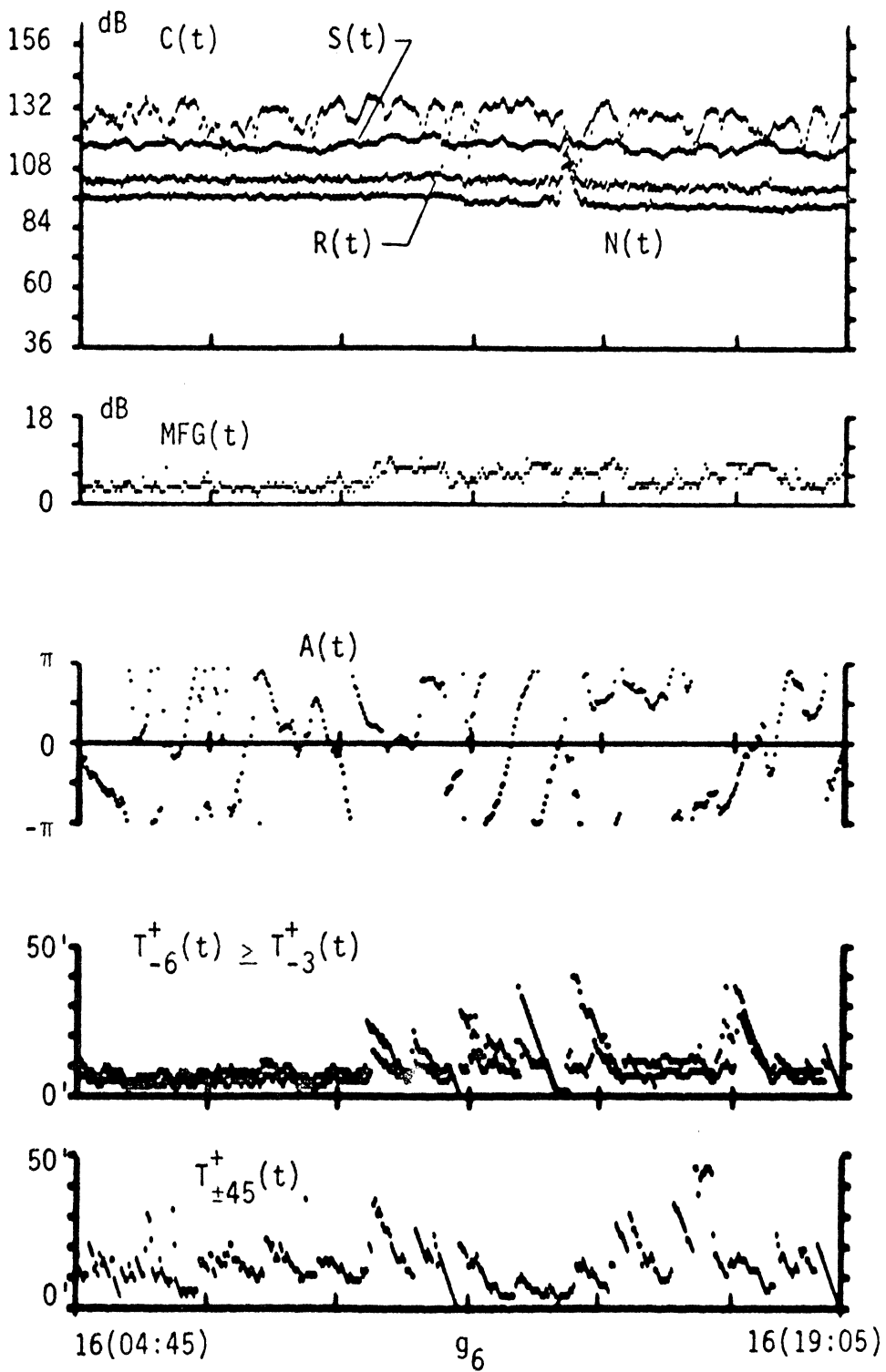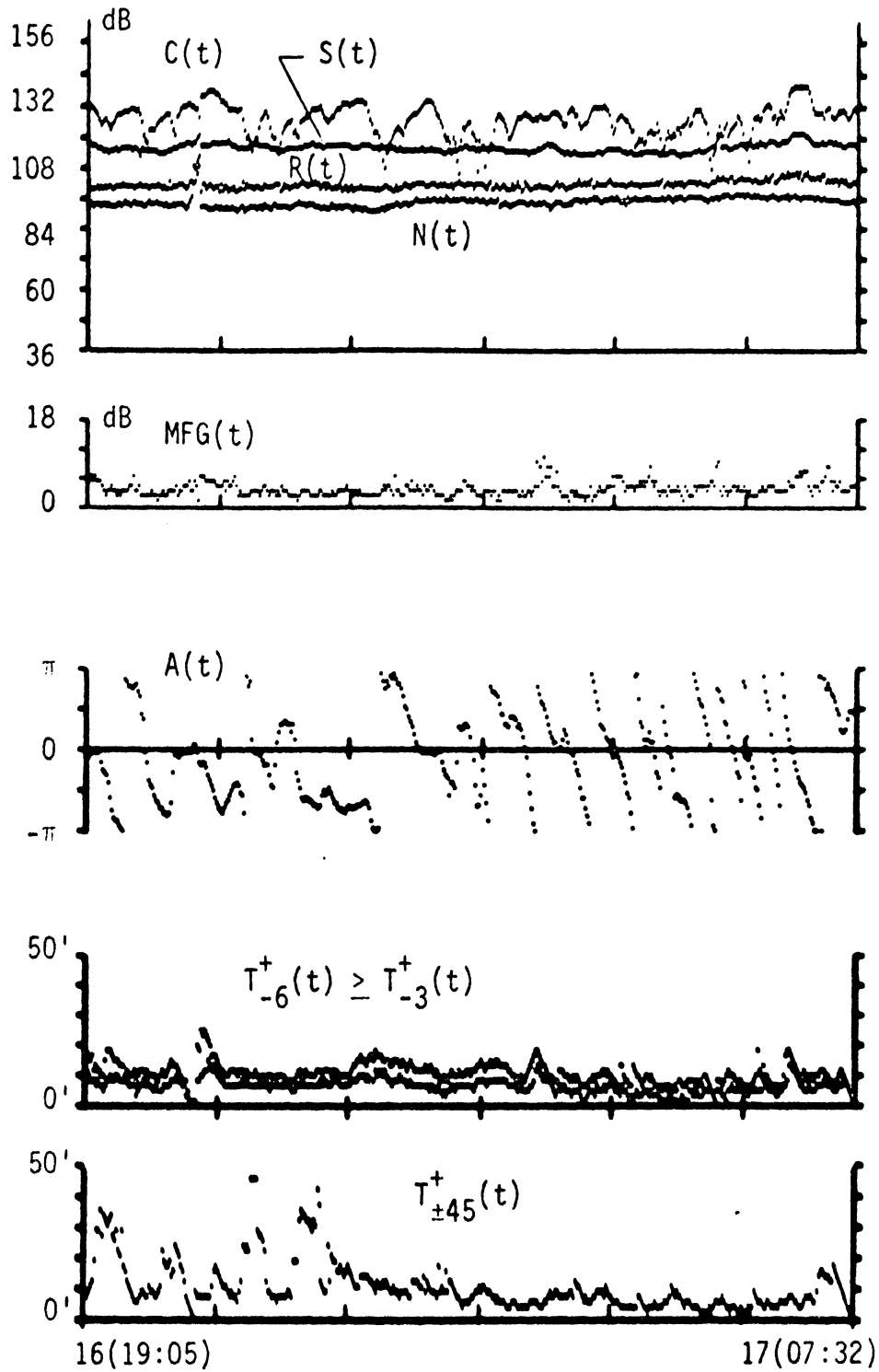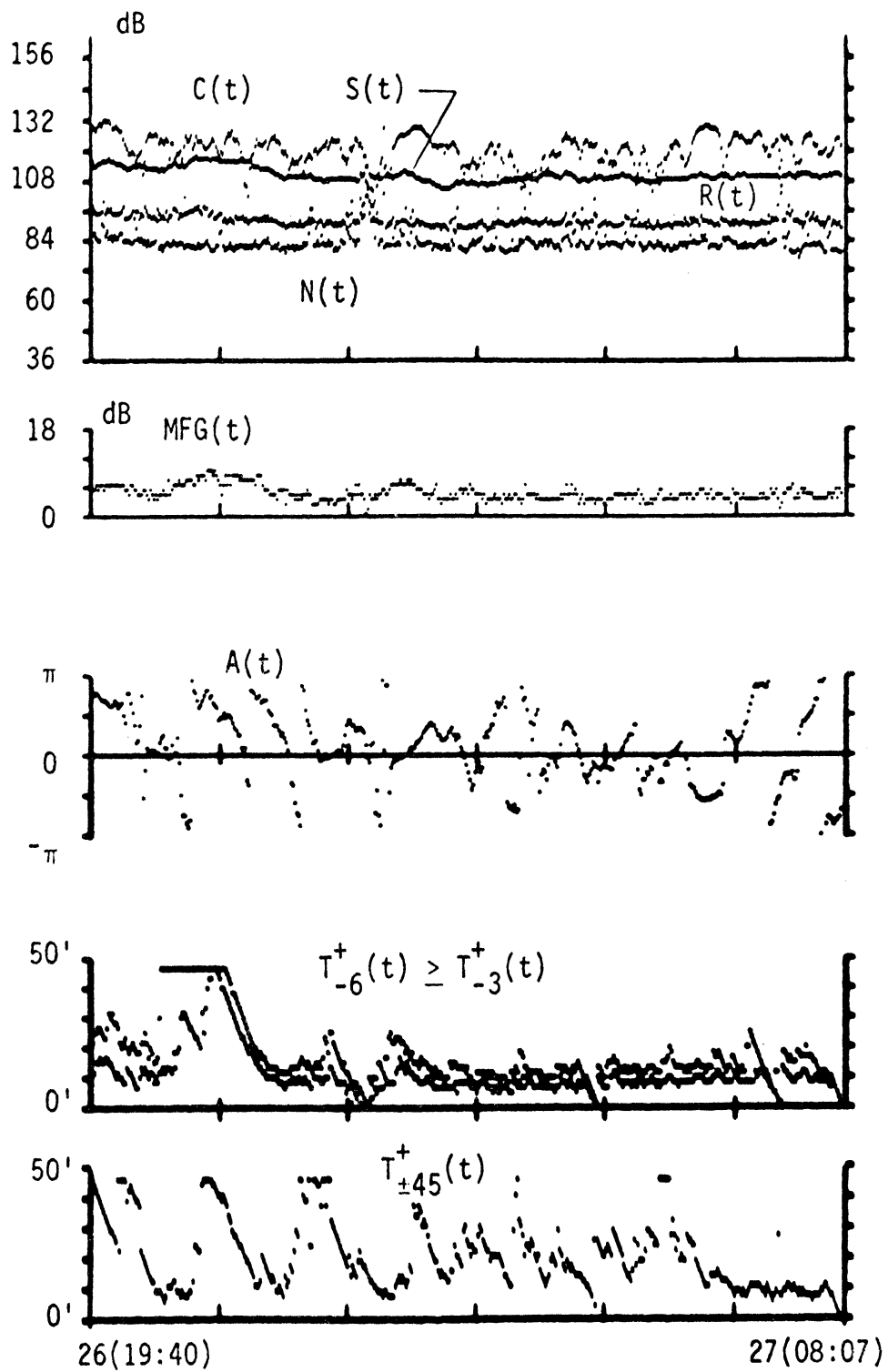
Fig. 3.16. Dual Graph 15
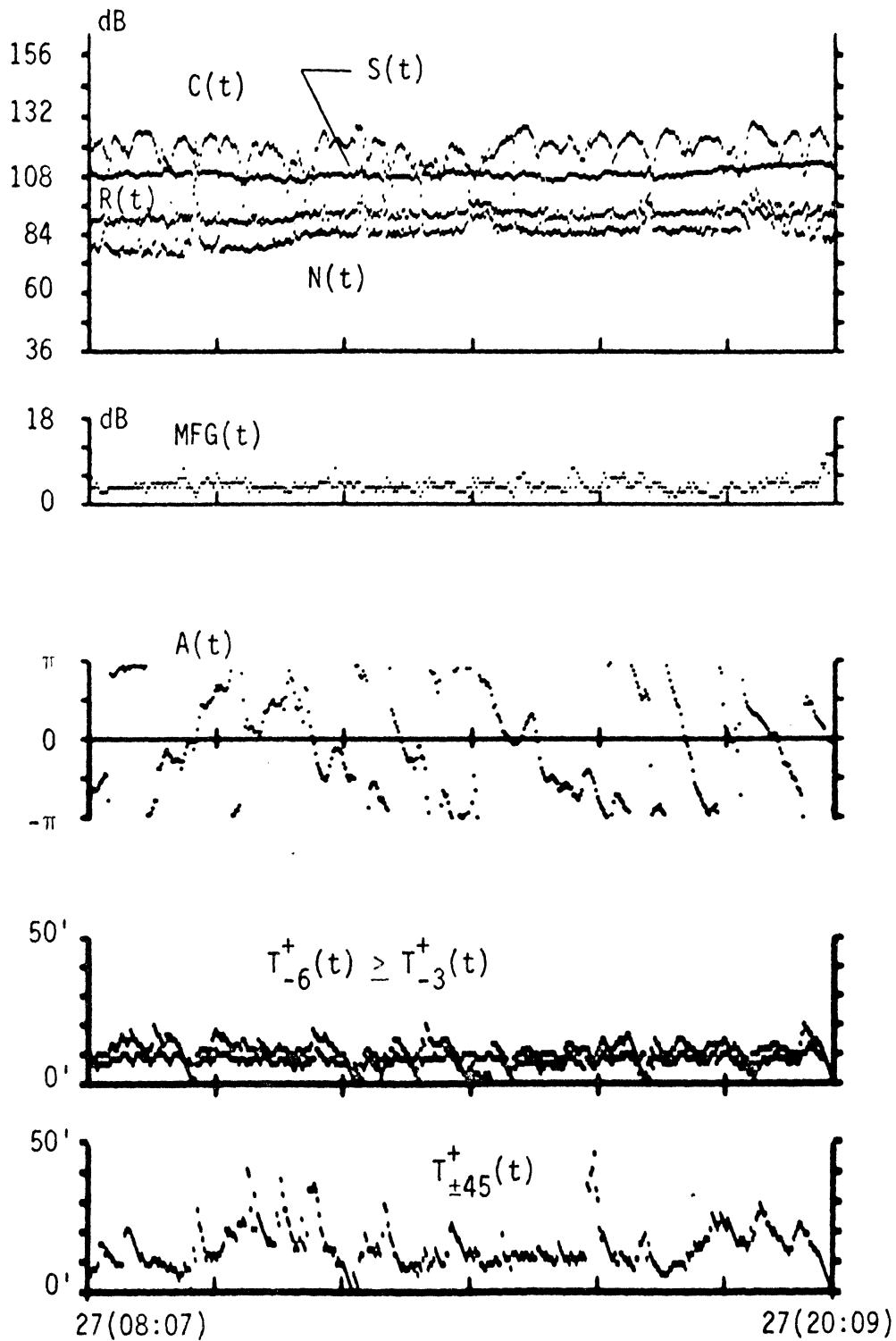
Fig. 3. 17. Dual Graph 16
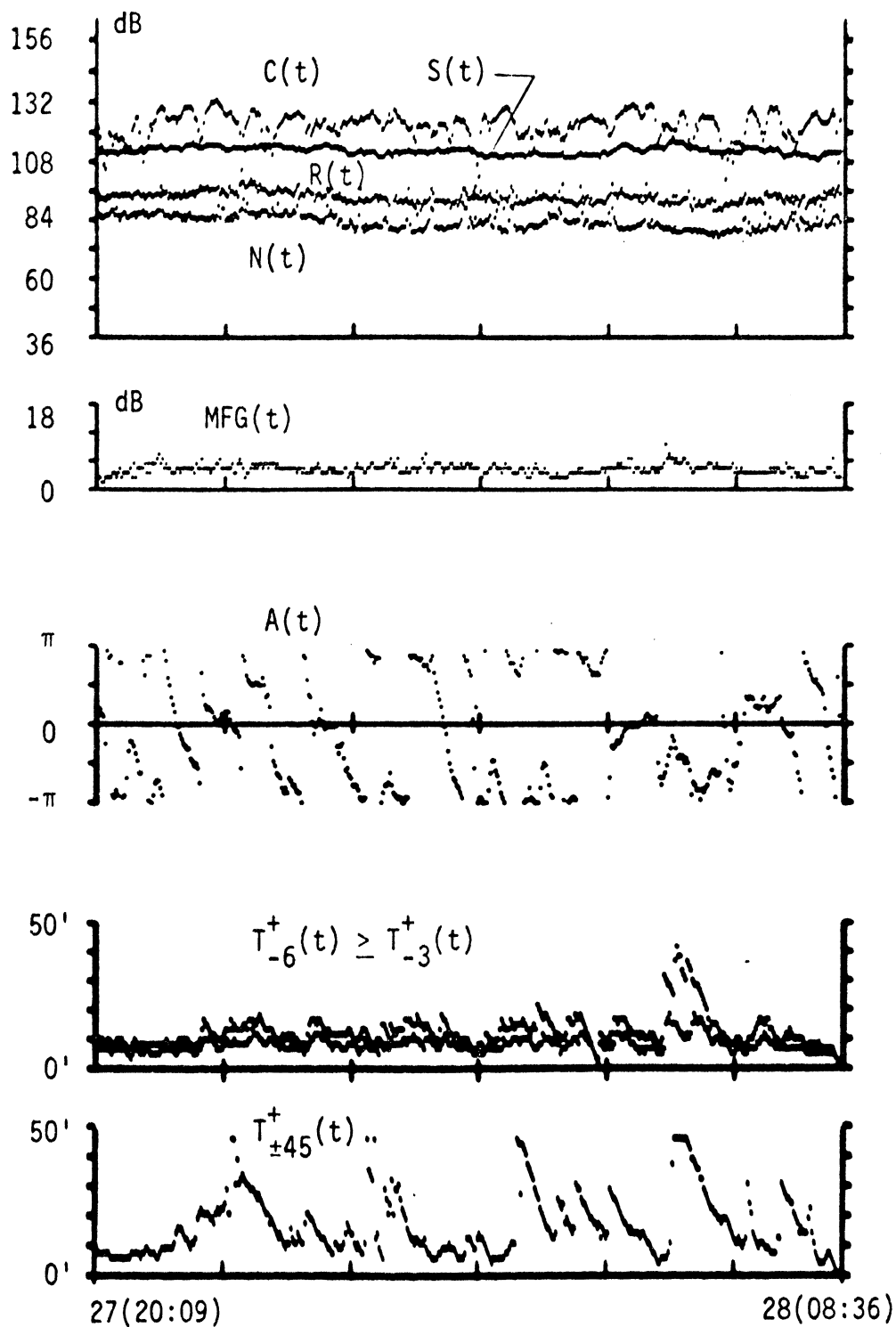
Fig. 3.18. Dual Graph 17
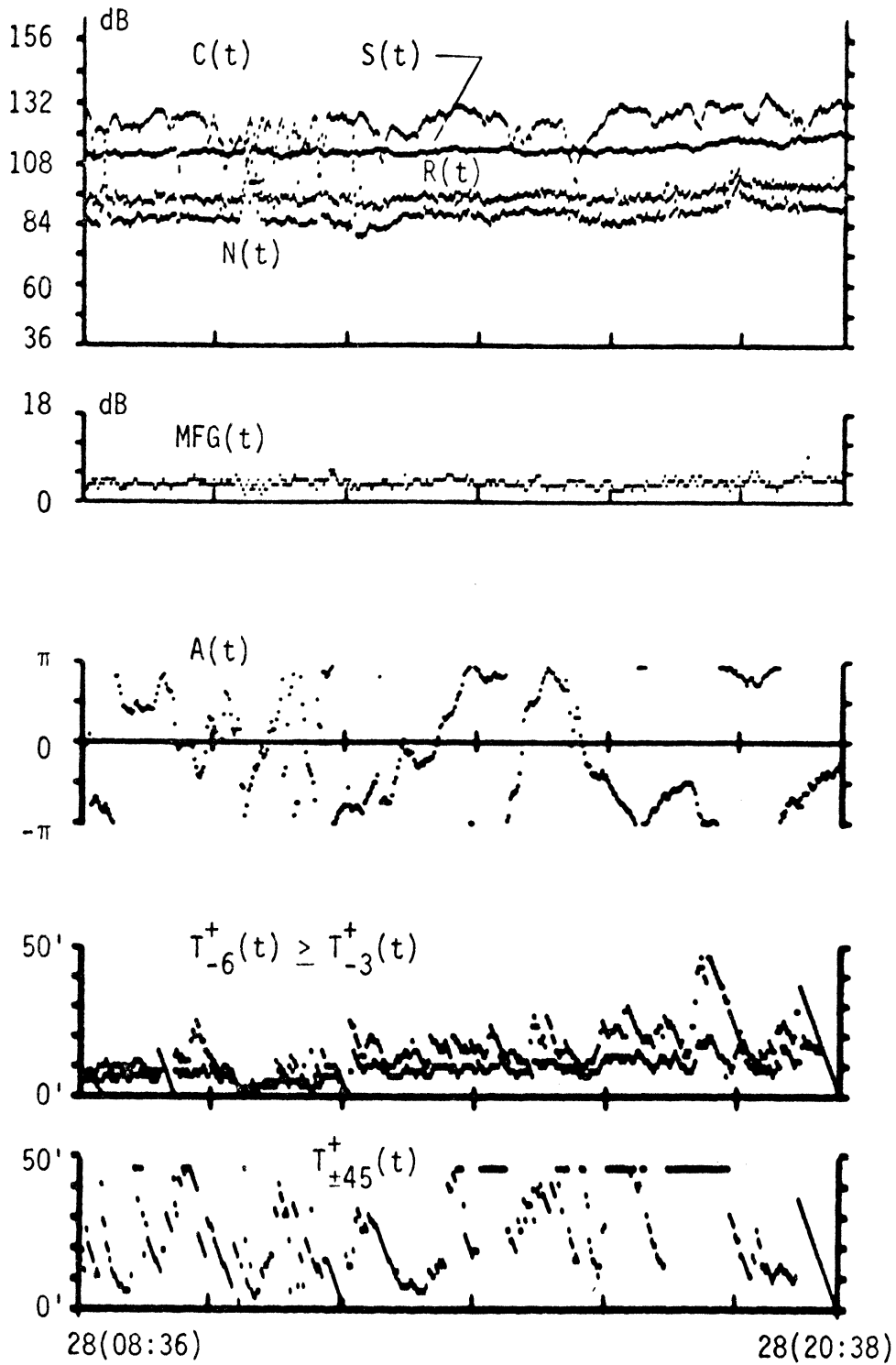
Fig. 3.19. Dual Graph 18
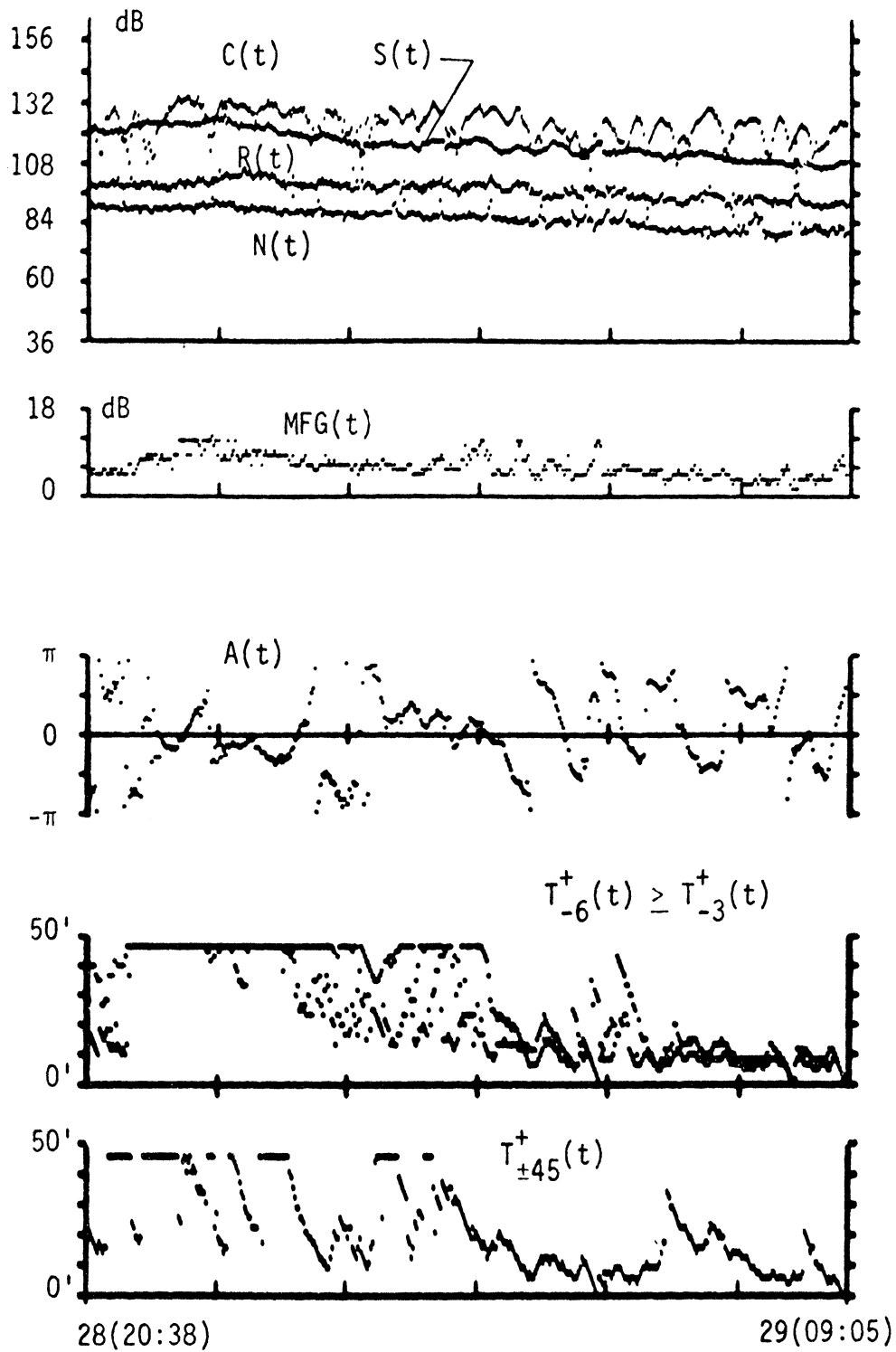
Fig. 3.20. Dual Graph 19

arrival time providing a verification of the assumption that ρ_{t_1, t_2} only needs to be evaluated at $\Delta\lambda = 0$.

The experimental results of DUAL processing are all relatively simple to compute and display. They are important because they reveal a wealth of information about the time-spread averaged channel and because they provide quantitative measurements of parameters that are very qualitative or not available in the $\hat{h}_t(\lambda)$ display of Chapter 4.

3.2 The Time Base Artifact of Data Files 9, 10, 11, and 12

From 18:46 hours on November 17 until 11:18 hours on November 25, the time base references at the transmitter and receiver were out of synchronism by approximately 1.7 millihertz. Data files 9, 10, 11, and part of 12 are during this time. Although the time base error was too small to have noticeable effects on power measurements, the artifact is reflected in the CDR grams, the carrier phase angle measurement, etc., as a constant rate of change in the propagation time of the channel. This rate measured from the CDR grams is approximately 14.3 milliseconds per hour or from the corresponding A(t) approximately 6 cycles of carrier phase per hour. These two measurements agree with each other and correspond to a 1.7 mHz reference offset.

Although this artifact is very noticeable in the phase striping patterns of CDR grams 9, 10, 11, and 12, the basic multipath

structure is not lost. Thus, these grams are still useful and, there-fore, retained.

3.3 Summary - A Preliminary Channel Model

A simple model of the UWAP channel in the Straits of Florida that reflects current knowledge and is consistent with MIMI measurement results and techniques provides a preliminary basis for more detailed modeling discussion later. To date, the surface effects have been modeled as a simple amplitude modulation. A simple model for the channel, which allowed for some reception unaffected by the surface, can be expressed as

$$h(t, \lambda) = a(t) h_{1_t}(\lambda) + h_{2_t}(\lambda)$$

The surface modulation is represented by $a(t)$, a narrow bandpass, 0.2 Hz bandwidth centered at 0.2 Hz, random process. The reverberation measurement, $R(t)$, is nominally a measurement of the power of $a(t)$. The two components $h_{1_t}(\lambda)$ and $h_{2_t}(\lambda)$, of multipath structure are quasi-time-invariant linear time-spread channels. The time dependence of $h_{1_t}(\lambda)$ and $h_{2_t}(\lambda)$ is implicit in the notation. The component of the multipath structure undergoing surface modulation is $h_{1_t}(\lambda)$. In some sense $h_{1_t}(\lambda)$ must therefore be a surface channel. The unmodulated component of the channel is $h_{2_t}(\lambda)$. Generally, in MIMI measurements of $h_t(\lambda)$ these two components are

not separated so that $\hat{h}_t(\lambda) \cong \hat{h}_{1_t}(\lambda) + \hat{h}_{2_t}(\lambda)$. The time variation remaining in $h_{1_t}(\lambda)$ and $h_{2_t}(\lambda)$ is due to slowly varying phenomena such as tides, internal waves, heating and cooling, currents, meanders, etc. This model will be expanded in more detail later.

CHAPTER 4

THE CDR GRAM DISPLAY

4.1 Introduction

In the discipline of signal processing, optimum filters receive extensive and intensive investigation with regard to theoretical, computational and implementation aspects. However, the weakest aspect of signal processing system is displays. Displays are also probably the most ignored aspect of signal processing systems. This is unfortunate because in problems of practical interest displays are as important as the receiver. This is because in practice many parameters of the signals and noise are unknown so that decision regions are difficult to determine. Therefore, when the situation allows, displays are often used. Because the human eye and brain provide a very adaptive or versatile pattern recognizer, the display-observer decision making mechanism usually provides better performance and much simpler system implementation than is otherwise practical. Thus, the display and observer often become an integral part of the signal processor, so that an optimum system implies optimum display as well as optimum filtering. A good display should be simple to generate, simple to interpret, and it should provide a maximum of information that is relevant to the objective at hand. In signal processing research, displays provide an additional

vital function, namely information obtained from the display provides qualitative data about the signals. This type of preliminary information provides the basis for the design of feasible decision-making equipment. That is, even when a display is not included in the final system, it can be an invaluable design tool.

Although this thesis is strongly supported by theoretical channel characterization and the well designed and implemented MIMI experiment, the new element of this thesis are the results obtained by the use of a unique display technique for channel propagation studies. Although the application is original, the display technique (or format) is due to a very creative individual, Charles I. Black of Texas Instruments Incorporated.

4.2 Description of Display

4.2.1 Display Format.
The major objective of the display is to very compactly illustrate a complex function of two independent discrete variables, $h(t, \cdot)$, where t is time and the second variable may be λ, time delay, or f, frequency or another independent variable. For the cdr (t, λ) the second independent variable is time delay. Figure 4.1 illustrates the basic format of the display, where the independent variables are the usual displacements in the plane (paper, CRT screen, etc.) and the display intensity, shade, or color at coordinate t, λ is a memoryless mapping of $h(t, \lambda)$. The display device used in this work, a Hathaway 731 recorder, has intensity

$$I(t', \lambda')=g[h(t', \lambda')]$$
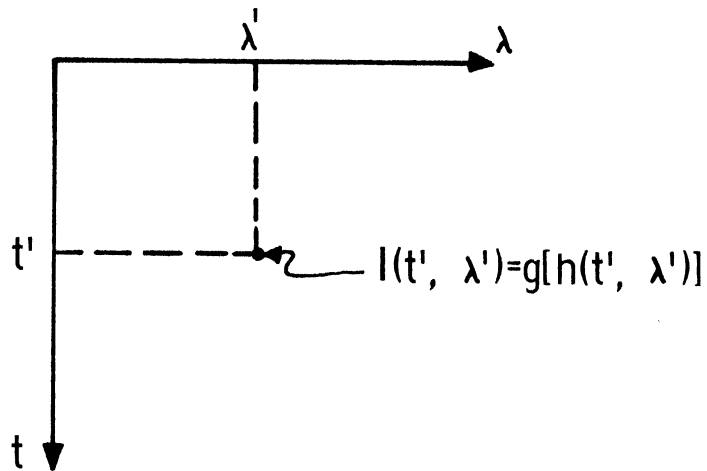
Fig. 4.1. Fundamental Display

modulation on white paper, where writing intensity may vary from white through gray to black. If g is the norm operator (or a variation), then the display format is a very conventional one commonly used in oceanography, seismology, sonar, speech research, etc. In these areas $h(t, \cdot)$ is often a spectrum $h(t, \cdot) = S(t, f)$. Table 4-1 lists some conventional mapping functions, $g(t, \cdot)$.

Table 4-1. Conventional Display Mappings

$$I_1(t, \cdot) = |h(t, \cdot)|$$

$$I_2(t, \cdot) = ||h(t, \cdot)||^2$$

$$I_3(t, \cdot) = \log |h(t, \cdot)|$$

Conventional displays have always mapped the complex function

$h(t, \cdot)$ into the positive reals. This display has been very valuable

in many areas of application; however, it has the disadvantage of

eliminating all the phase information in the generally complex-valued

$h(t, \cdot)$.

The inclusion of phase as well as magnitude into the display

is a new technique providing very valuable, additional information.

The display mapping function used is $I(t, \lambda) = \left(h_x(t, \lambda), \, h_y(t, \lambda) \right) +$

(b, b) where h_x and h_y denote the real and imaginary parts of h

and b is a constant gray scale bias. That is, the display intensity

function is now an ordered pair of real values with $h = (0, 0) \simeq$ gray

display, whereas in the conventional display $I(t, \lambda)$ was a positive

real value with $h = (0, 0) \simeq$ a white display. Finally, the ordered

pair $(I_x = h_x + b, \, I_y = h_y + b)$ are plotted side by side on the λ axis.

Figure 4.2 illustrates the mapping $g(h[t, \lambda])$ used in this thesis

which encodes both amplitude and phase information of the complex-

valued function $h(t, \lambda)$ into the otherwise conventional display.

Let us refer to this display as the OP (Ordered Pair) gram

and the conventional display will be called the PR (Positive Real)

gram. Since the intensity perception of the eye is approximately

logarithmic (that is, relatively insensitive to small changes in light

intensity) the dynamic range (with respect to intensity amplitude) of

the display is rather limited. In the conventional display the many
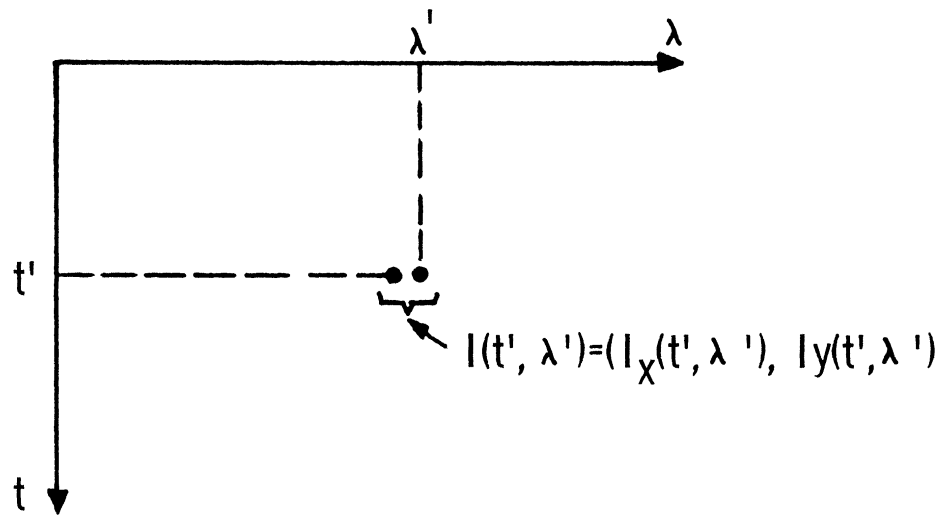
Fig. 4.2. The Ordered Pair Gram Display

variations of $g(t, \cdot)$ around the norm operator (e.g., the logarithm of the norm) are an attempt to map the dynamic range of the information function into the natural dynamic range of the display. Obviously, similar variations of the OP gram could be of interest for the same reasons, e.g.

$$I(t, \lambda) = \left(I_x(t, \lambda), I_y(t, \lambda) \right) = \left(\frac{h_x \cdot \log |h_x|}{|h_x|}, \frac{h_y \log |h_y|}{|h_y|} \right) + (b, b)$$

would preserve the information phase while compressing the range of the information amplitude. Such dynamic range compression techniques are not used in this thesis.

A display technique incorporating amplitude and phase

information as opposed to the conventional amplitude-only display has been described. The value of this added dimension in the display is great and its value in channel propagation studies will become clear in the subsequent material.

4.2.2 Amplitude and Phase Information in the CDR Gram.

The value of the OP gram in displaying cdr (t, λ) is in the tremendous quantity of qualitative and gross quantitative information available in a compact space. Typically, a gram of 6 to 12 hours of cdr (t, λ) is plotted onto an area less than 8-1/2 by 11 inches. Although quantitative amplitude measurements cannot be made from the CDR gram, relative amplitudes can be observed so that high-energy reception is distinguishable from low-energy reception, thus, primary multipath can be identified on the gram. (To relieve the observer of the task of this discrimination, thresholding based upon measured SNR is used, thus, allowing the observer to concentrate on the extraction of information and features from the primary multipath.) Likewise, at best, phase can only be measured to the nearest quadrant. However, trends of constant phase (in t or λ or both) can easily be observed as well as phase rates of change. This phase information tells much about the time invariance, randomness, stationarity, and correlatedness of the channel (reception). In one glance at a typical gram with its myriad of random patterns in t and λ the channel CDR is clearly stochastic. In addition, the majority of

primary multipath will have constant "phase patterns" of at least 5
to 15 minutes duration (i. e., on the t axis) indicating that the sto-
chastic channel process is very narrowband (remember the channel
being studied is over 50 Hz wide so that the channel random pro-
cess could change much faster than it does). If cdr (t, λ) = r(t, λ)
cdr'(λ) where cdr'(λ) is time invariant and r(t, λ) is a class of
very narrowband random processes the channel could be modeled as
quasi-time-invariant. In other words, the 100 second comb filter
used to obtain a high SNR representative CDR could easily be ex-
tended to 5 to 15 minutes without degrading the instantaneous CDR
measurement.

Although the amplitude and phase of cdr (t, τ) are grossly
quantified in the gram display, the basic nature of the reception is
retained. And, although the gram greatly compresses a large
quantity of information into a small region, much of the adaptive
recognition potential of a human observer is retained. This is very
important because, due to the unknown and complex nature of the
channel, rote application of electronic averaging, whether coherent
or incoherent, while greatly compressing the quantity of information,
will also mask much of the information unless the averaging process
is "matched" to the information process. (Even if matched elec-
tronic averaging was used to remove excessive redundancy the quan-
tity of data remaining would still be enormous and again a gram
display may be the best available means of displaying the averaged

information.)

4.2.3 Thresholding for Clutter Suppression. Often very low-energy multipath reception is readily detectable in the CDR gram by distinctive phase patterns. Although there is enough dynamic range in the gram to distinguish high-energy (primary) multipath reception from low-energy (secondary) reception, to do so requires considerable concentration. Thresholding of cdr (t, λ) based upon measured broadband signal and noise power, cleans up the gram, thus, relieving the observer of the distracting task of discriminating significant reception from insignificant reception. The result is that the general characteristics of the significant reception can be observed in a glance. In some cases, such as file 7, it greatly enhances the presence of a high strength reception that was not nearly so distinct in the unprocessed gram due to very strong phase patterns of the low-energy reception.

The thresholding introduces a quantitative energy measure into the gram which allows ready measurement and observation of the channel time-delay spread factor, L. If L was judged from the unprocessed gram it would be two to three times its values as estimated from the distinctive phase patterns and the large extent of very low level but coherent reception.

The threshold operation is based upon the broadband signal and noise measurements as expressed by

if $20 \log_{10} |\text{cdr}(t, \lambda)| \geq \max\{S(t) - 6\text{dB}, N(t) + 6\text{dB}\}$,

then $\quad \text{cdr}(t, \lambda) = \text{cdr}(t, \lambda)$

otherwise $\quad \text{cdr}(t, \lambda) = (0, 0)$.

That is, the instantaneous power of $\text{cdr}(t, \lambda)$ must exceed $S(t) - 6\text{dB}$ and $N(t) + 6\text{dB}$ to be considered primary reception.

Although the threshold processing is not always necessary, in much of the data it considerably enhanced the significant multipath reception and made possible valid interpretation of the $\text{cdr}(t, \lambda)$ gram.

4.3 Experimental Results

This section, consisting of the presentation and subsequent discussion of approximately 133 hours of $\text{cdr}(t, \lambda)$ data, is divided into four parts:

1. The CDR and threshold processed CDR gram displays, and discussions of

2. Parameter extraction from the CDR gram

3. Time invariance, correlatedness, and stationarity of $h_t(\lambda)$

4. Identification of two physical propagation modes.

4.3.1 CDR Data Presentation.
There are 19 data files each containing approximately 12 hours of CDR data. Table 3.1 and Figure 3.1 summarize the chronology of the data. Each data file is presented in a CDR gram and in a threshold processed CDR gram. The unprocessed grams are presented first, followed by the threshold

processed grams.

The CDR grams begin and end with a series of alternating black and while bars along the time spread axis, λ. There are 63 bars, 32 black and 31 white, each representing the 20 millisecond duration of the transmitted digit. Due to display device blooming, the black bars over extend into the white regions. Nevertheless, the time spread of the channel can readily be measured in units of 20 msec. Every 120 minutes a scan of this alternating black and white bar pattern is imposed. Along the time, t, axis in the margin the times, t_i, and time gaps, g_k, are annotated corresponding to the chronology summarized in Table 3.1, to provide a time element. Note that although the data is displayed in chronological order, events, g_k, denote the occurrence of time intervals where data was not obtained due to experiment down times.

Although the threshold processed CDR gram is the point of reference in subsequent discussion, both grams are presented in order to:

1. Provide a complete and unretouched representation of the channel.

2. Allow the reader to evaluate the threshold processing effects.

4.3.2 Parameter Extraction. Using a threshold processed CDR gram, several valuable parameters of the channel can be

11(17:16)

12(05:18)

12(09:27)
13(16:53)

14(01:36)

CDR GRAMS 1 & 2

Fig. 4.3

14(01:36)

14(09:29)
14(10:55)

14(15:29)

14(16:18)

15(03:06)
15(05:38)

15(07:17)

0

CDR GRAMS 3 & 4

Fig. 4.4

15(07:17)

15(10:13)
15(19:13)

16(04:45)

16(10:55)
16(12:52)

16(19:05)

0   1.2

CDR GRAMS 5 & 6

Fig. 4.5

16(19:05)

17(07:32)

17(12:06)
17(12:33)

17(18:46)

0   1.2

CDR GRAMS 7 & 8

Fig. 4.6

23(10:20)

23(22:47)

24(10:49)

0   1.2

CDR GRAMS 9 & 10

Fig. 4.7

24(18:42)

25(07:09)

25(11:18)
25(11:18)

25(19:11)

0   1.2

CDR GRAMS 11 & 12

Fig. 4. 8

25(19:11)

26(07:38)

26(19:40)

0   1.2

CDR GRAMS 13 & 14

Fig. 4.9

26(19:40)

27(08:07)

27(20:09)

0   1.2

CDR GRAMS 15 & 16

Fig. 4.10

27(20:09)

28(08:36)

28(20:38)

0   1.2

CDR GRAMS 17 & 18

Fig. 4.11

28(20:38)

29(09:05)

0   1.2

CDR GRAM 19

Fig. 4.12

11(17:16)

12(05:18)

12(09:27)

13(16:53)

14(01:36)

0   1.2

CDR GRAMS 1 & 2
CLUTTER SUPPRESSED

Fig. 4. 13

14(01:36)

14(09:29)
14(10:55)

14(15:29)

14(16:18)

15(03:06)
15(05:38)
15(07:17)

0   1.2
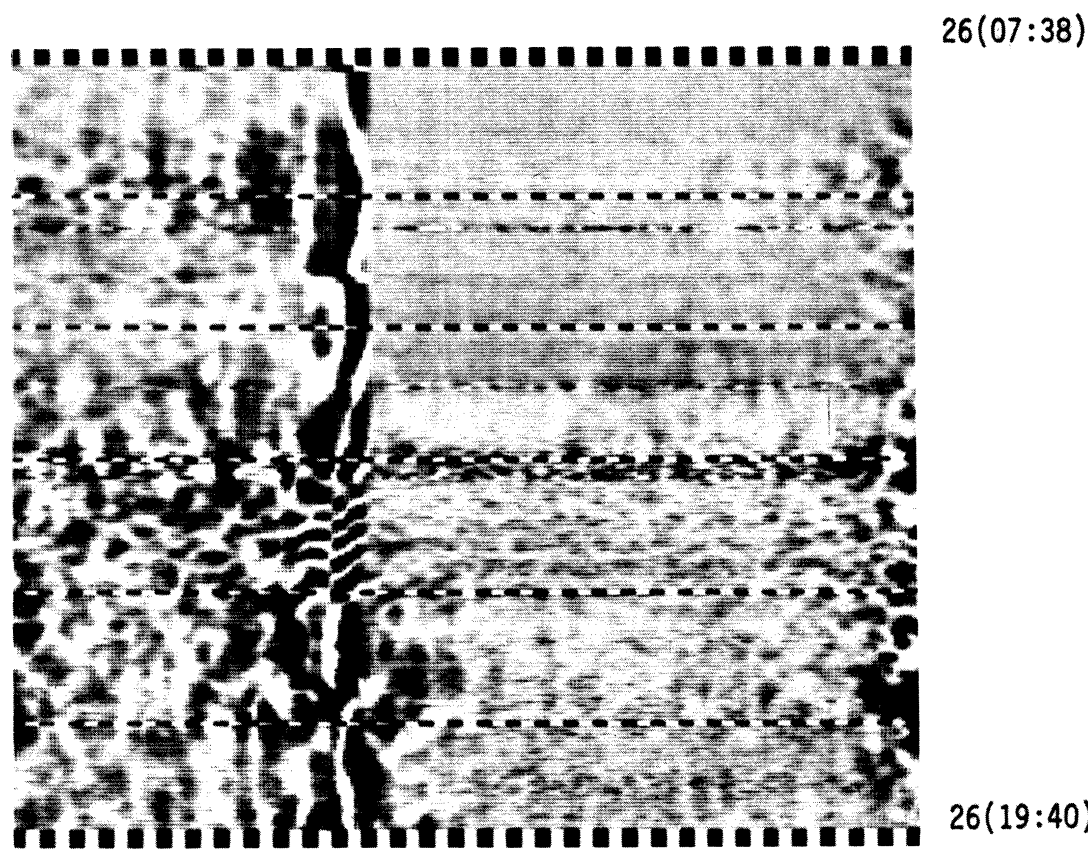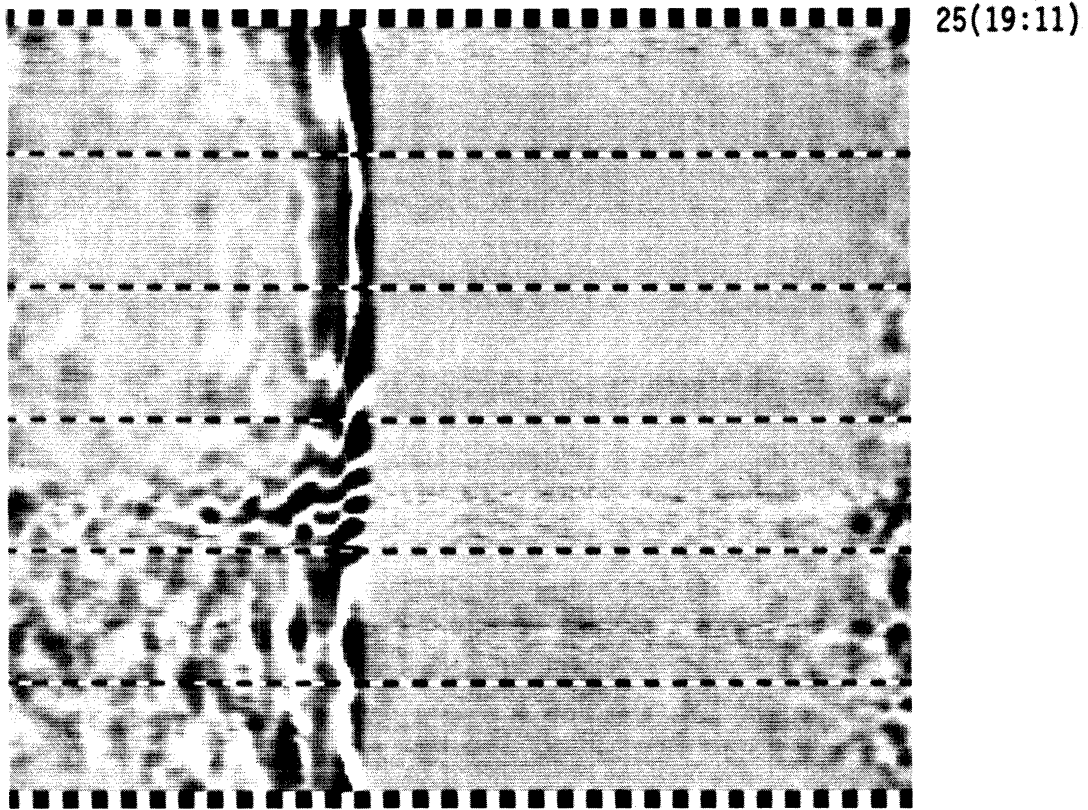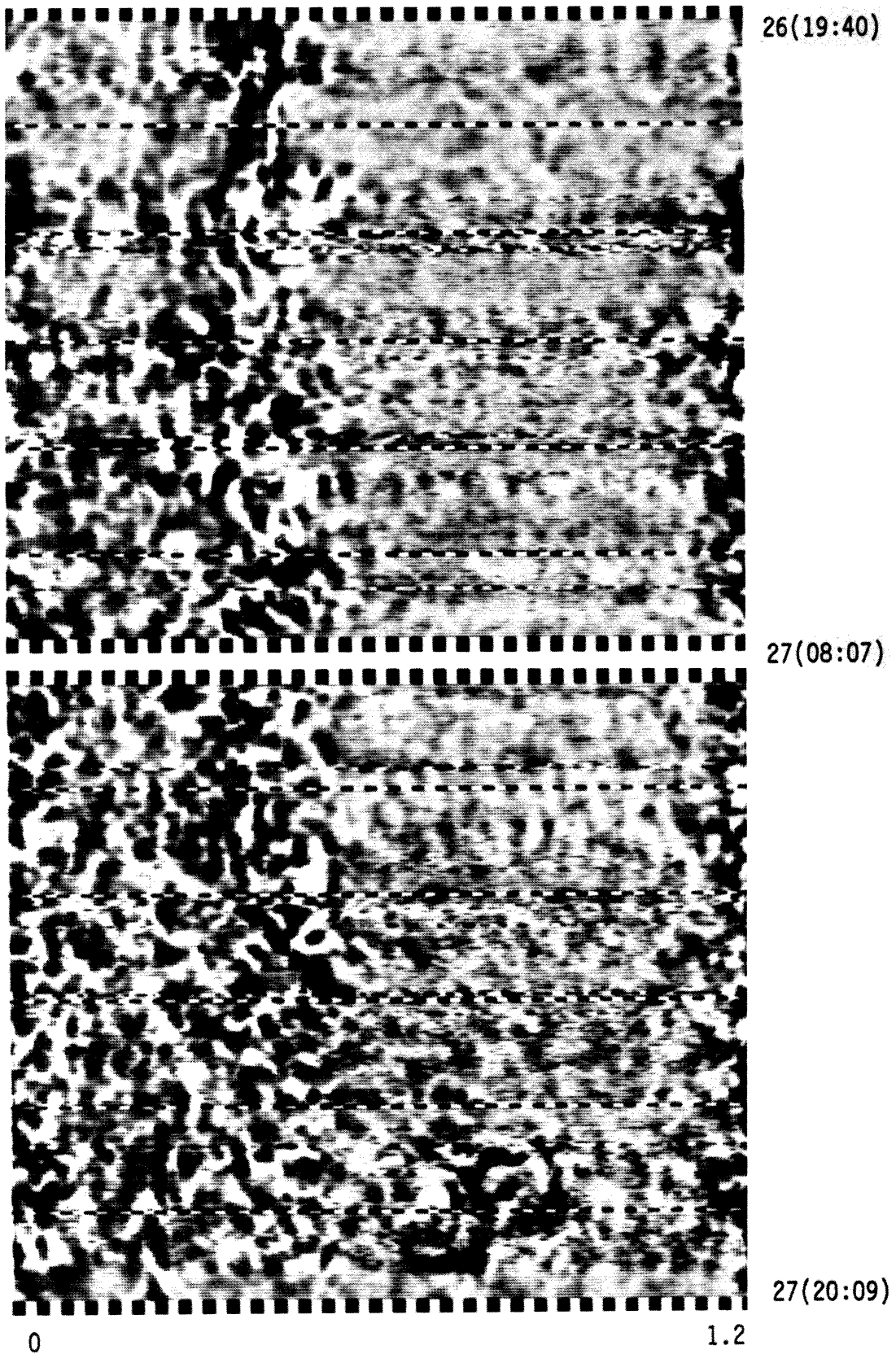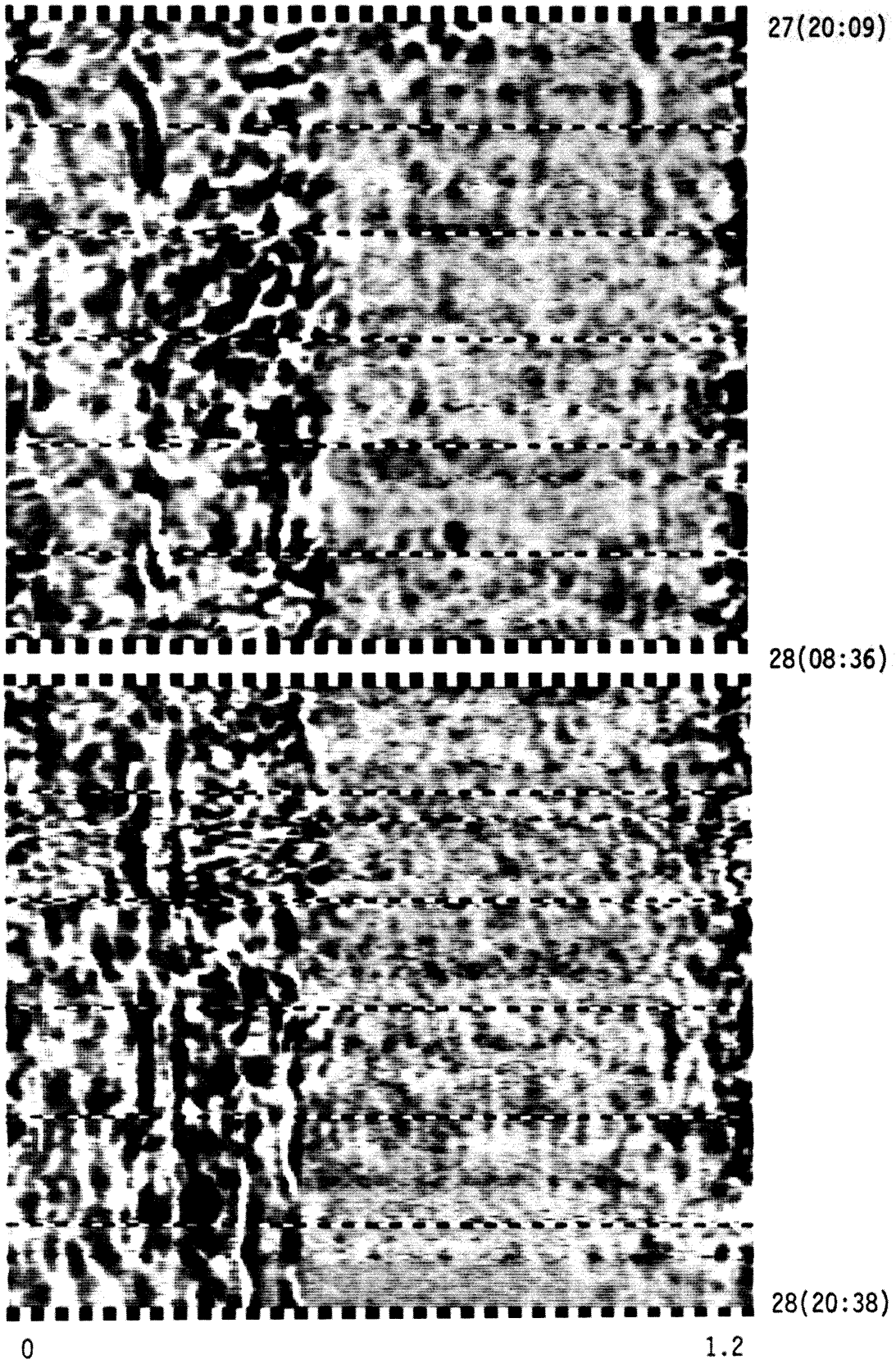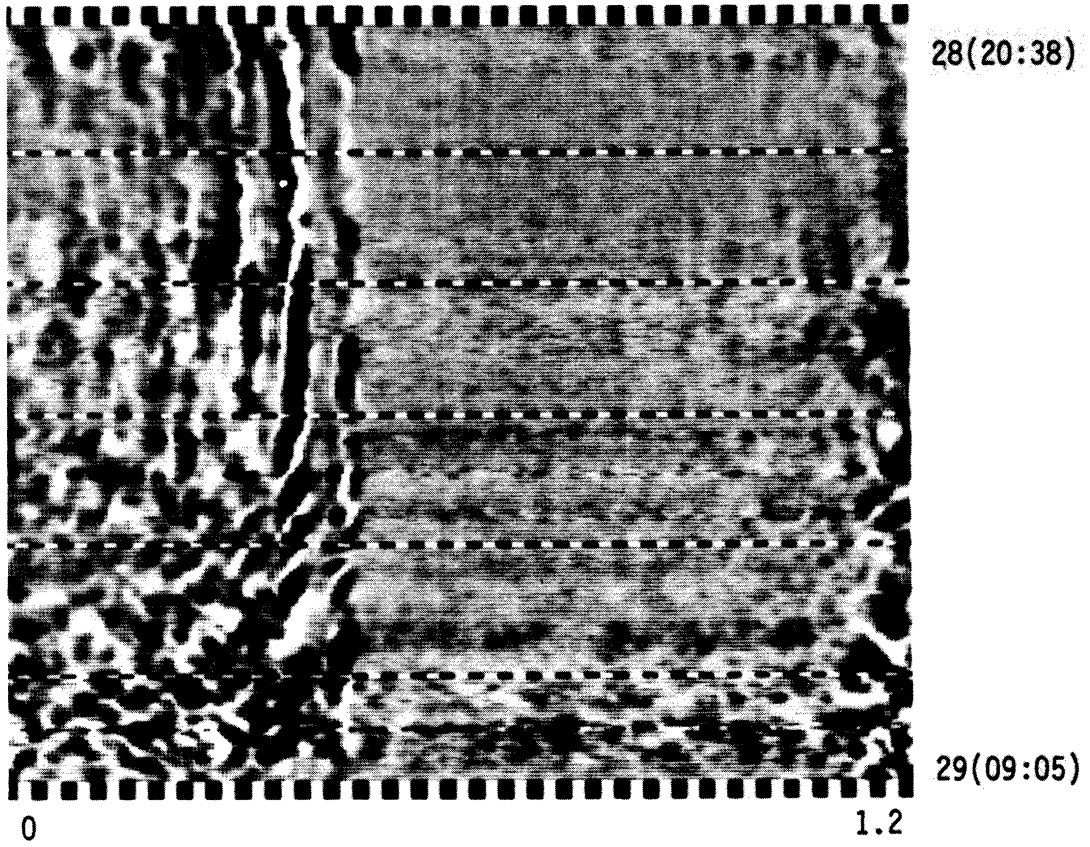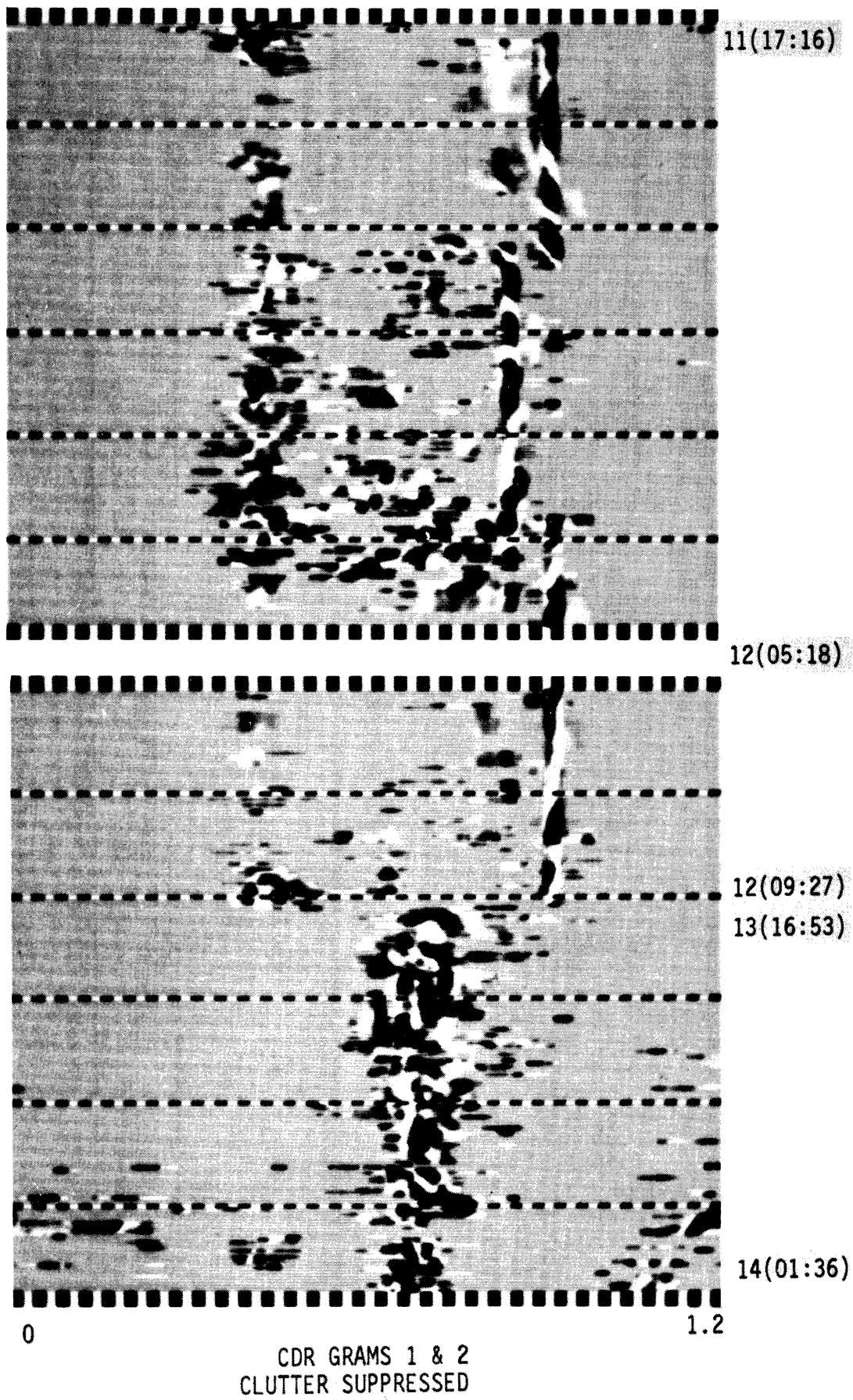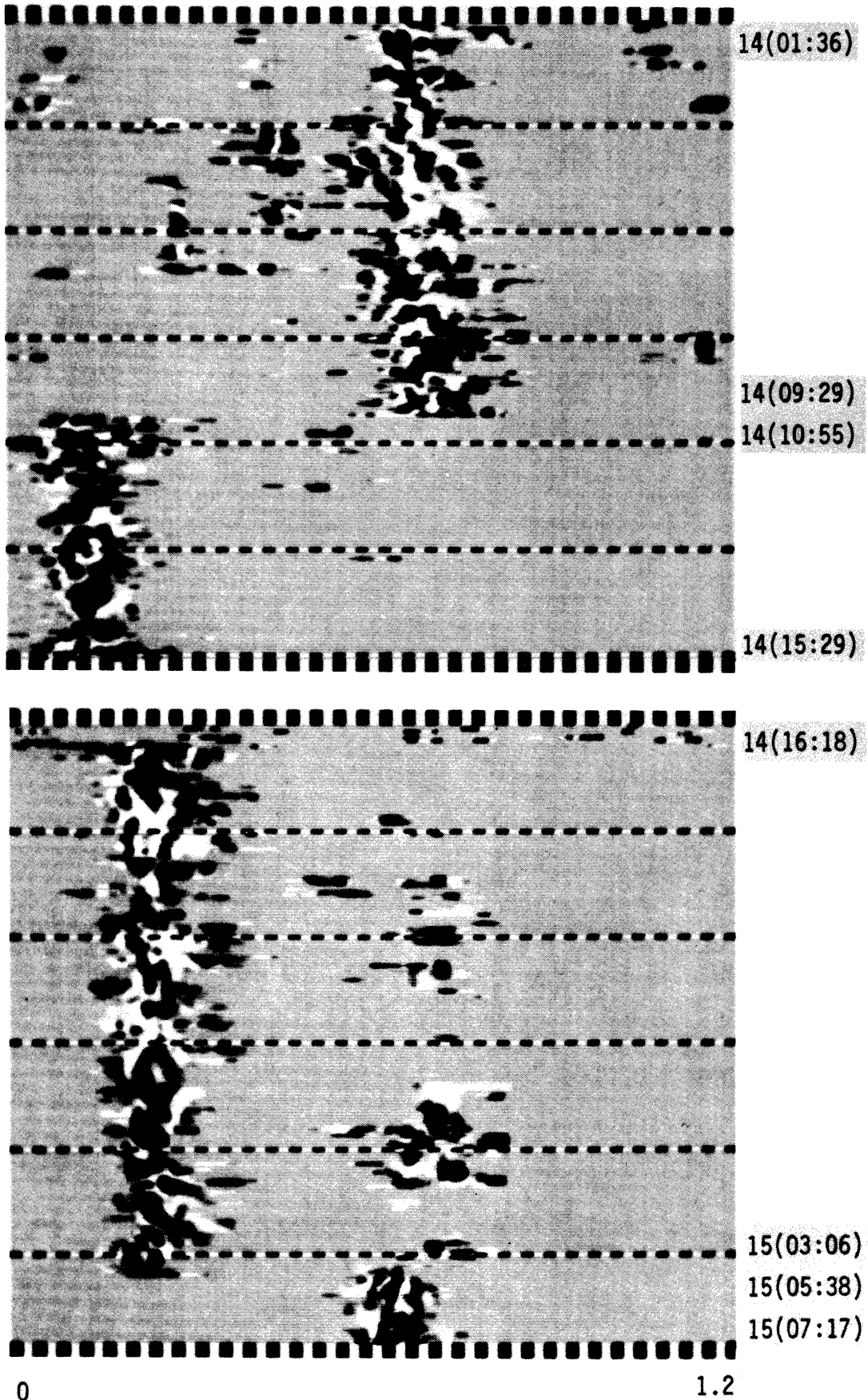
CDR GRAMS 3 & 4
CLUTTER SUPPRESSED

Fig. 4.14

15(07:17)

15(10:13)

15(19:13)

16(04:45)

16(10:55)

16(12:52)

16(19:05)

0   1.2
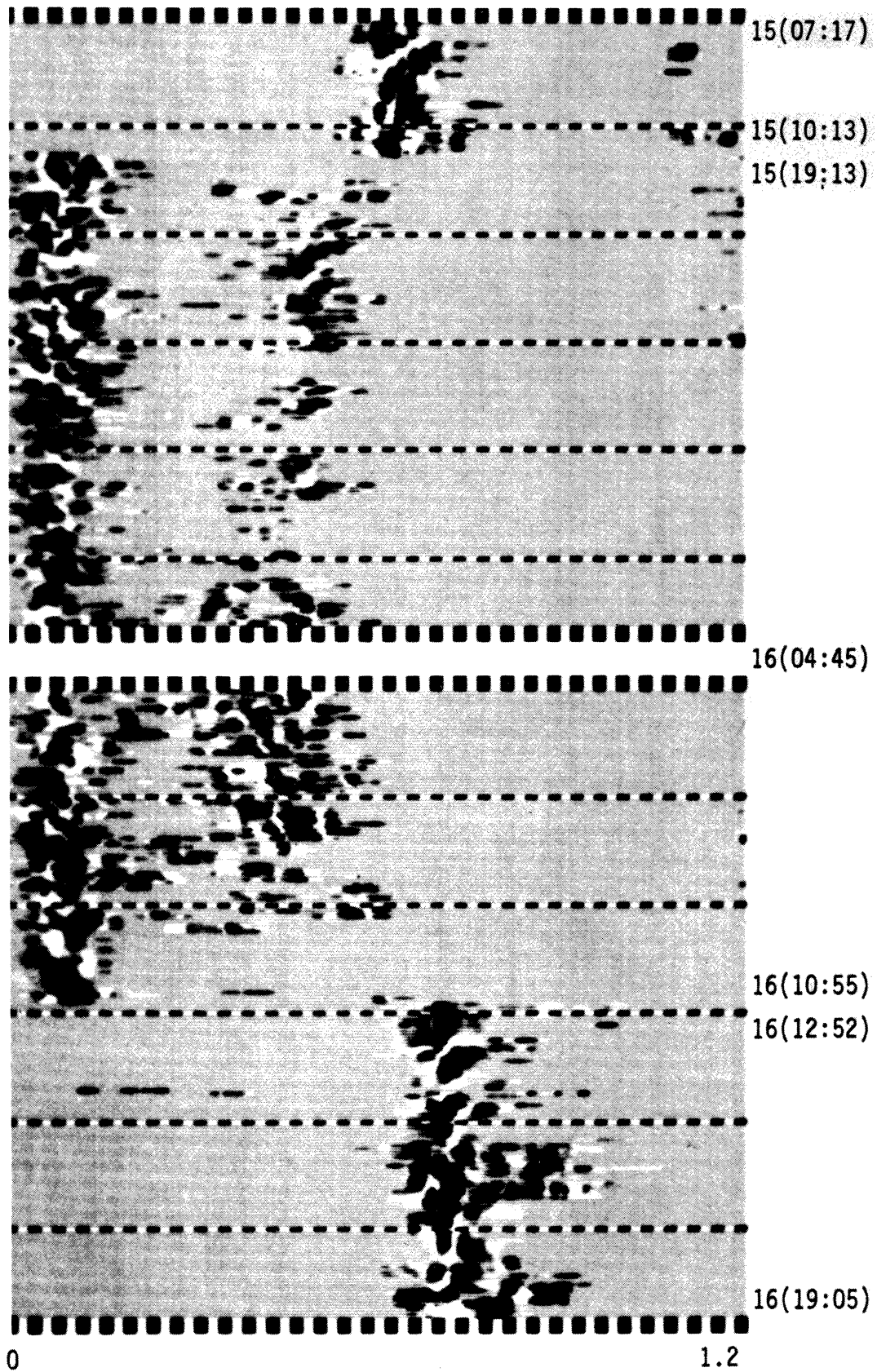
CDR GRAMS 5 & 6
CLUTTER SUPPRESSED

Fig. 4.15

CDR GRAMS 7 & 8
CLUTTER SUPPRESSED

Fig. 4.16

23(10:20)

23(22:47)

24(10:49)

0   1.2

CDR GRAMS 9 & 10
CLUTTER SUPPRESSED

Fig. 4. 17

24(18:42)

25(07:09)

25(11:18)
25(11:18)

25(19:11)

0   1.2

CDR GRAMS 11 & 12
CLUTTER SUPPRESSED

Fig. 4.18

25(19:11)

26(07:38)

26(19:40)

0   1.2

CDR GRAMS 13 & 14
CLUTTER SUPPRESSED

Fig. 4.19

26(19:40)

27(08:07)

27(20:09)

0   1.2
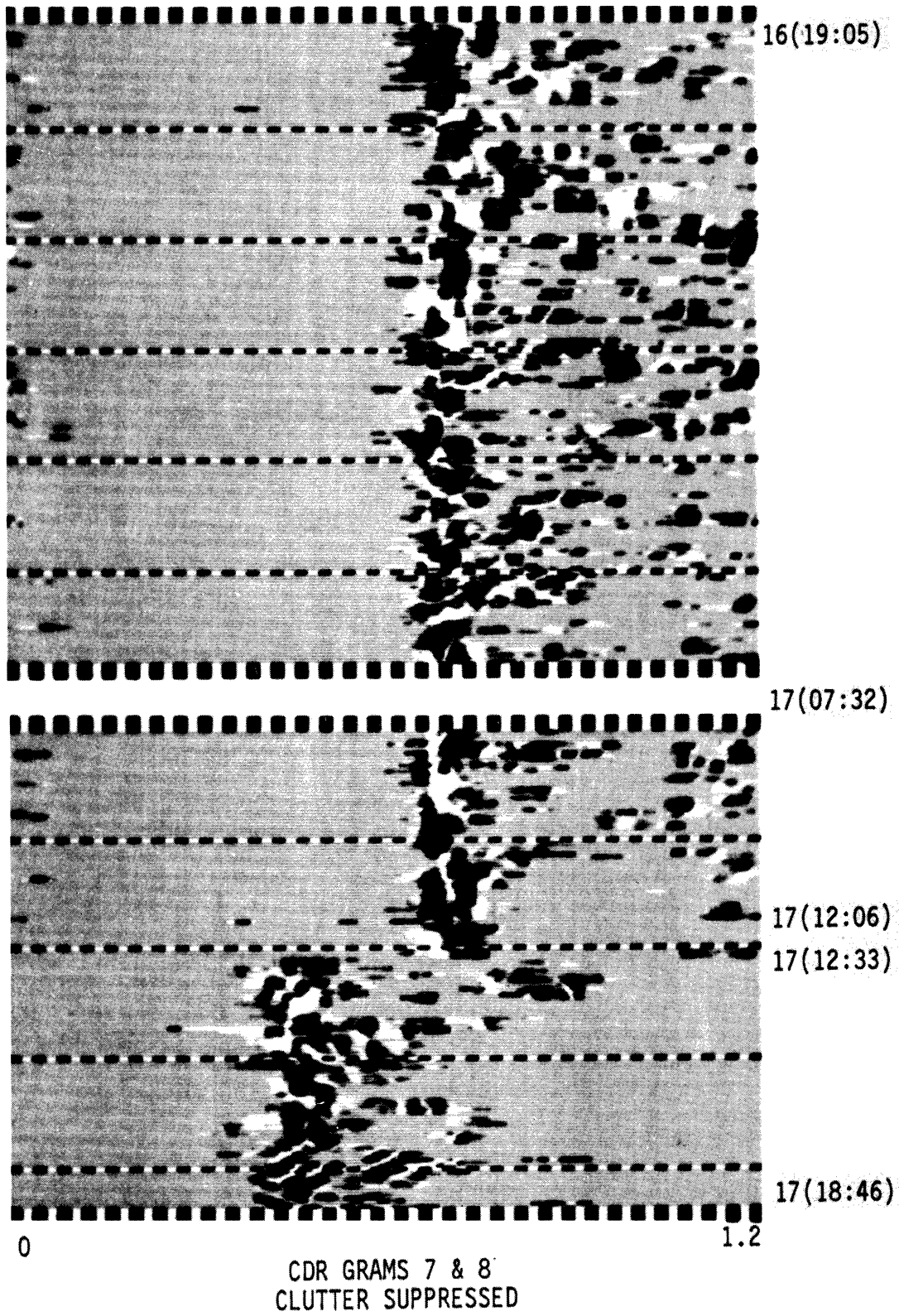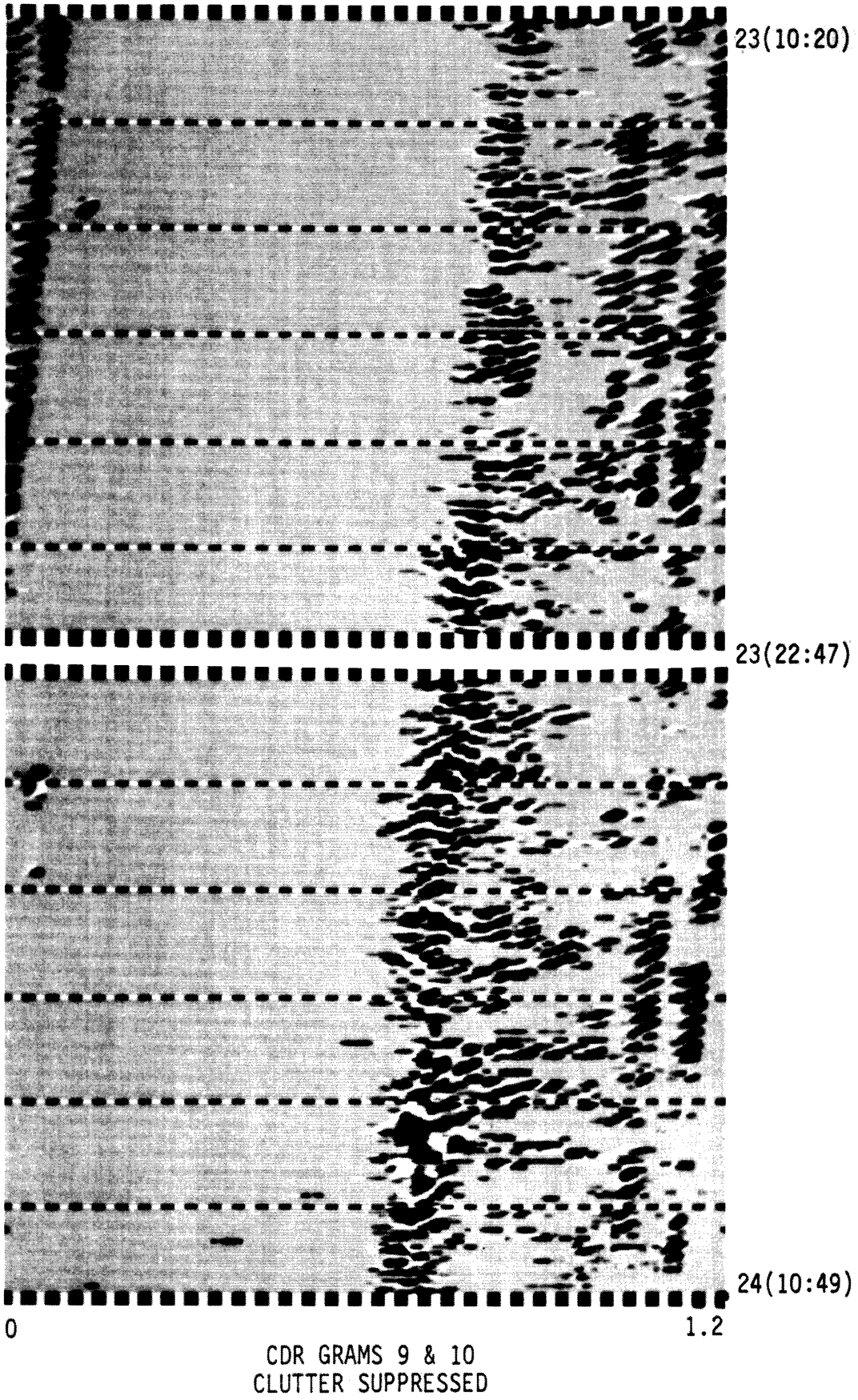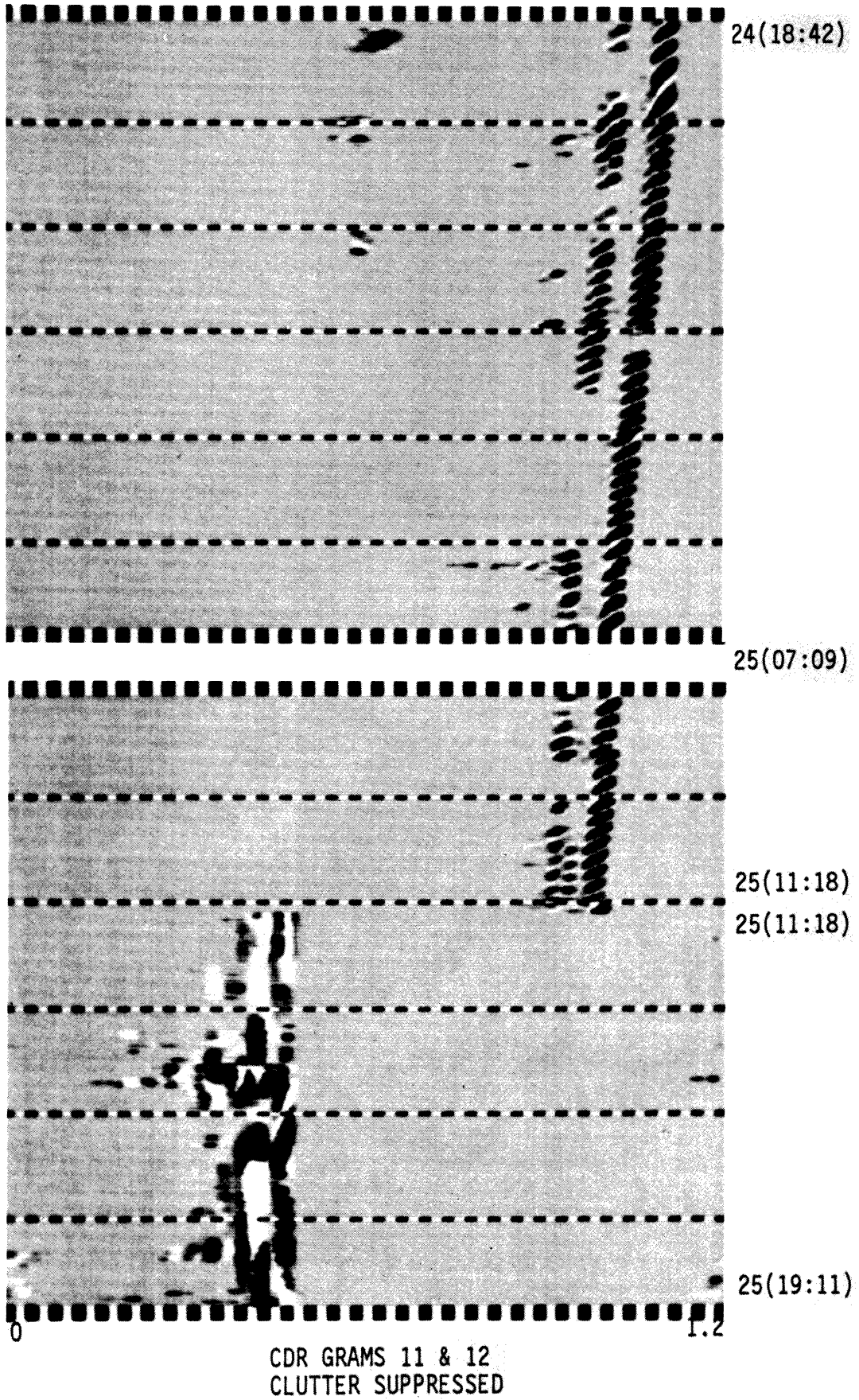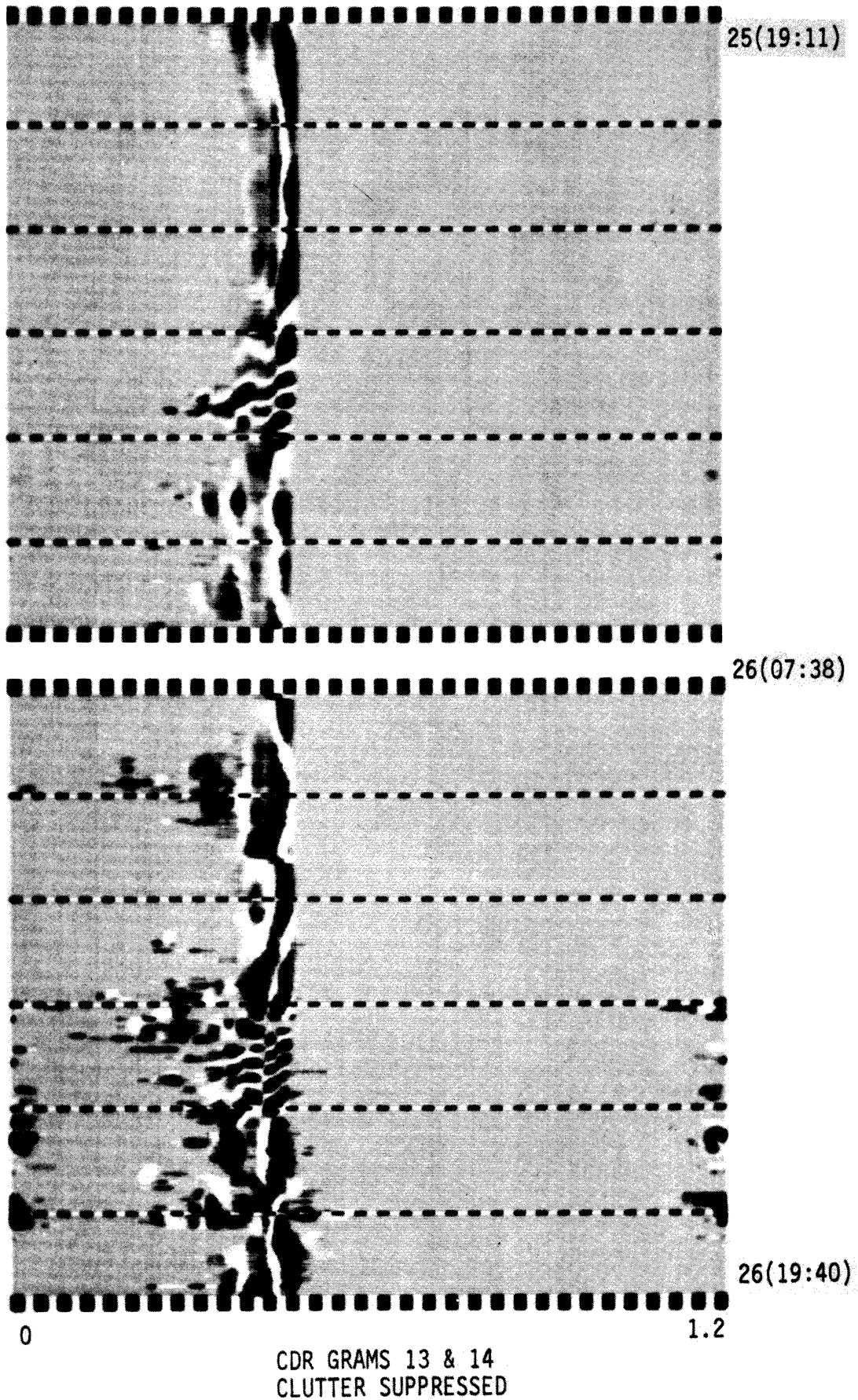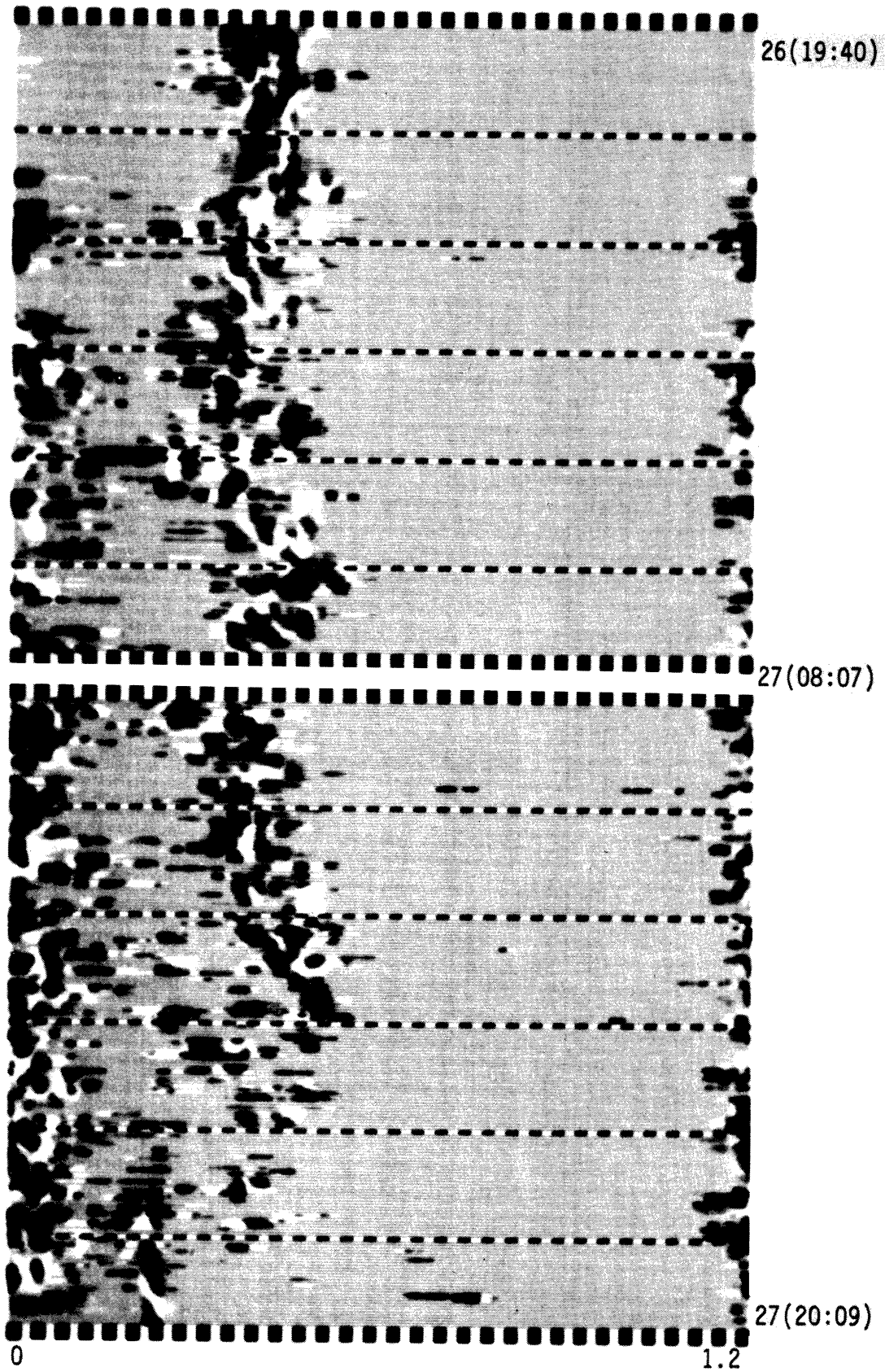
CDR GRAMS 15 & 16
CLUTTER SUPPRESSED

Fig. 4.20

27(20:09)

28(08:36)

28(20:38)

0   1.2
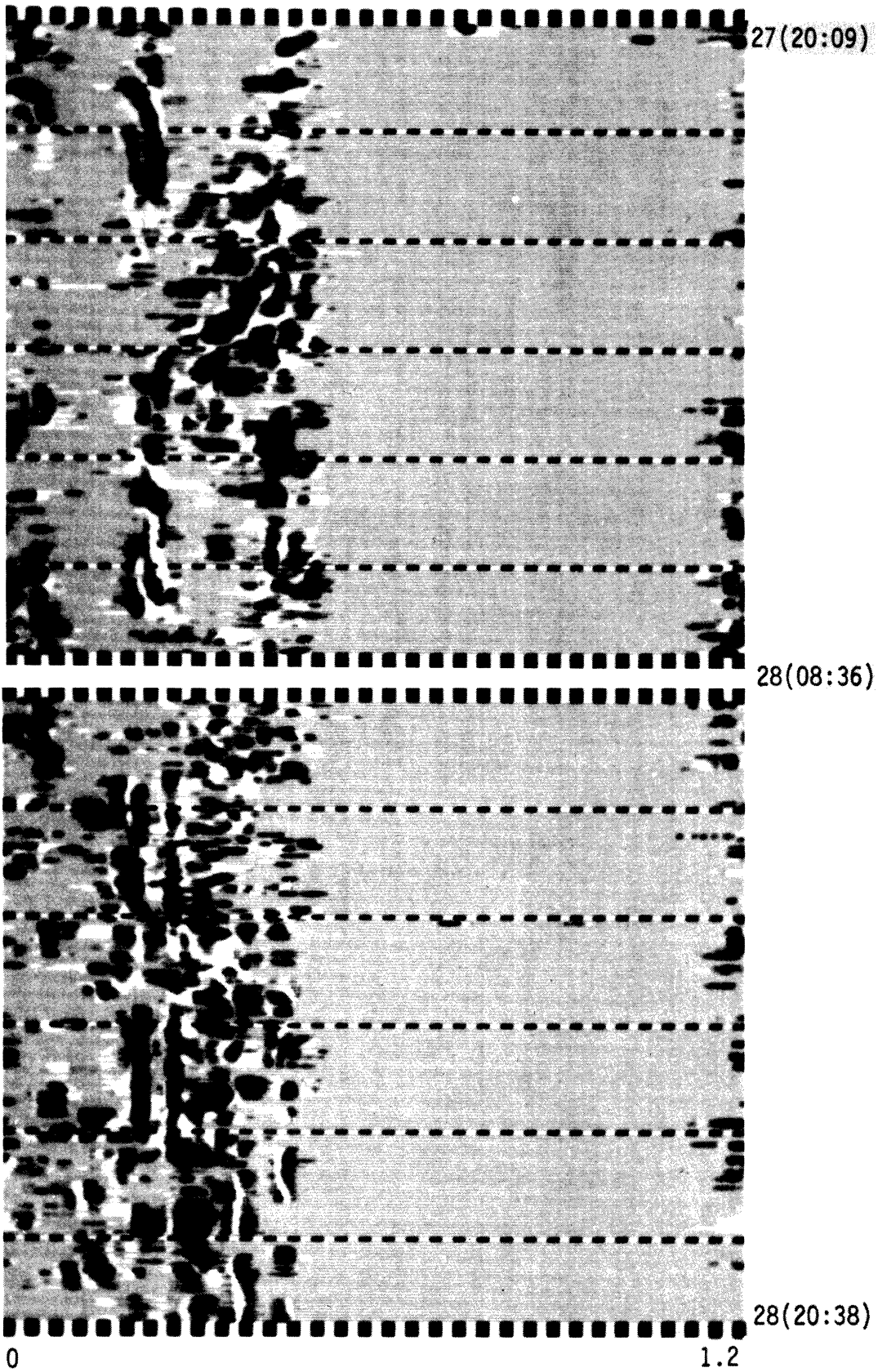
CDR GRAMS 17 & 18
CLUTTER SUPPRESSED

Fig. 4.21
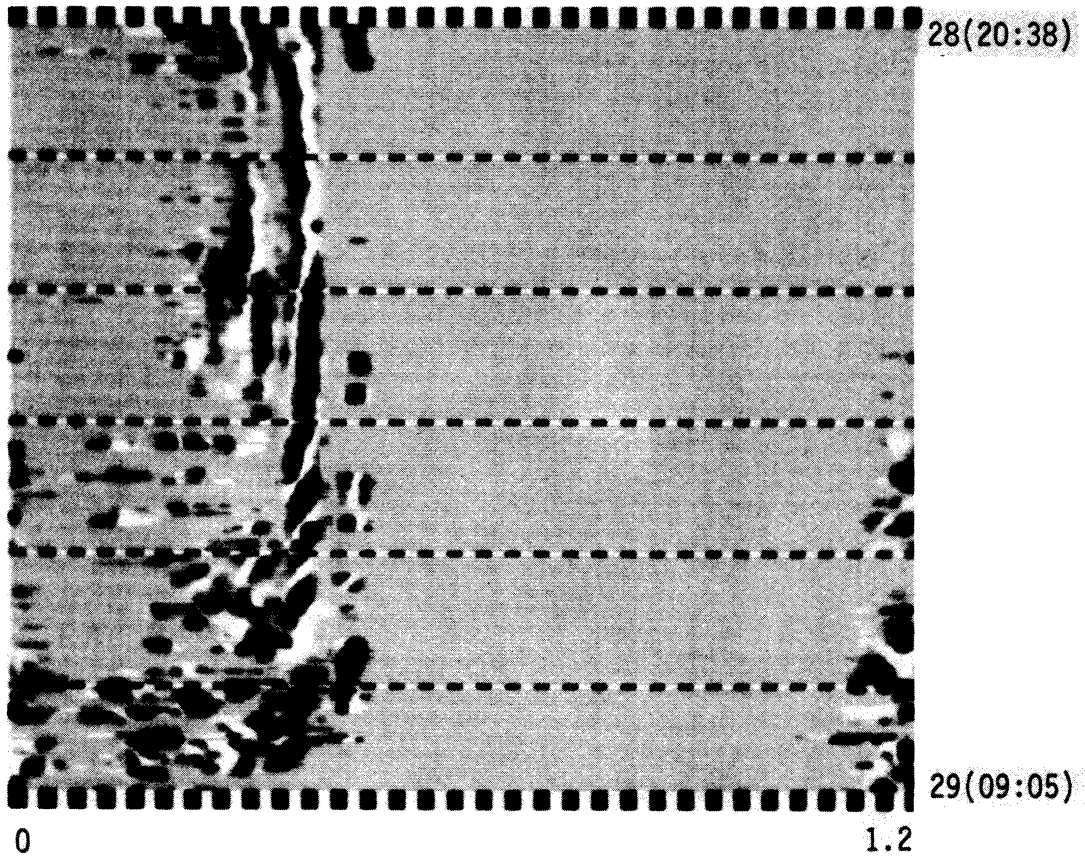
CRD GRAM 19
CLUTTER SUPPRESSED

Fig. 4.22

measured, some rather quantitatively, others qualitatively. Some illustrative examples follow.

<u>L</u>

A very important channel parameter is the time-delay spread coefficient (or multipath extent), L. In the data here, L is clearly less than T_p, the signal period. This condition, $T_p > L$, is required to avoid distorted measurements of the channel.[*] From the threshold processed grams, the channel has an L value of approximately 600 msec. If unprocessed grams are used, then L measurements are significantly affected by the preponderance of very low energy, but coherent, reception that is very detectable in the CDR gram. This unprocessed gram would imply L estimates more like 1200 msec. Since this insignificant (with respect to energy content) reception can influence L measurements so greatly, CDR grams must be threshold processed to obtain reliable L estimates.

Arrival Time Tracking, Path, or Mode Fading, and Multipath Resolution

Before this work, no information about the long-term time behavior of path propagation times has been ever measured. The behavior of path (or path group) arrival times is readily observable in the CDR gram (particularly if threshold processed). When paths are time resolvable on the gram, the individual arrival time of each

---

[*]Section 2.3.5. BL Effects on $\hat{h}$ (t, λ) Measurements.

path is easily observed. As illustrated in the CDR grams such paths have essentially constant arrival times for several hours. Typically, the arrival (or travel) time may change 10 milliseconds in 6 hours. The reception in files 9, 10, 11, and 12 appear to be moving more rapidly (and steadily). The time base in these files contains equipment induced accumulative error.* It can be seen that two-path arrivals butted side to side as in file 12 can be resolved and identified as two distinct paths in the CDR grams due to the phase discontinuity at the interface of the two arrivals. In previous CDR displays the resolution of such paths is observable on the basis of phase discontinuity and often an amplitude notch at the interface. However, previous presentations spanned very short periods of time, 5 to 15 minutes. It is important that the ability to resolve mildly interferring paths has not been lost in the CDR gram.

In high-interference reception, paths can be individually identified for only very short intervals (minutes), tracking of individual path arrivals is very difficult and probably pointless. The approach here is to be only concerned with the average arrival time of the very complex-looking gob of reception. This type of reception will be called clustered mode reception. Only the trend of this clustered mode travel time is of interest, since small random perturbations in a short-time average-travel-time measurement are simply

---

*See Section 3.2.

reflections of the highly interactive behavior of individual paths in the cluster. Generally the average arrival times of the cluster modes in the data here are constant for very long periods (hours). This observation is consistent with the previously observed behavior of individual paths. However, it cannot be concluded, only surmised, that the individual paths within the cluster have constant travel times. As a group of paths, they have a constant travel time, but as individual paths, they may be moving around within the cluster.

Thus, for the first time, based upon the CDR gram, statements can be made about the long term behavior of propagation path (or mode) travel times. It could be interesting to pursue this question in more detail. For example, individual path travel times could be correlated with each other and with large driving forces such as the tide, etc.

The CDR grams of data files 16, 17, 18, and 19 illustrate the ability of the observer to identify the superimposed reception of several distinct simple paths on a background of a cluster mode arrival. In addition, the individual path arrivals can actually be tracked (visually) in time through the cluster mode arrival. This type of reception, simple paths superimposed on cluster mode, has not been previously recognized or identified, and to do so with previous techniques would be virtually impossible.

Thresholding introduces enough quantitative amplitude measure into the CDR grams to provide observation of path and, even,

cluster mode fading in the CDR gram. This phenomenon has been surmised in the past from DUAL measurements but never observed before. Narrowband frequency selective fading of the CW signal has been observed for a long time. This is a phenomenon associated with multipath interference. However, path fading is a broadband phenomenon rather than narrowband and cannot be generally associated with multipath interference. Although extensive quantitative measurements have not been made of the total broadband power in a single path, broadband energy fading does not appear to be nearly as extreme as in the CW case so that in the broadband case energy fluctuation is a better term than fading. Although the CDR gram represents the UWAP channel more comprehensively than DUAL measurements, DUAL does provide quantitative data and the CDR gram is used now to note correlation between DUAL process behavior and channel structure observable in the CDR gram. In gram 13 the reception consists only of two distinct time resolved paths. The C(t) and S(t) curves in the associated DUAL plots indicate significant broadband power variation. The high correlation of C(t) and S(t) here is rather unusual and is a reflection of the lack of multipath interference, i. e., cluster mode reception is not present. Furthermore, the distinct absence of CW fading during this time is also a reflection of the absence of multipath interference. In other words, high correlation of C(t) and S(t) together with wide S(t) fluctuation and the absence of

CW fading are strong indications that the reception is of the simple type.

The art of extending DUAL measurements to hypothetical channel structure is subtle and is subject to complications. This is only an introduction to the concept which is implicitly developed throughout much of the remainder of this thesis.

The number of paths in simple reception is generally small, typically one to three paths. While cluster mode reception consists of many paths in a bundle or group, which may be spread over as much as 600 milliseconds of time delay, resulting in highly interactive and random multipath interference. This is reflected in DUAL measurements by CW fading and constant $S(t)$ measurements.

Usually, reception consists of combined simple reception plus cluster mode reception, for example, grams 1, 2, 3, 9, 10, 14, 16, 17, 18, and 19. Let us call this complex type reception. Grams 4, 5, 6, 16, 17, and 18 also illustrate two simultaneous cluster modes. Simple type reception is reflected in the distinctive behavior of the DUAL measurements $C(t)$ and $S(t)$. However, in complex reception, the cluster mode component dominates the $S(t)$ and $C(t)$ measurements so that the presence of the simple component is not detectable in the DUAL measurements. CDR gram 1 is a particularly interesting example of complex reception where the two paths in the simple component are strongly fluctuating. The two paths are fading and building completely out of phase with each other. This

dramatic behavior so clearly represented in the CDR gram is not reflected in the DUAL measurements due to: (1) cluster mode masking and (2) the out of phase fluctuations average each other out. Averaging and masking effects on DUAL parameters could be avoided by making measurements on individual paths or modes. Possibilities of such measurements are discussed in Section 6.3.

The application of CDR grams for arrival time tracking, multipath resolution and path or mode fading has brought exciting new observations and aspects to UWAP channel studies.

4.3.3 Time Invariance, Correlatedness, and Stationarity of $\hat{h}(t, \lambda)$.

The general UWAP channel has been modeled as a linear, stochastic, doubly spread system with a channel digit response $h(t, \lambda)$ where λ is the time delay parameter. MIMI measurements filter out the frequency spread component of $h(t, \lambda) = a(t) h_1(t, \lambda) + h_2(t, \lambda)$. Thus, the MIMI measurements provide a singly (delay) spread system for study. This system is denoted by $\hat{h}(t, \lambda) = h_1(t, \lambda) + h_2(t, \lambda)$.

In abstract channel modeling or characterization, additional assumptions of uncorrelatedness and wide-sense stationarity of the channel are highly desirable for mathematical convenience. Verification of such assumptions is no mean task. An in-depth study of these questions for the UWAP channel is not the objective of this work, but some preliminary efforts have been made. The purpose here will be only to show that these assumptions are reasonable.

Time Invariance

At normal transmission levels $\hat{h}(t, \lambda)$ measurements using

one minute integration provide reliable (high SNR) estimates. Con-

tinuous measurements show that $\hat{h}(t, \lambda) \cong \hat{h}_{t_1}(\lambda)$, $t_1 < t < t_2$ with

$t_2 - t_1$ approximately 5 to 15 minutes, i. e., for time intervals of

5 to 15 minutes the UWAP is a time invariant channel. This has been

reported in MIMI references spanning several experiments [2], [15],

[16], [17]. Using previous display techniques to determine time

invariance durations was feasible but somewhat awkward. Therefore,

the measurement technique CANDOR presented in 2. 3. 4 was imple-

mented. However, the CDR gram provides a less quantitative but

comprehensive means to judge not only durations of total channel time

invariance, but durations of time invariance of individual components

(paths and modes) of the CDR. That is, simple reception time in-

variance durations are significantly greater than for cluster modes

or the components of the cluster mode microstructure. This behav-

ior is apparent in CANDOR measurements only during simple mode

reception. During complex reception such behavior is quite observ-

able in the CDR gram, although not so in CANDOR measurements.

In all measurements and discussions of time invariance, the

structure of interest is in the CDR phase while pure gain variation

is normalized out. Besides general curiosity, the great interest in

channel time invariance is motivated by the tremendous practical

need to minimize data quantities for meaningful channel representation.

For example, by using S(t) and a single normalized cdr (t, λ) from each time invariant interval, the quantity of data required to represent $\hat{h}(t, \lambda)$ is reduced by an order of magnitude. This translates into an order of magnitude savings on data storage requirements and post-processing times. Thus, studies that would be a practical impossibility become feasible.

Correlatedness

The cdr (t, λ) = $\hat{h}(t, \lambda)$ is a family of random processes with indices t and λ. In this section properties of the channel with respect to the λ parameter are of major interest. The time parameter will be demoted to the role of subscript in the notation to emphasize λ, $\hat{h}(t, \lambda) \triangleq \hat{h}_t(\lambda)$.

Since ensemble averages are not available, ergodicity and stationarity assumptions on $\hat{h}_t(\lambda)$ allow the correlation properties of $\hat{h}_t(\lambda)$ to be studied using time averages. Since $\hat{h}_t(\lambda)$ are zero mean, * the normalized auto-covariance of the CDR is estimated by

$$\text{Covh}_t(\mu) = \frac{\sum_{\Lambda} \hat{h}_t(\lambda) \, \hat{h}_t^*(\mu-\lambda) \, \Delta\lambda}{\| \hat{h}_t(\lambda) \|}$$

The auto-covariance analysis fulfills two purposes: to study the λ-correlatedness of the channel and to investigate an alternative

---

*The mean of $\hat{h}_t(\lambda)$ is estimated $M_h = \sum_{\lambda} \hat{h}_t(\lambda)$ and subtracted to assure zero mean $\hat{h}_t(\lambda)$.

statistical representation of the channel. Here only λ-correlatedness is the topic. The complete $Covh_t(\mu)$ analysis of the CDR data is presented in gram format with a discussion of $Covh_t(\mu)$ as a represen- tation of the channel in Chapter 5.

The gram display of $Covh_t(\mu)$ is inadequate for highly quanti- tative measurements. However, two preliminary observations are immediately obvious:

- $Covh_t(\mu)$ is nominally "constant" for several hours at a time

- $h_t(\lambda)$ is approximately uncorrelated most of the time

$Covh_t(\mu)$ is nominally "constant" means the width of the significant portion of $Covh_t(\mu)$ is "constant" and no significant changes in $Covh_t$ (μ) are apparent for large durations of t. This condition implies that time averaging of $Covh_t(\mu)$ is a reasonable method of obtaining better statistical estimates of $Covh_t(\mu)$.

Under normal conditions, cluster mode reception, $Covh_t(\mu)$ quickly falls well down from $Covh_t(o)$ withing two digit durations, i.e., $Covh_t(4) \simeq 0.1\ Covh_t(o)$. To be considered completely uncor- related $Covh_t(\mu)$ should fall within one digit duration. However, considering $L \simeq 300$ to 600 msec, or 15 to 30 digits, $\hat{h}_t(\lambda)$ is approximately uncorrelated under normal conditions. The paths in simple mode reception often appear to be well correlated.

In files 9, 10, and 11 several resolved paths are present and spread widely in time delay. The $Covh_t(\mu)$ grams of this reception

indicate considerable correlation between paths. However, based on past experience, this type of reception is rather anamolous and has only been observed in November and December.

Although more detailed and quantitative investigation are desirable, those efforts have been left for later work. The preliminary conclusion here is that the MIMI channel under normal conditions is approximately uncorrelated.

Stationarity

The concept of wide-sense stationarity involves 1st and 2nd moment statistical properties of the channel. In our notation the UWAP channel is WSS with respect to t, if and only if

$$E\hat{h}(t, \lambda) = M(\lambda)$$

and

$$E\hat{h}(t, \lambda) \hat{h}*(s, \lambda) = R(t-s, \lambda)$$

These conditions are impractical to verify. The assumption that the UWAP channel is quasi-stationary appears very reasonable for intervals of time necessary for DUAL and $\hat{h}(t, \lambda)$ measurements as indicated by experimental results showing channel durations of time invariance on the order of 5 to 15 minutes. For these orders of time, physical arguments that the ocean is a very high inertia system must further support such an assumption.

However, for longer periods of times the UWAP is generally assumed to be non-stationary. The attitude prevails that one minute

of stationarity was all that was needed to make measurements, why push it further?

However, the question of what is the full extent of the quasi-stationary behavior of the UWAP channel is important. Although answering this question is not the purpose of this work, preliminary bases for extending the quasi-stationarity assumption to several hours are presented in the hope of motivating further thought on this subject because an answer to this question could have tremendous effects on future propagation experiments and models.

With a little thought, it should be clear that simply because $C(t)$, $S(t)$, and other DUAL parameters are not constants does not mean the channel is non-stationary. Moreover, the channel could be stationary to within a pure (broadband) time-varying gain. Or some modes or parameters, rather than the total process, may be stationary in some sense. For example, possibly the cluster mode reception is stationary but the simple mode reception is not. Or perhaps, just a parameter such as arrival times of either modes or paths are stationary. The point is that many possibilities exist and just because one approach hits a dead end, the search should not be given up. The following discussion presents, possibly disconnectedly, several preliminary results supporting the possibilities of some long term quasi-stationarity in the channel.

Quasi-Stationarity of Structure

Given the channel structure at any particular time, say complex with a single cluster mode and two simple paths, the most fundamental notion of quasi-stationarity must include "constant" structure for long periods. More specifically, if the complex structure of a cluster mode and two paths remains, and parameters, such as arrival times and delay spread, are constant, some underlying notion of quasi-stationarity must be present, if not in the structure process, then at least in some of the key parameters of the structure.

The "constant" structure of the channel is also illustrated in the auto-covariance grams by the long periods of "constant" decorrelation time. It is intuitively agreeable that the basic nature of a high-inertial system, such as the ocean where the most significant driving force, the tide, has a 12 hour period, has been observed to be very slowly changing.

The most obvious mechanisms disrupting the structure of the channel are the variability (coming and going, and $S(t)$ variation) of the simple paths.

Quasi-Stationary and Some Average Channel Parameters

Practical considerations of storage, display, and computation often dictate averaging of the time delay, λ, aspects of the channel. The discussion here centers on speculation about the stationary nature of the channel based upon λ-averaged measurements.

The preliminary report [1] on the experiment from which the

data in this thesis was obtained, contained sample mean and standard deviation analyses of the DUAL parameters C(t), S(t), R(t), and N(t). The samples used to compute these statistics represented 102 second coherent measurements of the channel and they were taken continuously from contiguous 102 second intervals. Then, the sample statistics were computed using three hour sliding averages on the mean and 25-minute sliding averages for the standard deviations.

Generally, the mean statistics are constant over periods of several hours. During those exceptions to this statement the channel structure consisted of the simple type where variations are wide and C(t), S(t), and R(t) are highly correlated.

The standard deviation measurements are discussed individually. The C(t) standard deviation, σ_c, displayed considerable fluctuation about a constant average level. This fluctuation rate was driven by the deep CW fades, which occur throught the experiment except during conditions of simple type channel structure. The S(t) standard deviation, σ_s, was quite constant throughout, R(t) and N(t) standard deviation measurements, σ_R and σ_N, were relatively constant throughout, except for shipping noise spikes. More details and a presentation of this statistical data is available in Reference [1]. Except for shipping interference and during simple type structure these results support hypotheses of long term (several hours) quasi-stationarity of the channel.

Another λ-averaged channel measurement, which supports the

quasi-stationary hypothesis, is the CANDOR measurement. CANDOR

involves the computation of the normalized cross-correlation coeffi-

cient of $\hat{h}(t, \lambda)$,

$$\rho(t, \ t-s) \ = \ \frac{\sum \hat{h}(t, \ \lambda) \ \hat{h}*(t-s, \ \lambda) \ \Delta\lambda}{||h_t(\lambda)||^{\frac{1}{2}} \ ||h_{t-s}(\lambda)||^{\frac{1}{2}}}$$

where $||h_t(\lambda)|| \ = \ \sum |h_t(\lambda)|^2 \ \Delta\lambda$.

In an average-λ-sense $\rho(t, \ t-s) \ = \ \rho(s)$ implies WSS of $h(t,$

$\lambda)$ where any pure (broadband) time varying gain is normalized out.

Although $\rho(t, \ t-s)$ was computed for all t with $\Delta t = 102$ seconds

and all $s-t$ in $[0, \ 48 \ \text{minutes}]$ with $\Delta(s-t) = 102$ seconds, the con-

dition $\rho(t, \ t-s) \ = \ \rho(s)$ was not fully tested. However, the -3 db

and -6 dB decorrelation times, T^+_{-3} and T^+_{-6}, were plotted for all

t, $\Delta t = 102$ seconds in Section 3.1.

The parameters display constant values of 5 to 15 minutes

most of the time, corresponding to the channel's nominal duration of

time invariance. Thus, preliminary indications are that the λ-average

WSS test of $\hat{h}_\lambda(t)$, $\rho(t, \ t-s) \ = \ \rho(s)$ may be successful. Finally, the

normalized cross-correlation statistics of $\hat{h}_\lambda(t)$ appear to be time

invariant for much greater lengths of time than $\hat{h}_t(\lambda)$ itself is time

invariant.

Although this discussion on quasi-stationarity has been highly

speculative, the data base relatively small and the measurement

techniques compromised, the discussion is constructive because the results presented were obtained using practical measurement techniques and they provide an early intuitive basis for serious efforts in determining the quasi-stationary properties of the UWAP channel.

4.3.4 Identification of Two Physical Propagation Modes. As pointed out earlier, there often appear to be two kinds of received multipath structure present in the CDR grams. First, a group of closely packed paths with very random appearing structure but a relatively constant average time of arrival has been denoted as cluster mode reception or structure. Although the delay spread of this cluster mode type structure is relatively constant for several hours at a time, during various periods of the experiment this spread can vary considerably. For example, in file 9 and 10 the cluster mode spread is approximately 300 milliseconds, while in file 4 the spread is approximately 150 milliseconds. In addition, on some occasions, see data files 4 and 5, two cluster modes appear in the channel's structure.

The second type of structure identified in the CDR gram consists of a small set of clearly resolved paths. Usually one to three paths are present and, although definitely resolvable, all within 120 milliseconds of delay spread. The paths are generally well correlated.

Trace these two basic modes of propagation throughout the two weeks of data. Often the two modes are separated so that they can easily be studied individually. However, they can be superimposed as in files 16, 17, 18, and 19, so that, although they are being

visually identified, individual study would be difficult since simple delay gating would no longer isolate the modes.

These two modes appear independent and are clearly contrasting in nature. The natural conclusion is that two distinct physical mechanisms or modes of propagation are operating. Physical reasoning together with some simplified propagation analysis of the Straits of Florida provide a convincing argument that the cluster mode and simple mode structures are bottom, RBR, and surface RSR, SRBR, or surface duct propagation modes, respectively. The reasoning for these conclusions is expressed in the following paragraphs.

Since significant Doppler spread energy has been noted and attributed to surface wave interaction with propagation, there certainly must be a surface mode of propagation in order for this interaction to occur. Furthermore, since Doppler spread activity correlates well with the presence of simple mode structure, the conclusion is that the simple structure is a surface mode of propagation. Other information further substantiates this conclusion. Greater variability in propagation (loss, speed, etc.) is anticipated in a surface mode because of the relatively unstable water column. This fluctuating water column is driven by the sun (heating), clouds (cooling), winds, currents, etc., which produce a fairly dynamic propagation media (i.e., unstable water column). This expected variability in the surface mode is reflected in the $S(t)$ variation in files 11, 12, and 13 where only simple type reception is present. This amplitude

variation in the simple paths is also evident in file 1.

During simple mode reception S(t) is typically higher than during complex or cluster mode reception. Because greater losses are associated with surface reflections than bottom reflections there may be some question as to whether the surface mode is a channel, near the surface but not reflecting from it, or a refracted, surface reflected (RSR) mode. However, direct surface interaction appears to be the only significant spreading mechanism so that RSR is the more logical choice. Indirect frequency spreading surface mechanisms include modulation of the sound velocity due to pressure variations caused by waves or direct modulation of the acoustic signal, a pressure wave, by induced pressure waves from the surface waves. However, these are rather implausible explanations because the velocity is rather insensitive to such small pressure perturbations, and nonlinear phenomenon from pressure wave interaction is a negligible higher order effect.

The cluster mode reception is identified as refraction-bottom-reflected (RBR) propagation. In shallow depth water temperature is continually decreasing and pressure increases; if the temperature gradient is high sound velocity decreases with depth. Thus, a sound ray is refracted downward until it is reflected from the bottom upward only to be refracted downward again. Figure 2.3 is a ray trace of the Straits of Florida illustrating several RBR paths as well as RSR propagation. In contrast to the surface the deep water

column is very stable due to the lack of many of the dynamic driving

(200 meters and deeper) forces at the surface. Therefore, propaga-

tion variability with time will be much less for RBR. However,

simplified RBR ray theory in the Straits of Florida predicts many

closely stacked up arrivals [11], providing excellent support for a

quasi-stationary uncorrelated Gaussian process due to many small

scale variations and interactions in the received RBR propagation.

CDR grams 9 and 10 contain two apparent surface paths (along the

right hand margin and continuing through CDR gram 14) and what ap-

pears to be basically RBR (i. e., many paths) but displaying the non-

characteristic feature of resolved individual arrivals. It is not clear

what drives this variation in RBR propagation, possibly deep internal

waves, or a changing surface layer depth.

Thus, although some very complicated results can be obtained

and uncertainty exists, two contrasting propagation modes identified

in the CDR gram, have been logically associated with the two major

modes of propagation.

Decomposition of the Delay Spread UWAP Channel

The CDR gram and the DUAL measurements suggest and

provide the means for further measurements and experiments to

substantiate the identification and to better study and understand these

two modes. The CDR gram illustrates the possibility for a decom-

position of the UWAP channel into two natural subchannels by very

simple time-delay gating. Previously, measurements such as DUAL,

CANDOR, etc., have been measurements on the total channel, which is constructed of two very different and interesting subchannels. Such measurements can be made individually on the two channels whenever they are noninterfering. Such analysis has already proved interesting when simple mode is present alone, files 11, 12, and 13. Here DUAL and CANDOR results are quite different than the normal measurements dominated by cluster mode. $S(t)$ and $R(t)$ measurements of the decomposed channels can be particularly interesting. Since cluster mode is almost always present, previously little opportunity has been presented to extensively correlate variable $S(t)$ with individual paths or even simple mode structure, or to correlate $R(t)$ activity with simple mode $S(t)$ activity. However, individual CW measurements are impossible with single hydrophones and individual $R(t)$ measurements may be impractical. Thus, individual $S(t)$ measurements will be compared with total channel $C(t)$ and $R(t)$ measurements. Nevertheless, such studies should be very interesting, informative, and simple to implement.

Subchannel Modeling

Two very distinct types of propagation, which can often be isolated, have been identified in the CDR gram and individual study has been suggested. Since the subchannels are so contrasting in nature, the appropriate models and modeling techniques will be quite different. The cluster mode structure appears to be a perfect candidate for stochastic, quasi-stationary, uncorrelated Gaussian modeling where statistical methods appear most useful.

The simple mode structure seems best suited for non-random parameter tracking techniques. Each path of the mode can be resolved and its parameters, amplitude, phase, duration, and arrival time may be individually tracked and studied. The paths and their respective parameters can be correlated with each other, environmental measurements, etc.

4.4 Summary

The author feels that the ordered pair gram display of the channel digit response, $cdr(t, \lambda)$ is a breakthrough for MIMI signal processing and will provide new insight in underwater acoustic propagation study. The display presents a more complete picture of the multipath structure of the UWAP channel, its complexity and simplicity, and its variability, for much longer durations than has been possible previously. For the first time, the whole of the channel can be simply presented and comprehended.

In general, the value of the CDR gram is the compact and useful presentation of the tremendous quantity of qualitative and gross quantitative information inherent in the $cdr(t, \lambda)$ data. For example, a CDR gram spanning several hours of time is easily displayed on an 8-1/2 by 11 inch area. Multipath structure can be readily detected and identified as simple or complex, the duration (hours, days, etc.) of each general structure is easily observed. The simultaneous reception of a simple and complex structure, whether non-overlapping

or superimposed in time delay, is readily identified. Visual correlation of the general channel structure with key scalar functions (e.g., DUAL parameters) representing the channel are simply achieved by observing side-by-side plots of such parameters and the corresponding CDR grams.

The CDR gram is equally as important as a springboard or testing ground for new post-processing ideas of UWAP data as it is for the direct extraction of information from the display. A significant attribute of the CDR gram is that without any processing, several parameters can be at least semi-quantitatively estimated. This means the computing time of several special post-processing algorithms can be avoided. Even more importantly, the gram provides preliminary information on parameters and their behavior so that the probability of success and the basic nature of the algorithm can be intelligently surmised without the time consuming task of blindly defining, implementing, and evaluating an algorithm. The value of this ability to rather effortlessly obtain preliminary algorithm design and evaluation can not be over emphasized.

The simple and complex types of structure are so contrasting in nature that an observer immediately wants to classify them. Based upon propagation theory, these two types of structure are readily hypothesized to be very distinct physical propagation modes. The simple reception is apparently a surface related mode and the complex reception must be a bottom mode. Immediately, several ideas

are generated. When the two modes are non-interferring in time delay or only one mode is present, they may be studied separately. For example, S(t) or CANDOR analyses can be independently performed on the modes. Surface reverberation measurements from DUAL can easily be correlated with the presence of the surface mode. Since the two modes are so different in nature, measurement and modeling approaches most suitable for each mode are likely to be quite different. Observations of the CDR grams clearly indicate tremendous data reduction may be possible without significantly compromising the quality of the data base or the representation of the channel which the data base provides. The possibilities are indeed vast and exciting. But most importantly, new ideas using or generated from the CDR gram will provide a greater understanding of the UWAP channel and piece by piece useful and reliable models and experimental methods will be developed.

CHAPTER 5

OTHER CHANNEL REPRESENTATIONS

Although the CDR, $\hat{h}_t(\lambda)$, appears to be a useful represen-

tation of the UWAP channel, other likely candidates are briefly

presented and discussed. The alternatives investigated, the chan-

nel digit spectrum, $S_t(f)$ and the channel covariance function,

$Covh_t(\mu)$, provide some information about the MIMI channel, but

they appear considerably less interesting than the cdr (t, λ) .

5.1 Channel Digit Spectrum, $S_t(f)$

The channel digit spectrum is a logical alternative repre-

sentation of the UWAP channel. The CDS denoted by $S_t(f)$ is the

Fourier transform of the time spread channel digit response,

$\hat{h}_t(\lambda)$, taken with respect to the time spread variable λ ,

$$S_t(f) = \left| \sum_{\lambda \in \Lambda} \hat{h}_t(\lambda) \, e^{i 2\pi f \lambda / \Lambda'} \right|$$

where

$$f \in [-63, 62] \quad , \quad \Lambda' = 252$$

$$\Delta\lambda \cong 5 \text{ msec} \quad \text{and} \quad \Delta f = \frac{1}{T_p} \cong 0.833 \text{ Hz}$$

Since 252 is not an integer power of two, the usual fast Fourier transform algorithm could not be used to compute $S_t(f)$ here [27]. However, 252 is a high composite number, $252 = 3 \cdot 3 \cdot 7 \cdot 2 \cdot 2$, so that an efficient but very specialized FFT algorithm could have been used [30]. However, a more general computational algorithm called the Chirp Z-Transform, CZT, was used here [29], [31]. The advantages of the CZT, obtained at the expense of increased computer memory requirements, are:

- The CZT expresses the Fourier transform as a convolution. Thus, fast convolution techniques using the conventional FFT algorithm may be used to obtain computation efficiency.

- Λ' is an arbitrary integer variable in the CZT. In the conventional FFT Λ' is restricted to integer powers of 2.

This discussion is not intended as a detailed development of computational techniques such as the FFT, CZT, or fast convolution. These techniques are well documented in the open literature.[*] This is simply a straightforward application of an algorithm that does not contain the restriction of conventional FFT analysis.

---

[*]References [26]-[31].

This added flexibility is important because varied MIMI experimental conditions and objectives dictate different signal periods. That is, Λ varies and is never an integer power of two since maximal length binary sequences are always one less than a power of two, so that $\Lambda = \text{Integer} \cdot 2^{n} - 1$. Thus, the CZT algorithm provides efficient and versatile signal processing, spectral analysis, correlation and convolution, of MIMI signals. Another approach to this same problem is currently being studied from the signal design aspect of the problem [14]. The major equations and a Fortran listing of the CZT are in Appendix B.

Since $S_t(f)$ is positive real valued, the positive real (PR) gram format discussed in Section 4.2 is the natural technique for displaying it. These CDS grams are organized by files as summarized in Table 3.1. The time variable, t, runs down the gram and frequency is across the gram. Since the transmitted signal main lobe has a ± 50 Hz main lobe

$$\frac{\sin \pi f T_p}{\pi f T_p}$$

and the reception is filtered sharply at ± 50 Hz , only the ± 50 Hz region of $S_t(f)$ is displayed. However, $S_t(f)$ was computed from -100 Hz to $+100$ Hz and the power in the main lobe -50 to $+50$ Hz

was computed

$$MLP_t = \sum_{f=-63}^{63} |S_t(f)|^2$$

The ratio of MLP_t to S(t) is an indicator of the analog prefiltering integrity and, likewise, it is a measure of the over sampling of the current MIMI sampling rates.

This ratio expressed in decibels, $10 \, Log_{10} \, MLP_t/S(t)$, was nominally -0.1 ± 0.075 dB for all the data presented, or $MLP_t = 10^{-0.01} \, S(t) = 0.975 \, S(t)$. That is, approximately 97.5 percent of the total reception energy is within the ± 50 Hz band. Thus, for practical purposes, including sampling rate aliasing concern, the sidelobes are negligible.

The CDS grams do not appear to reveal the basic nature of the channel as the CDR grams. The first impression of the CDS grams is sameness; they are all alike. However, there is some information unavailable in the CDR grams. Most of the received energy is nominally in the ± 30 Hz band around center. However, the band from -30 to 0 Hz generally has more energy than the corresponding 0 to 30 Hz band. This phenomenon is particularly emphasized during simple mode propagation, e. g. , file 9. Although there are probably more informative ways to display or otherwise

CDS GRAMS 1 & 2

Fig. 5.1

14(01:36)

14(09:29)
14(10:55)

14(15:29)

14(16:18)

15(03:06)
15(05:38)

15(07:17)

-50   -25   0 Hz   25   50

CDS GRAMS 3 & 4

Fig. 5.2

15(07:17)

15(10:13)
15(19:13)

16(04:45)

16(10:55)
16(12:52)

16(19:05)

-50   -25   0 Hz   25   50

CDS GRAMS 5 & 6

Fig. 5.3

16(19:05)

17(07:32)

17(12:06)
17(12:33)

17(18:46)

-50   -25   0 Hz   25   50

CDS GRAMS 7 & 8

Fig. 5.4

23(10:20)

23(22:47)

24(10:49)

-50   -25   0 Hz   25   50
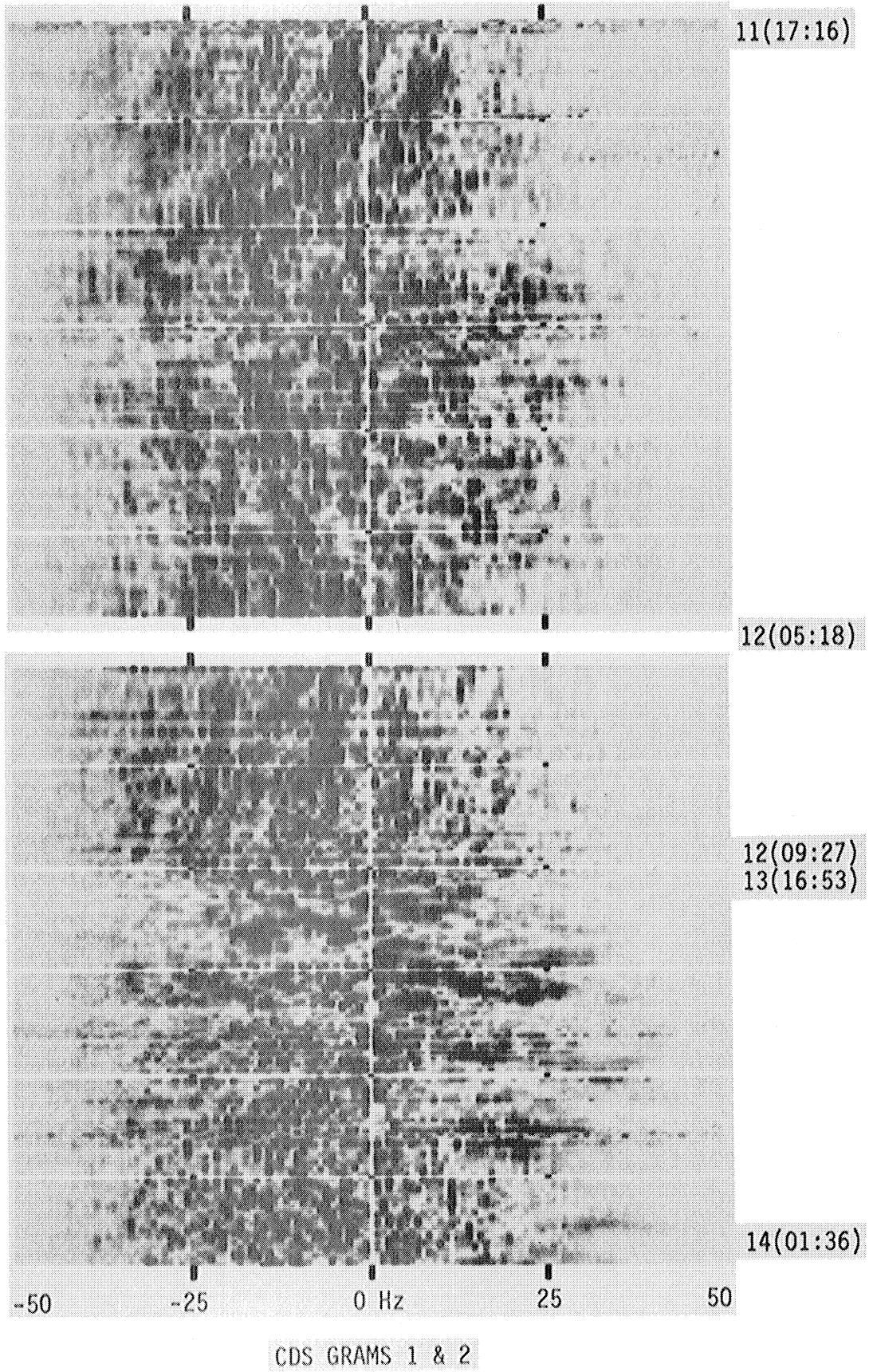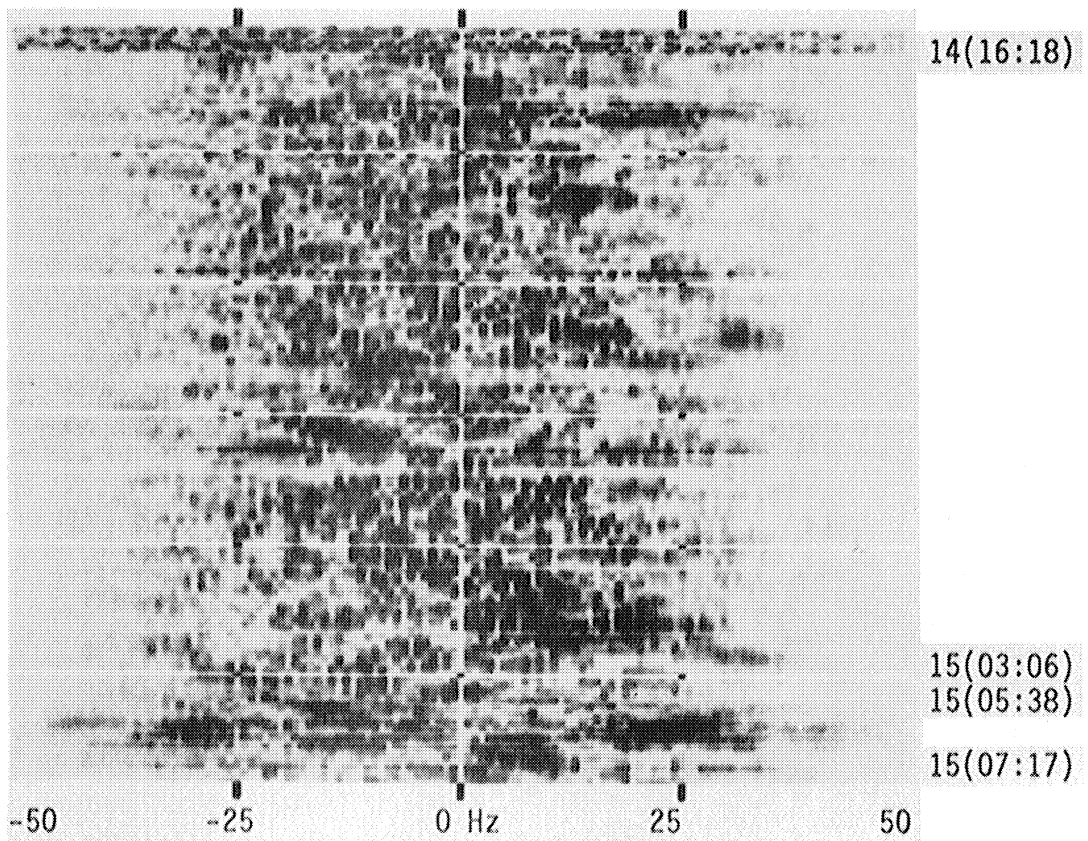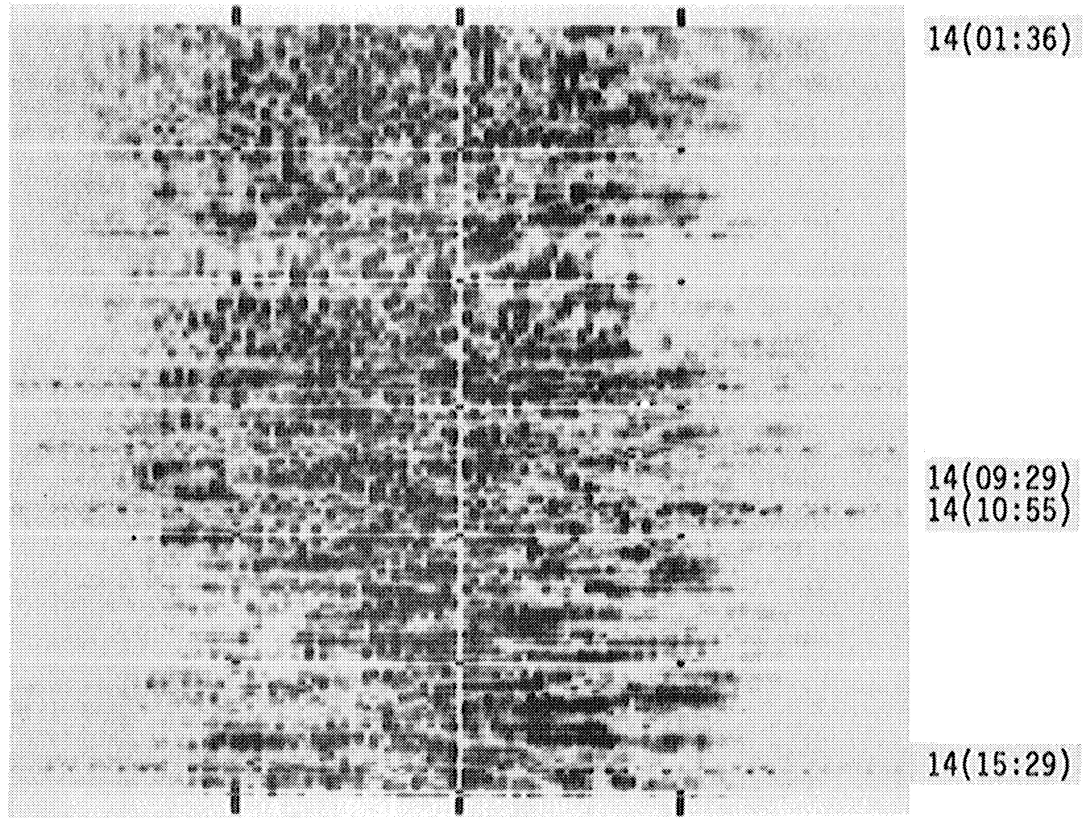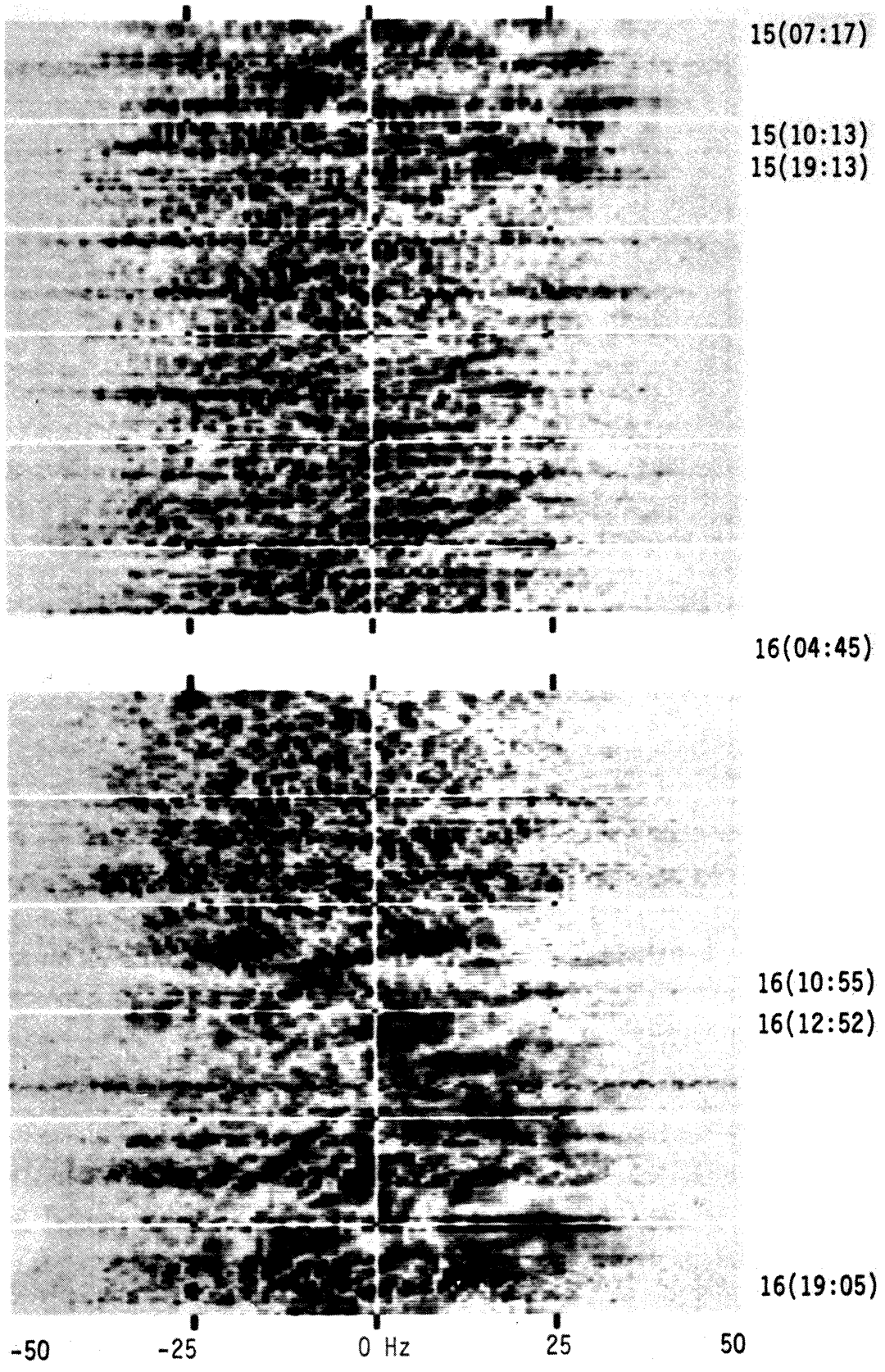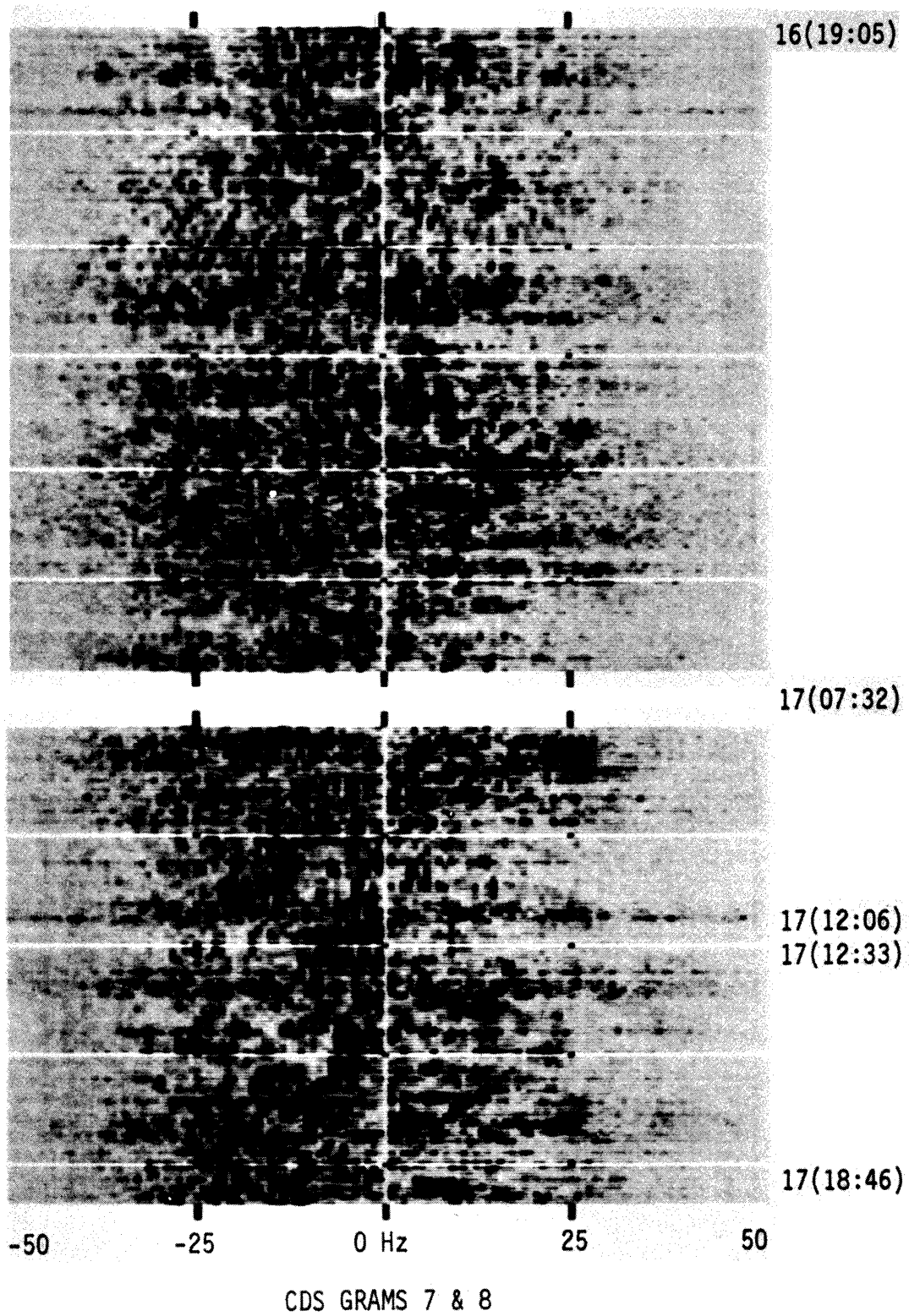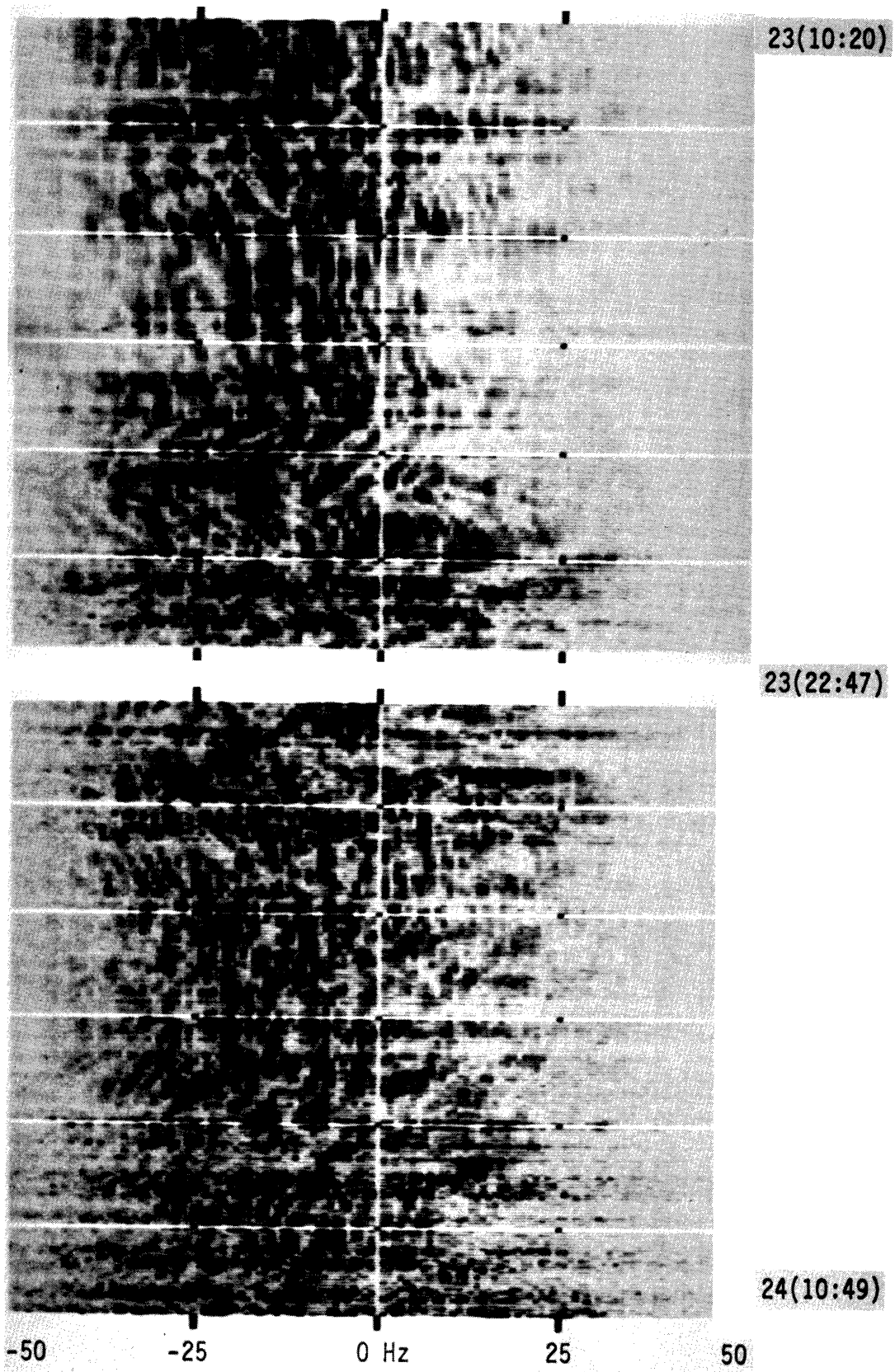
CDS GRAMS 9 & 10

Fig. 5.5

CDS GRAMS 11 & 12

Fig. 5.6

132

25(19:11)

26(07:38)

26(19:40)

-50   -25   0 Hz   25   50

CDS GRAMS 13 & 14

Fig. 5.7

26(19:40)

27(08:07)

27(20:09)

-50   -25   0 Hz   25   50

CDS GRAMS 15 & 16

Fig. 5.8

134

27(20:09)

28(08:36)

28(20:38)

| -50 | -25 | 0 Hz | 25 | 50 |

CDS GRAMS 17 & 18

Fig. 5.9

28(20:38)

29(09:05)

-50   -25   0 Hz   25   50
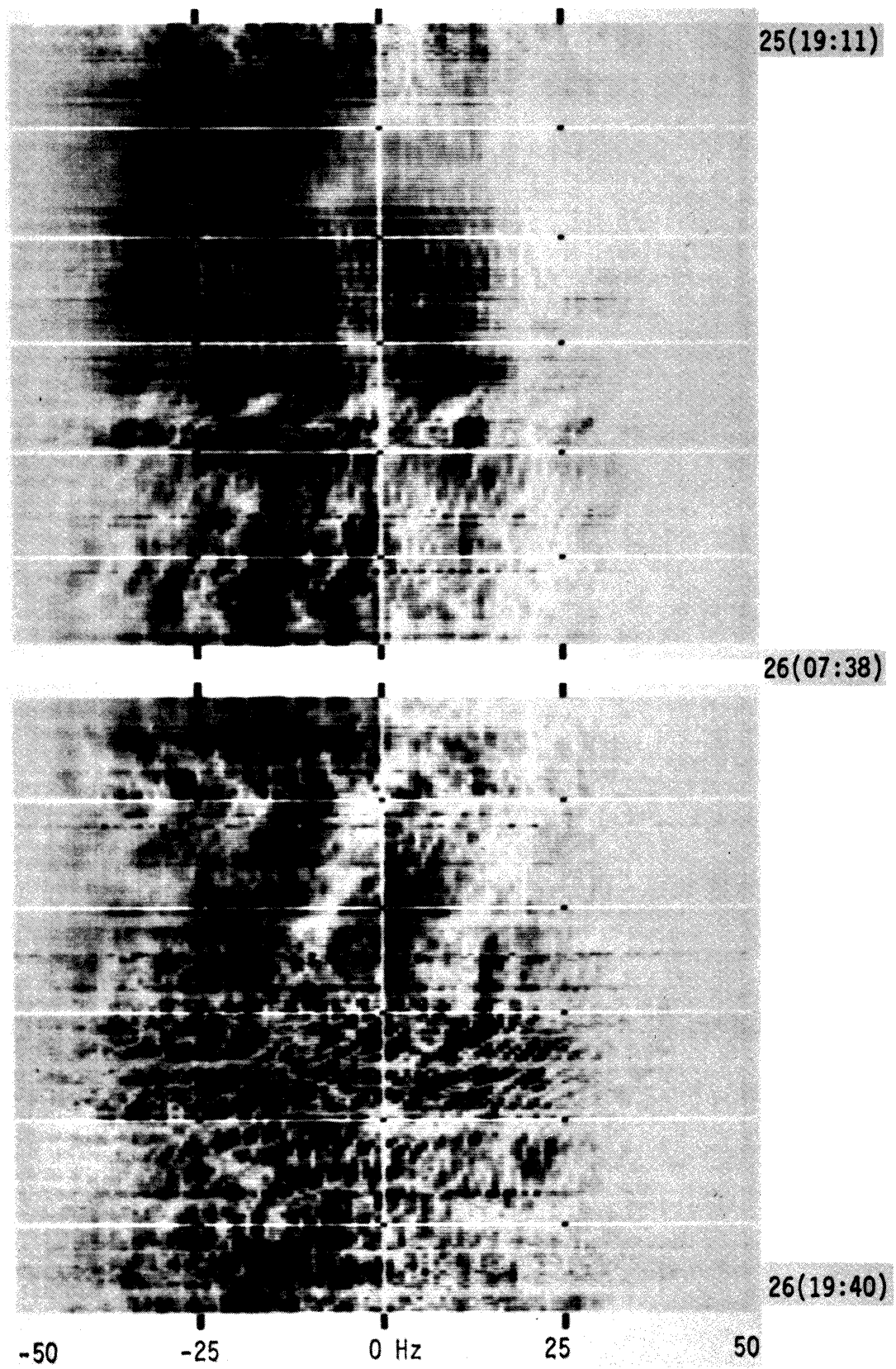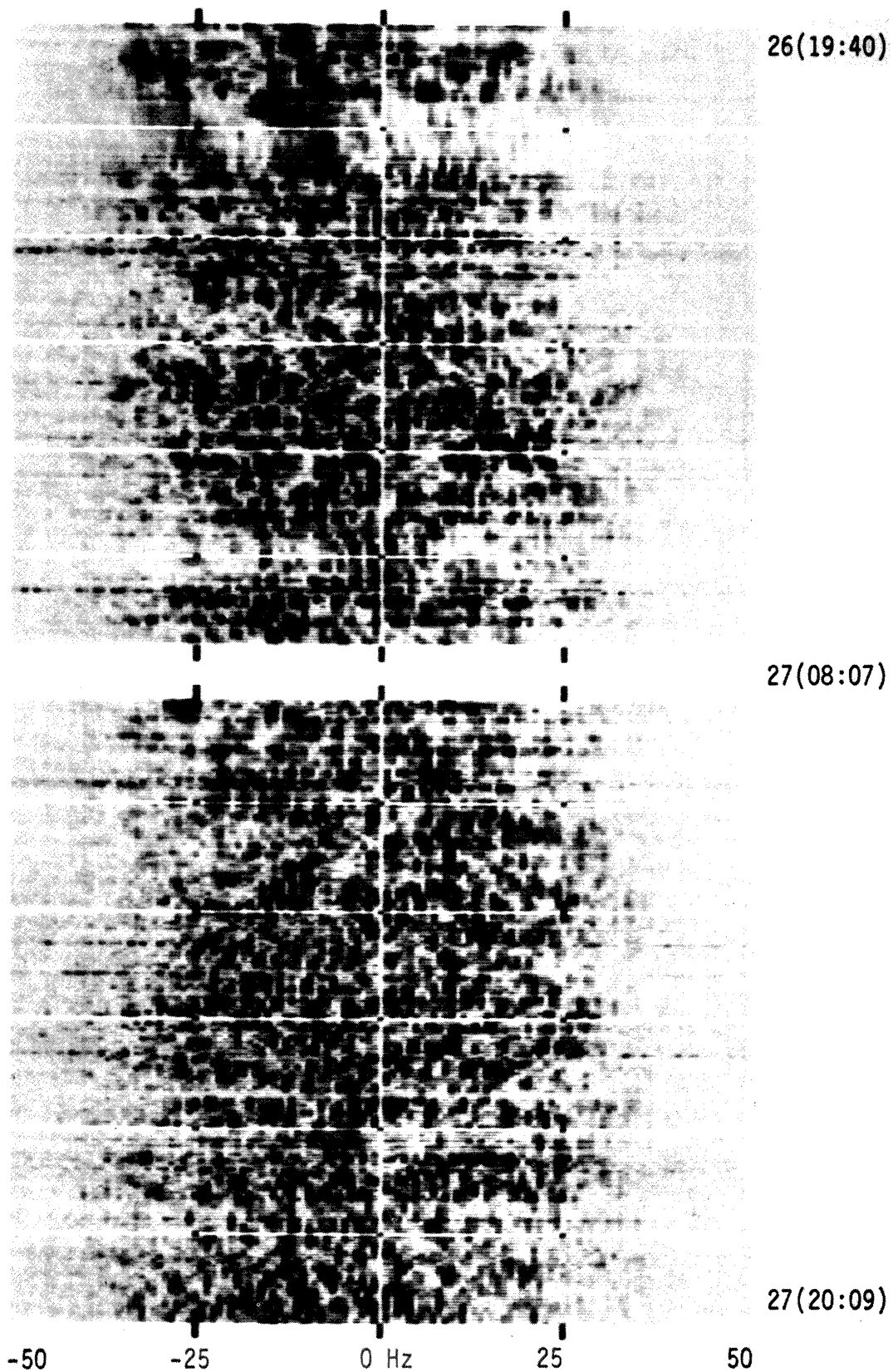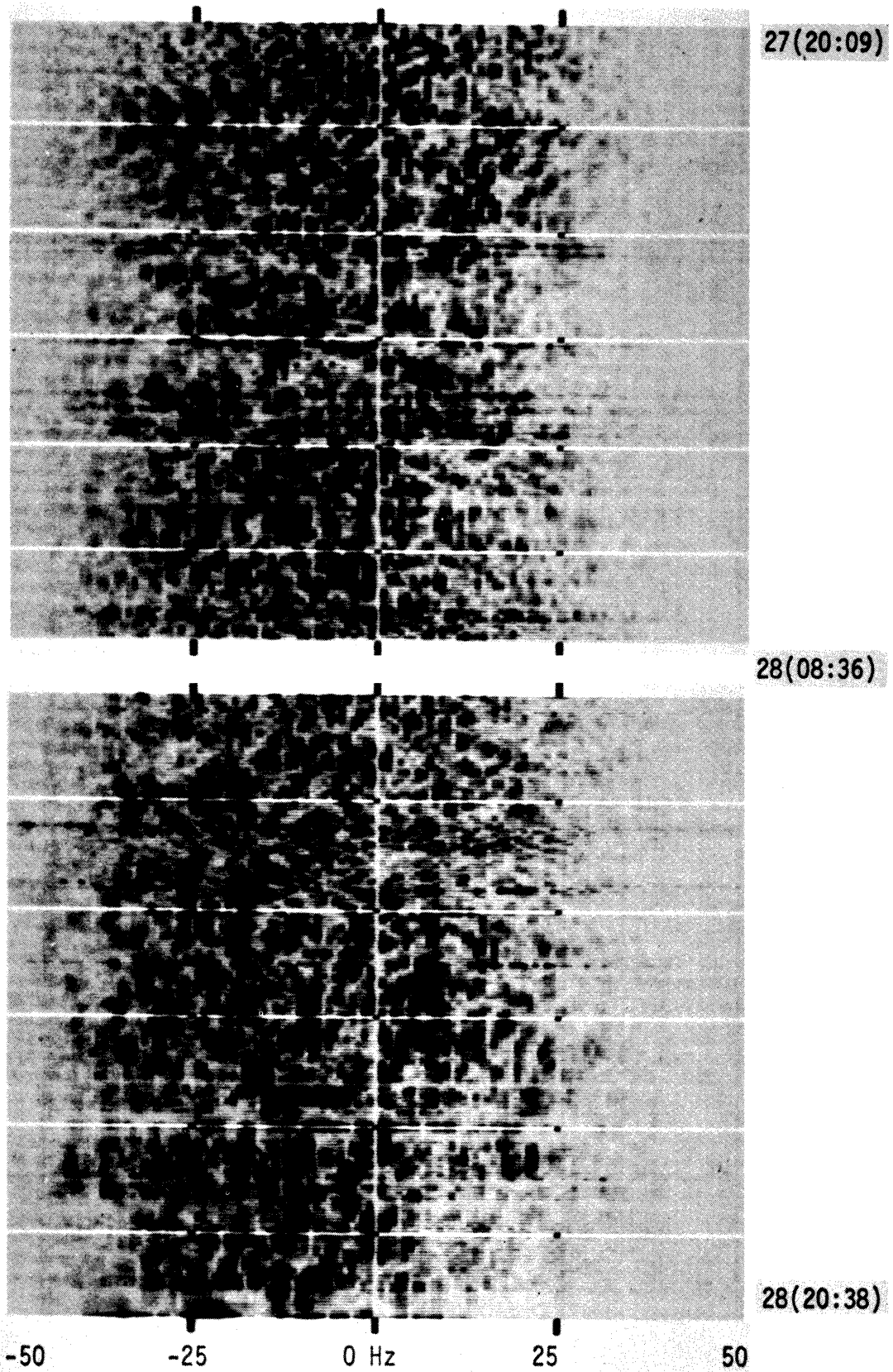
CDS GRAM 19
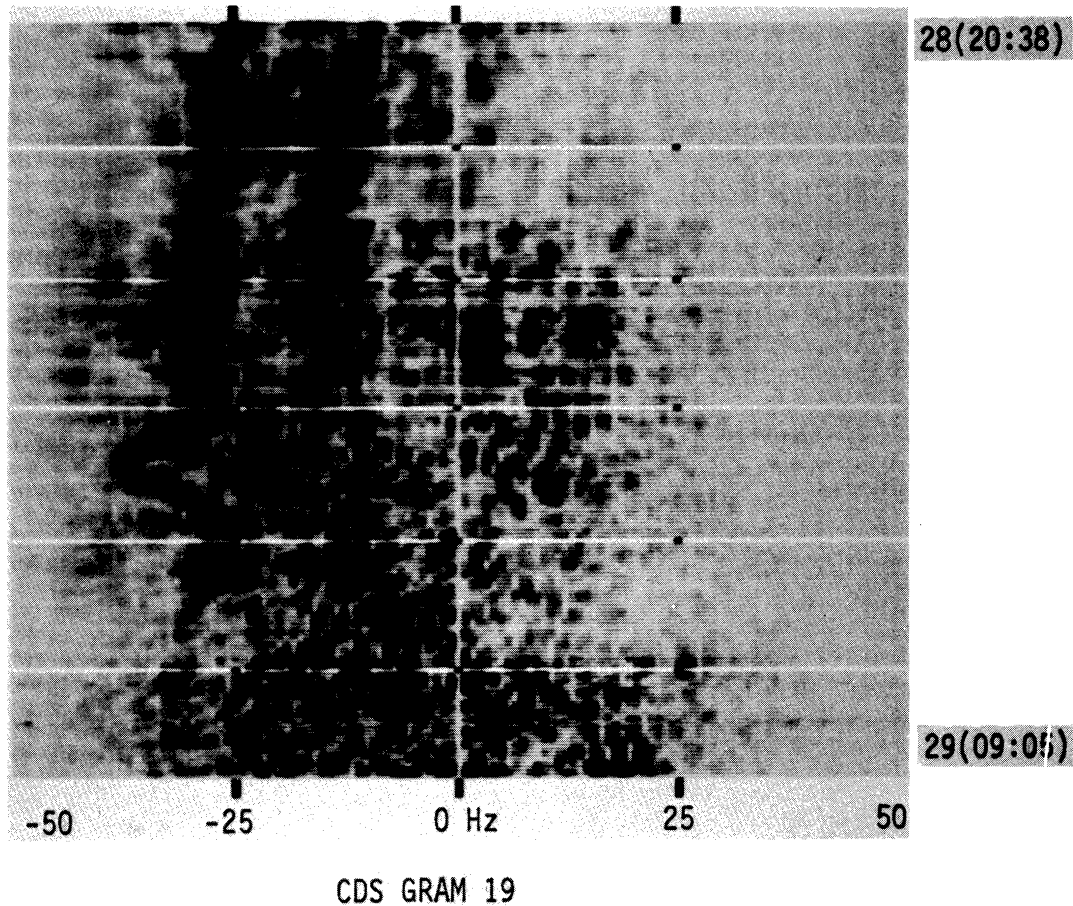
Fig. 5.10

process $S_t(f)$, the CDS does not appear nearly as revealing a repre-
sentation of the UWAP channel as the CDR.

5.2 The Channel Auto Covariance

Under normal conditions, cluster mode reception, arguments
have been made of quasi-stationarity. Gaussianness of $\hat{h}_t(\lambda)$ can be
argued on the basis of the cluster mode reception consisting of the
relatively large number of closely spaced random multipath arrivals.
Assuming ergodicity, time averages are used to estimate the mean
and auto covariance functions of $\hat{h}_t(\lambda)$.

Since $\hat{h}_t(\lambda)$ is zero mean,[*] the normalized auto covariance

of the CDR is estimated by

$$\text{Covh}_t(\mu) \; = \; \frac{\cong \; \sum_{\Lambda} \hat{h}_t(\lambda) \; \hat{h}_t^*(\mu-\lambda)\Delta\lambda}{\| \hat{h}_t(\lambda) \|}$$

$\text{Covh}_t(\mu)$ is complex-valued conjugate symmetric function. The

computations were performed using fast convolution techniques and

the results of this analysis on all of the CDR data are presented in

ordered pair format. A tremendous amount of information appears

to be lost in going from the CDR gram to the COVH gram. As with

the CDS, the COVH grams generally leave an impression of "same-

ness" and certainly do not convey the physical characteristics so

vividly illustrated in the CDR gram. Possibly $\text{Covh}_t(\mu)$ is a very

incomplete statistical representation of the channel. However, any

statistical representation is likely to wash out the physically dis-

tinctive features of the channel. The preliminary conclusion

drawn here is that $\text{Covh}_t(\mu)$ is probably an inadequate repre-

sentation of the UWAP channel. However, the CDR gram and

$\hat{h}_t(\lambda)$ are very rich in physical information about the UWAP channel

---

[*]The mean is estimated $M_{h_t} = \sum_{\lambda} \hat{h}_t(\lambda)$ and subtracted to

assure zero mean $\hat{h}_t(\lambda)$.

and clearly should be the primary base for MIMI experiments at this time.

The $\text{Covh}_t(\mu)$ grams are presented on a one-to-one basis corresponding to the CDR grams. The $\text{Covh}_t(\mu)$ grams are OP grams as are the CDR grams. The general format of the COVH grams are otherwise similar to the CDR grams. Alternating black and white bar patterns are plotted every 100 minutes and the black and white bar durations in μ correspond to the 40 msec width of the correlation triangle resulting from an ideal 20 msec pulse in the CDR. The significant extent of $\text{Covh}_t(\mu)$ appears to be approximately 40 to 60 or 80 msec in the gram. That is, the channel appears to be uncorrelated within one to two transmission digits. In files completely consisting of simple mode reception, more correlation is present. In general, $\text{Covh}_t(\mu)$ gives a strong impression of "sameness" which supports contentions of stationarity and indicates that time averaging should be a valid means for obtaining better estimates of $\text{Covh}_t(\mu)$.
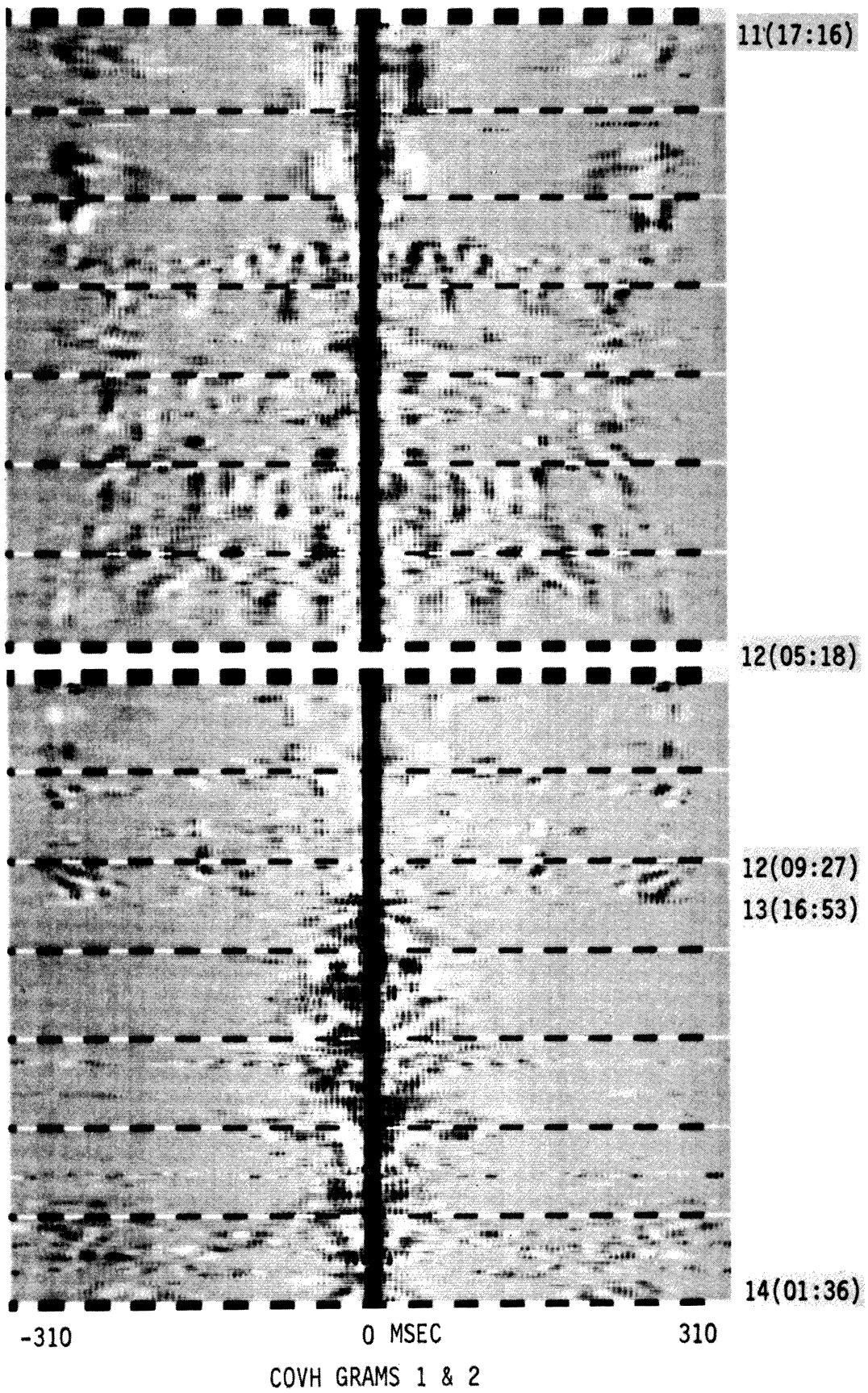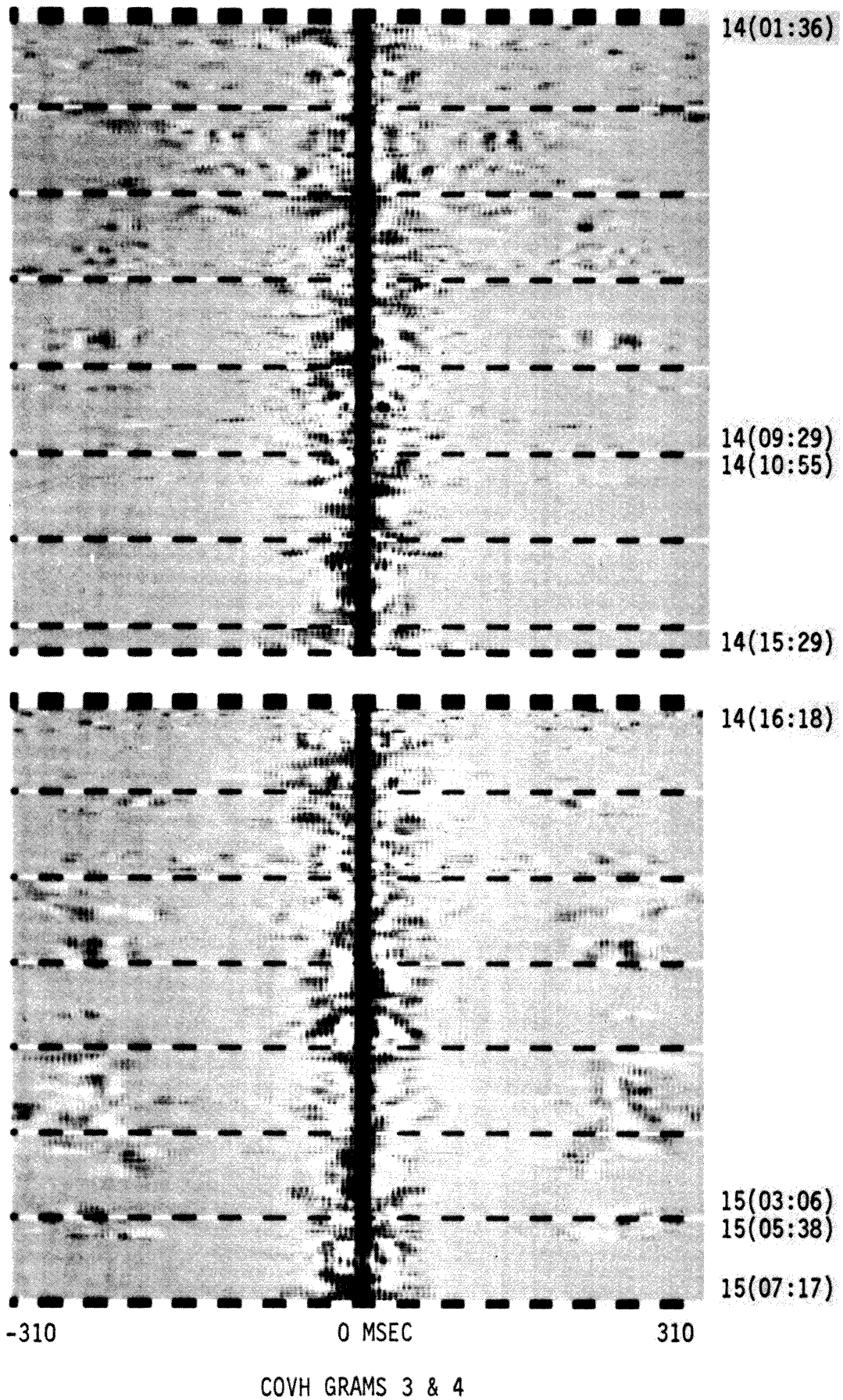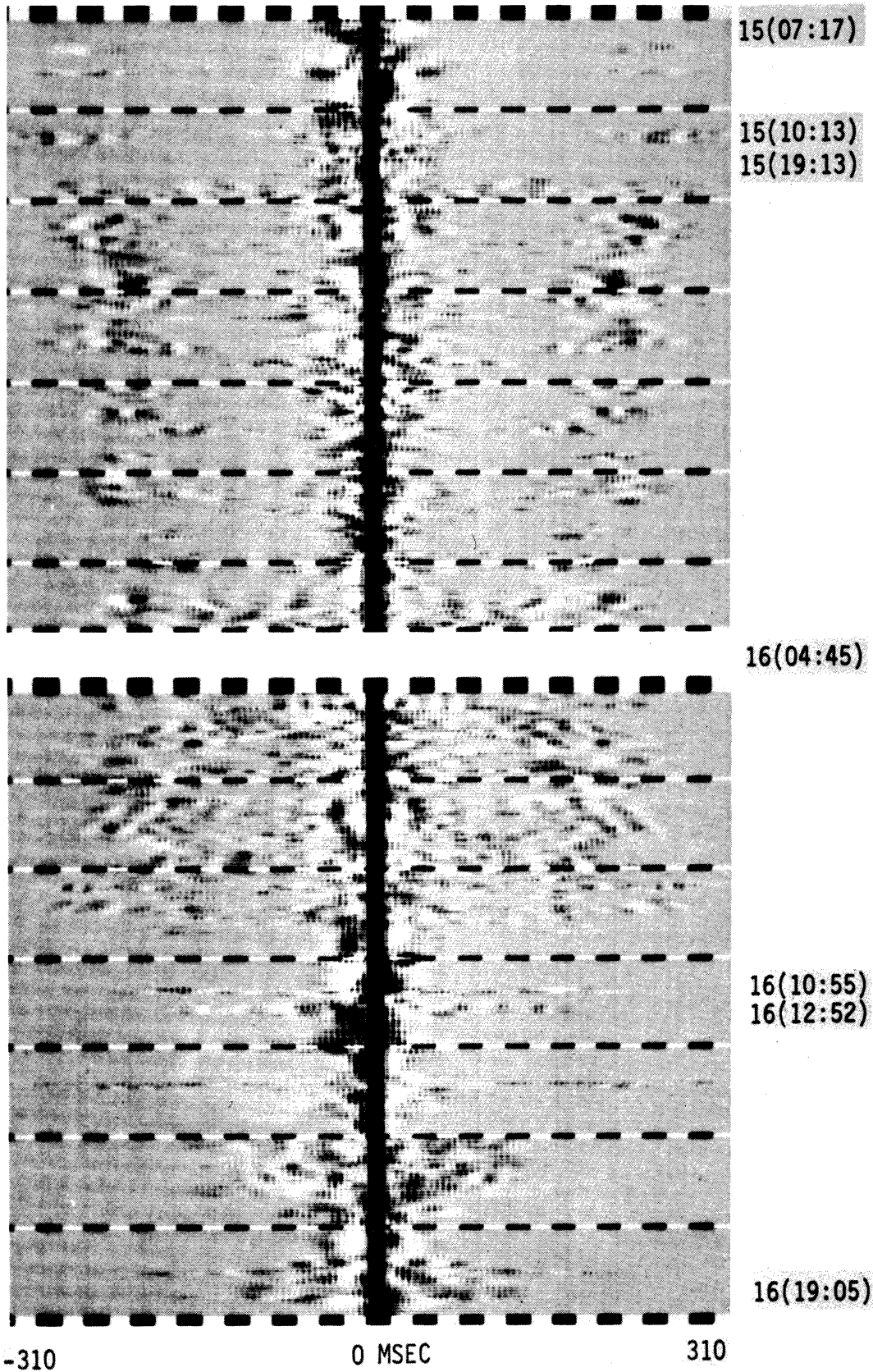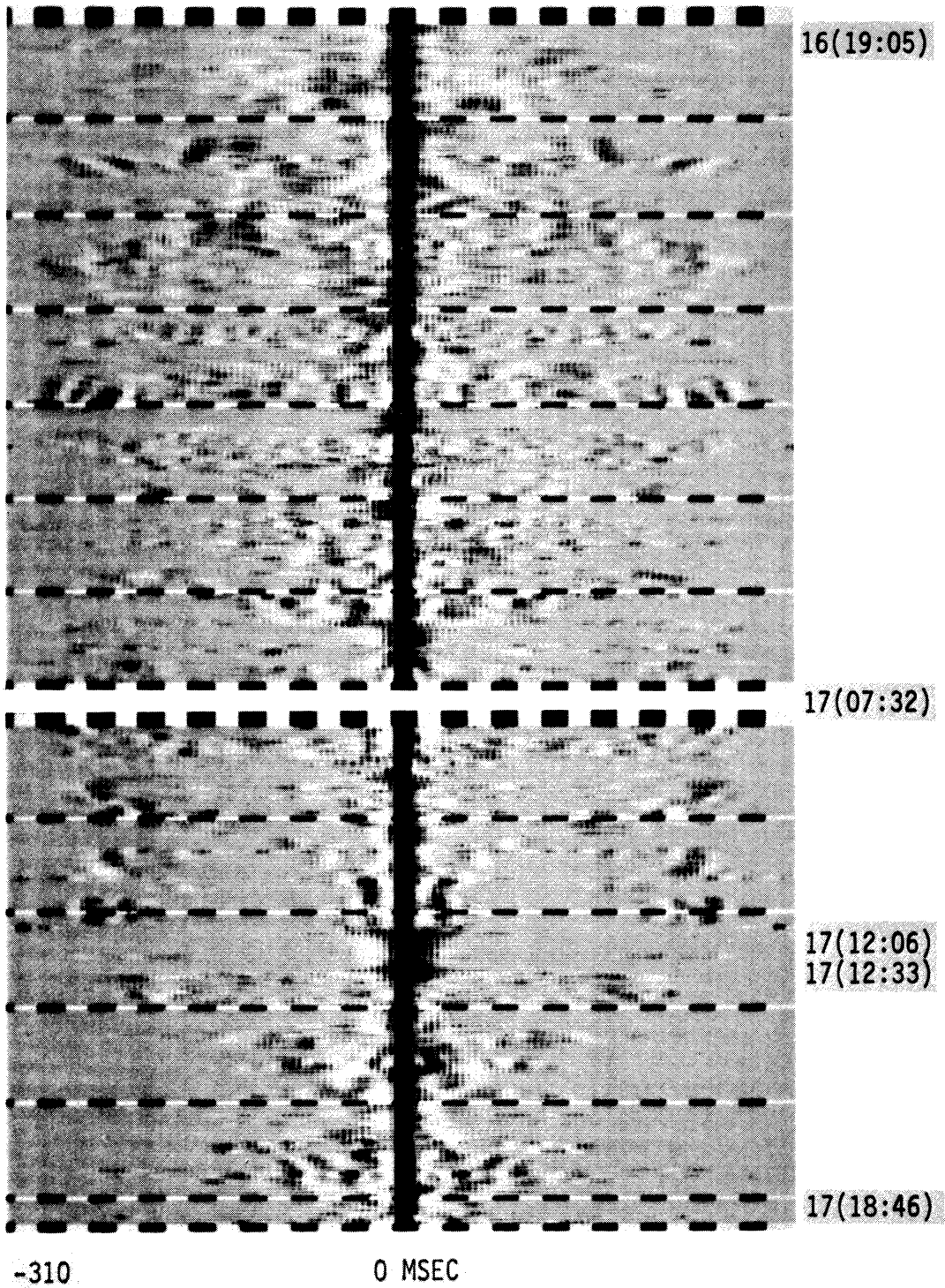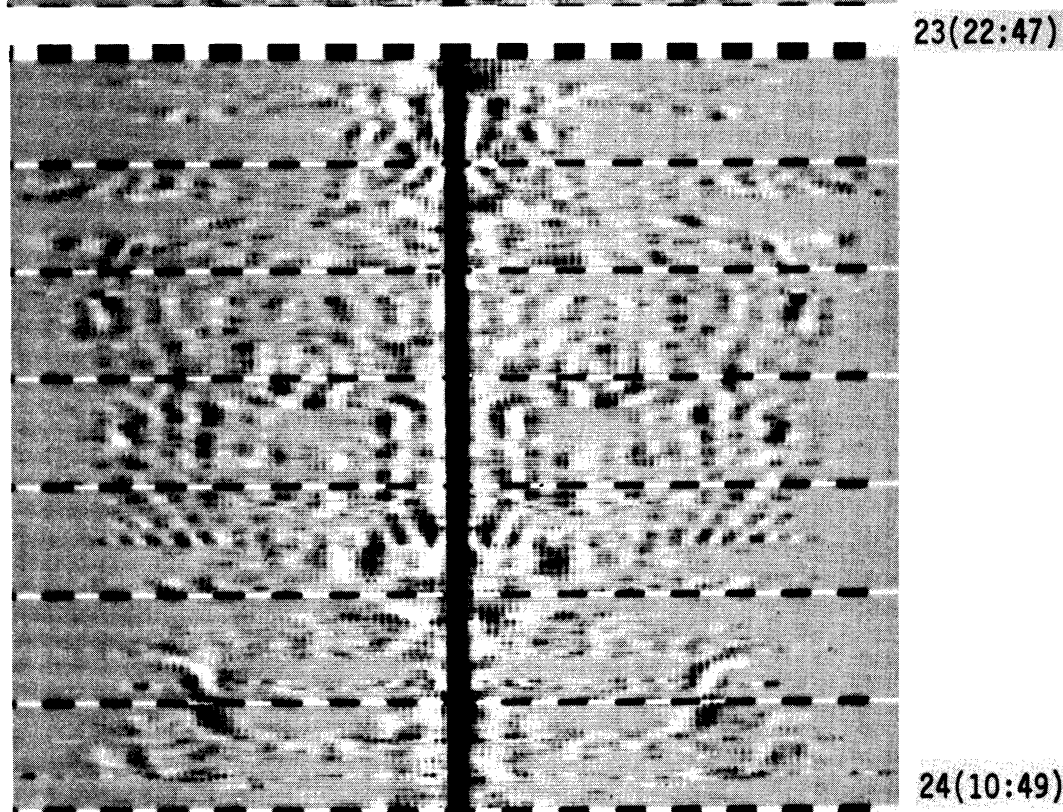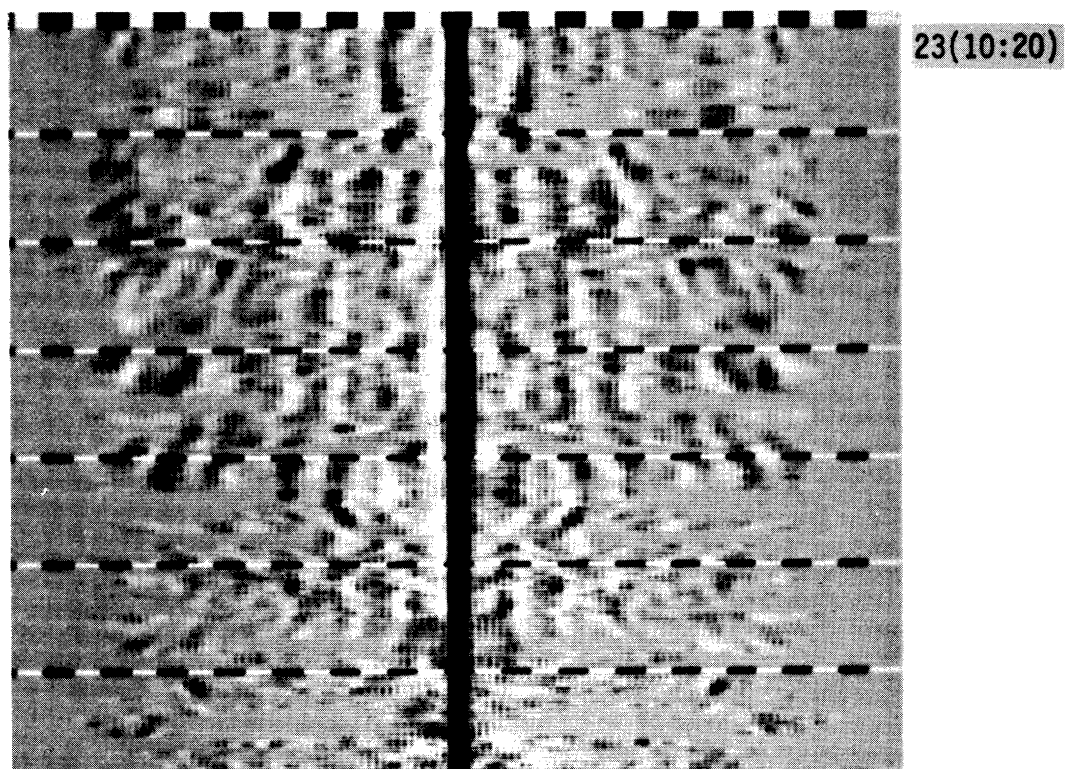
138

COVH GRAMS 1 & 2

Fig. 5.11

14(01:36)

14(09:29)
14(10:55)

14(15:29)

14(16:18)

15(03:06)
15(05:38)

15(07:17)

-310   0 MSEC   310

COVH GRAMS 3 & 4

Fig. 5.12

140

15(07:17)

15(10:13)
15(19:13)

16(04:45)

16(10:55)
16(12:52)

16(19:05)

-310   0 MSEC   310

COVH GRAMS 5 & 6

Fig. 5.13

16(19:05)

17(07:32)

17(12:06)
17(12:33)

17(18:46)

-310   0 MSEC

COVH GRAMS 7 & 8

Fig. 5.14

COVH GRAMS 9 & 10

Fig. 5.15

24(18:42)

25(07:09)

25(11:18)
25(11:18)

25(19:11)

-310   0 MSEC   310

COVH GRAMS 11 & 12

Fig. 5.16

144

25(19:11)

26(07:38)

26(19:40)

-310   0 MSEC   310

COVH GRAMS 13 & 14

Fig. 5.17

26(19:40)

27(08:07)

27(20:09)

-310   0 MSEC   310

COVH GRAMS 15 & 16

Fig. 5.18

27(20:09)

28(08:36)

28(20:38)

-310   0 MSEC   310

COVH GRAMS 17 & 18

Fig. 5.19

28(20:38)

29(09:05)

-310   0 MSEC   310
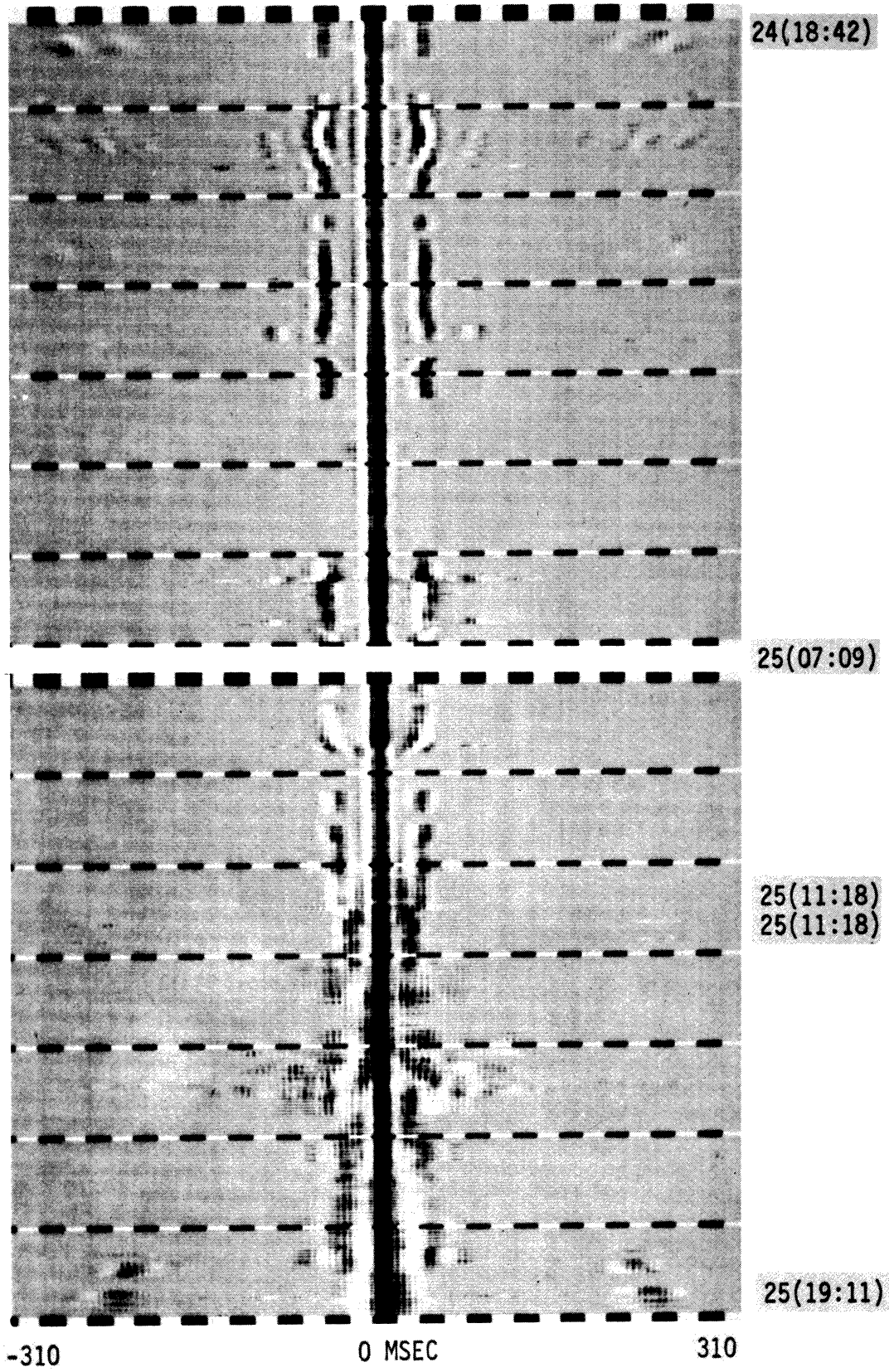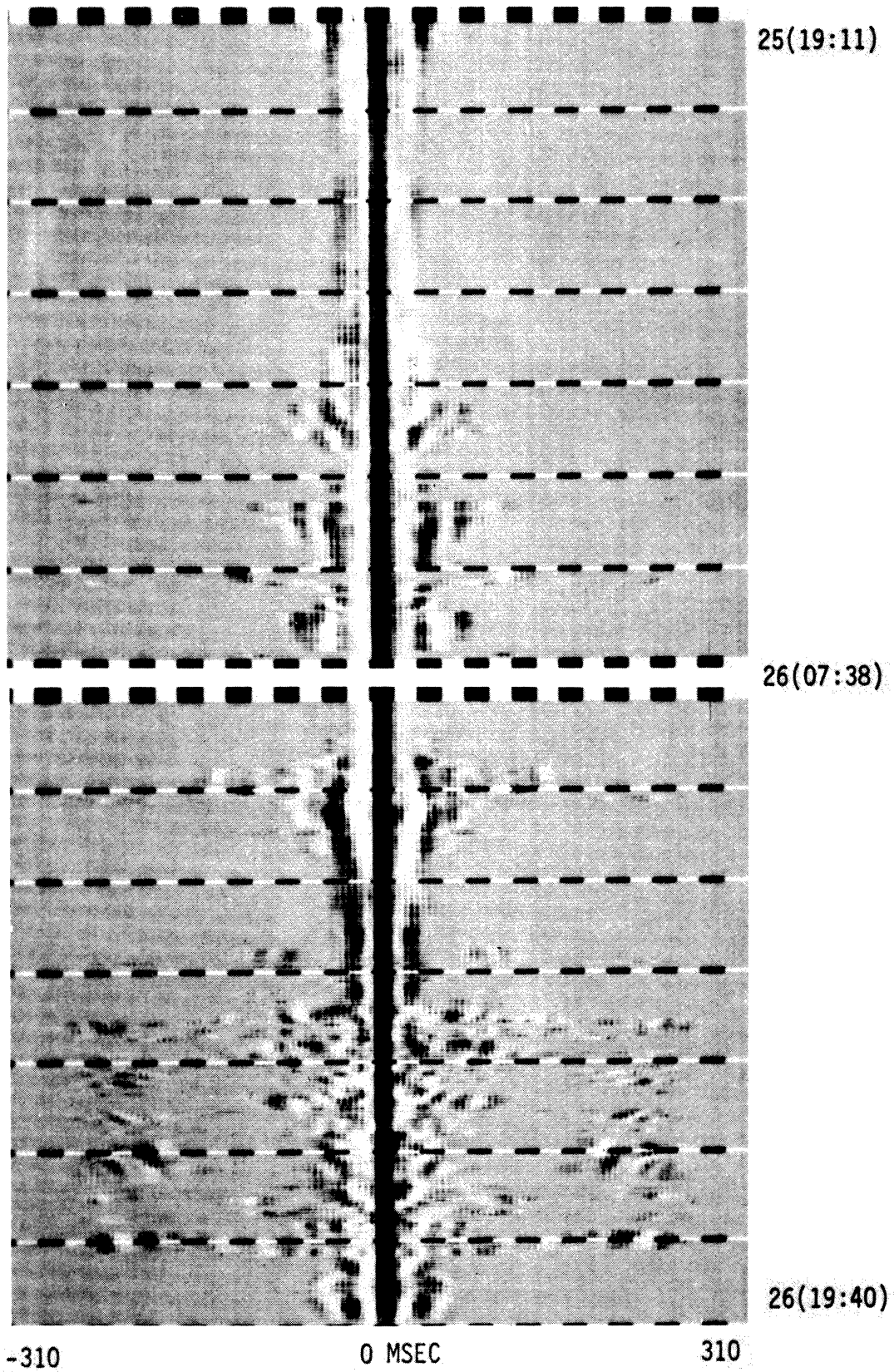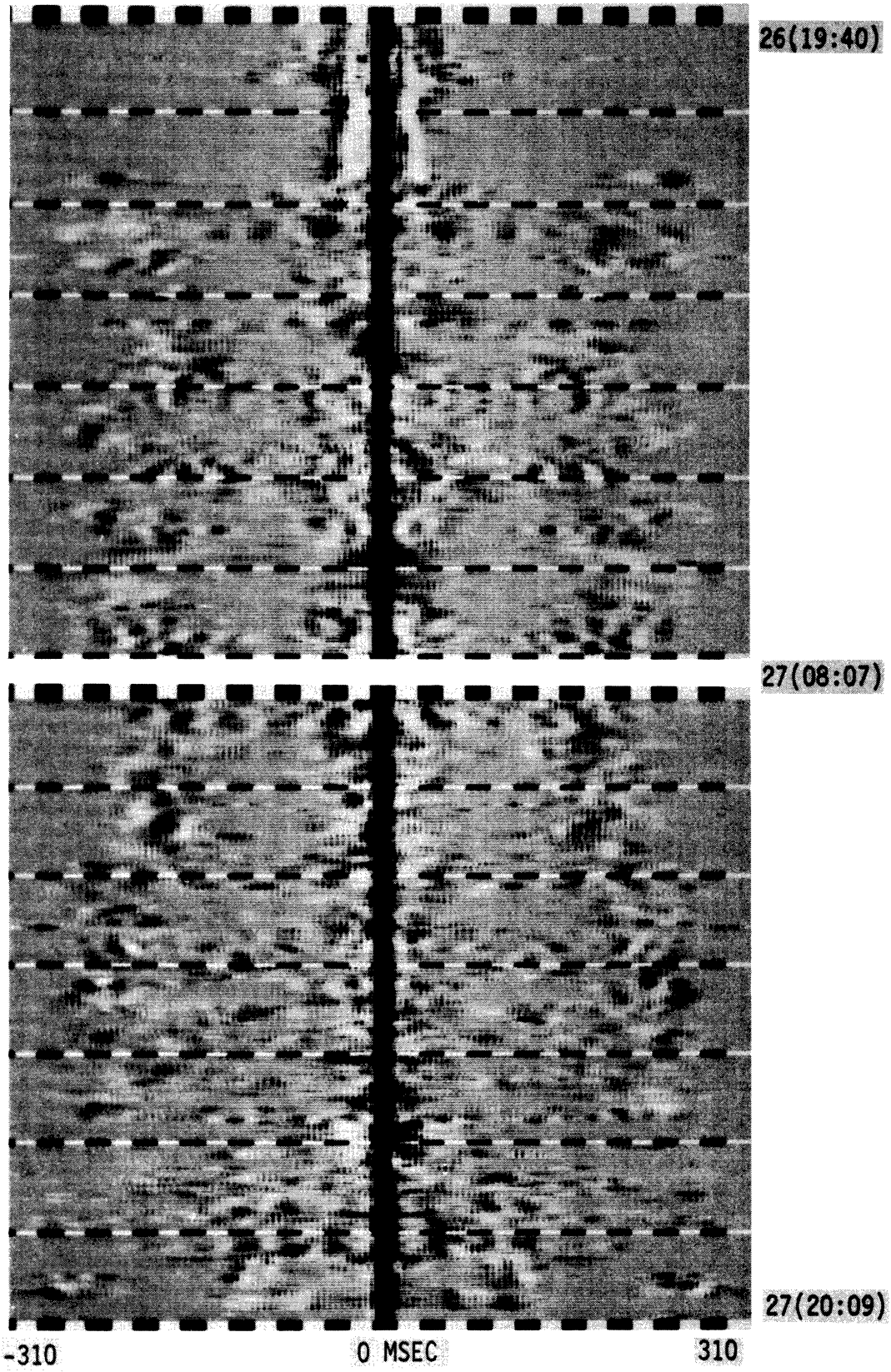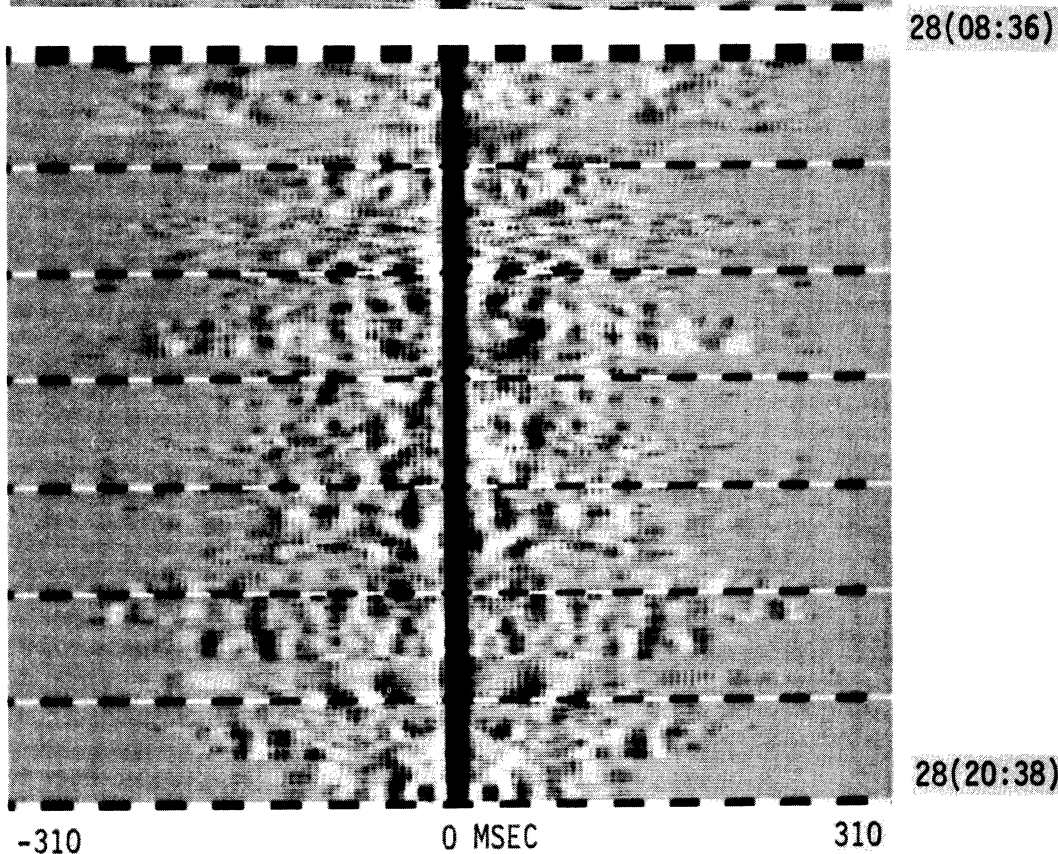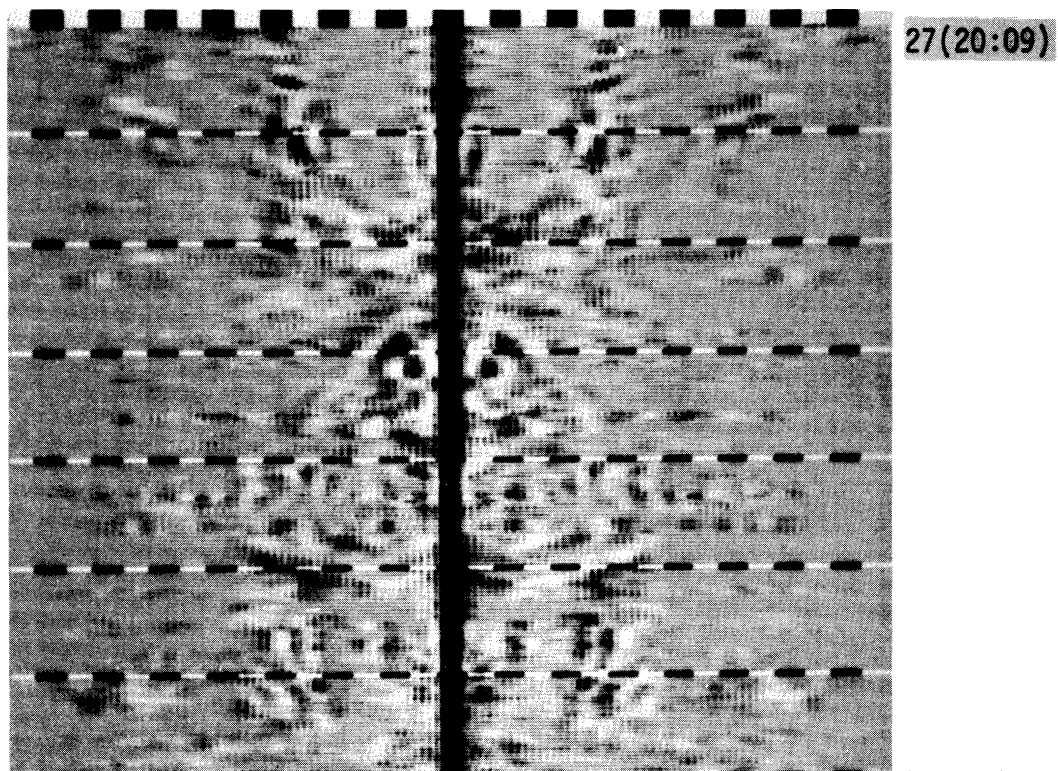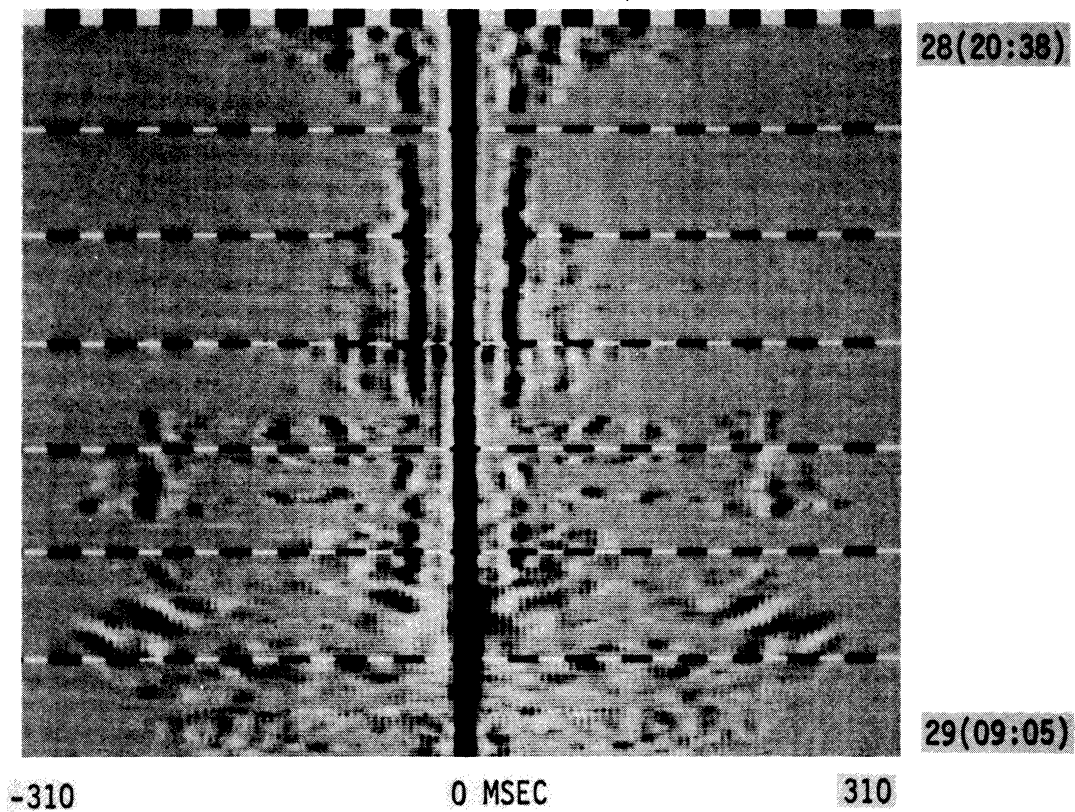
COVH GRAM 19

Fig. 5.20

CHAPTER 6

CONCLUSIONS

The contribution of this work is the presentation, application, and interpretation of a simple display of long time-series of the underwater acoustic channel digit response, or multipath structure, for the first time.

The display has been demonstrated to be particularly useful in three areas:

1. elementary information extraction, which includes:

    1.1 measurement of arrival times, delay spread, time-invariance durations, and structure duration

    1.2 classification of structure into simple, cluster, and complex modes

    1.3 path and mode resolution

2. correlation of multipath reception characteristics with power measurements

3. association between observed multipath structure and physical propagation modes. The simple mode structure is recognized as a surface interacting mode and cluster mode is, most likely, refracted, bottom-reflected propagation.

The conclusion is that the channel digit response display is a promising research tool for acoustic propagation studies. However,

much work remains to gather more propagation data and to obtain experience with the display. These efforts should provide new and useful inputs for physical and abstract underwater acoustic propagation modelling.

GENERATING A-SCAN PLOTS WITH THE 731 RECORDER

The DUAL plots in Chapter 3 illustrate the capability of a raster-scanning recorder for presenting data in an A-scan format. The Hathaway 731 recorder was the particular device used in this thesis. Many other similar and inexpensive commercial devices are available. In general, this type of device has several advantages over an X-Y plotter including speed, silence and reliability. At times, the disadvantage of data formatting may exist; however, this is not true in many cases. If the paper motion direction is selected as the axis for the independent variable, the formatting task is trivial. This is illustrated below by outlining the formatting task using Fortran-like statements.

Outline of Formatting Task

1. Declare a dependent variable plotting array of N variables

    Dimension   Depvar (N)

    Integer   Depvar

2. Clear Depvar (I) (I=1, N, 1) i.e., intensity off

3. "Format" the integer variable X

    a. Scale X, assume X is positive

    $X' = X*N/XMAX$

XMAX is generally 2^{15} since variables are single

precision (16 bit) integer variables

Typical values of N are 500 or 1000 providing 9 to

10 bits of dynamic range in the plotting variable,

i. e. , 54 to 60 dB of amplitude (voltage) dynamic

range.

    b.   Depvar (X') = Intensity ON

4.   Trigger the scan

    Call plot 731 (Depvar, N)

5.   Wait for scan completion

6.   Clear those "Intensity ON" elements of Depvar(I)

    Depvar(X') = 0 (Intensity Off)

7.   Return to 3. to format and plot next scan (each scan corres-

ponds to an increment on the independent variables, i. e. ,

$t = t + \Delta t$) .

This outline is for the plotting of a single dependent variable.

The DUAL plots are multiple dependent variables which are a simple

extension of the above outlined procedure.

A procedure similar to the above was programmed in Fortran

in about two hours. The procedure ran quickly. Each plot scan was

formatted and plotted in the 50 msec sweep time of the 731. The

paper speed was approximately an inch per second.

The 731 is very suitable for producing A-scan plots at speeds, silence and reliability not available in X-Y plotters with a very simple and fast formatting algorithm. Such devices can be used effectively for nonimpact alpha-numeric printing, too.

Appendix B

CHIRP-Z-TRANSFORM

This is a brief presentation of the basic equations and Fortran listings of the CZT algorithm used in this thesis for computing the channel digit spectrum. Denote the finite, discrete Fourier transform of f(t) by $F(\omega)$ where $\omega = 0 , \ldots , N - 1$ and $t = 0 , \ldots , N - 1$.

Then

$$F(\omega) \quad \overset{\Delta}{=} \quad \frac{1}{N} \sum_{t=0}^{N-1} f(t) \; e^{-i\omega t/N} \qquad (B.1)$$

Using the identity $(\omega - t)^2 = t^2 - 2\omega t + \omega^2$ or $-\omega t = (\omega - t)^2/2 - t^2/2 - \omega^2/2$, Equation B.1 becomes

$$F(\omega) \quad = \quad \frac{1}{N} e^{-i\omega^2/2} \sum_{t=0}^{N-1} f'(t) \; e^{i(\omega-t)^2/2} \qquad (B.2)$$

where

$$f'(t) \quad = \quad f(t) \; e^{-it^2/2}$$

But

$$\sum_{t=0}^{N-1} f'(t) \; e^{i(\omega-t)^2/2}$$

is just the convolution of f'(t) with $e^{it^2/2}$.

Thus Equation B.2 can be evaluated using the fast convolution (FFT) technique.

The only significant practical difficulty is obtaining the results of an aperiodic convolution from periodic representations. This result is achieved by simply augmenting f(t) with enough zeros so that for the region of interest, $\omega = 0$, ..., N - 1 , the aperiodic and periodic results are the same.

This may seem to be a hard way to evaluate Equation B.1. Why not evaluate Equation B.1 with an FFT in the first place? For values of N not equal the a power of two a versatile and efficient FFT algorithm does not exist.

The fast convolution technique was also used to compute the channel auto covariance $Covh_t(\mu)$.

The major subroutines in the CZT are :

1. CZT   - the basic algorithm

2. CZT∅   - initialization

3. FXCV   - fast convolution

4. FXCTC - an in-place Cooley-Tukey FFT

All arithmetic is 16 bit block floating point. The arrays IX1 and IY1 are the real and imaginary parts of the data vectors. (IX1, IY1) is both the input vector, f(t) , and the output vector, F(ω) . Similarly, (ICX, ICY) is the $e^{-i\omega^2/2}$ vector, IEZ is the

FFT coefficient vector, $e^{-i\omega t/N}$ and (IFX, IFY) is the $e^{-it^2/2}$

transform vector. ICHAR is the block floating point characteristic.

```
      SUBROUTINE CZT (IX1, IY1, ICX, ICY, IEZ, IFX, IFY, NL, N,
      ICHAR)
      DIMENSION IX1(1), IY1(1), ICX(1), ICY(1), IEZ(1), IFX(1),
      IFY(1)
C     IZ1  = I/O DATA BUFFER
C     ICZ  = CZT COEF
C     IFZ  = FFT(CZT COEF)
C     IEZ  = FFT COEF
      LOGICAL ISW, ISW2
      DATA ISW/. FALSE. /, ISW2/. FALSE. /
      IC0=0
      IC1=0
      IF (ISW) GO TO 10
      CALL CZT0 (ICX, ICY, IFX, IFY, IFC, IEZ, NL, N)
      ISW=. TRUE.
C     DO CZT
10    CONTINUE
      N2=N*2
      N2P=LOG2(N2)
      NL2=NL*2
C     Z=Z*EXP(-I*2*PI*N**2/NL2)
      CALL CMPY (IX1, IY1, IX1, IY1, ICX, ICY, NL)
      NL1=NL+1
      N2M=N2-NL1+1
      CALL CZERO(IX1(NL1), IY1(NL1), N2M)
C     FAST CONVOLUTION OF IX1 WITH IFZ
C     WHERE TRANSFORM OF IFZ WAS PRECOMPUTED
      ISW2=. TRUE.
      CALL FXCV(IX1, IY1, IFX, IFY,IFC, IEZ, N2P, IC0, ISW2)
C     Z=Z*EXP(-I*2*PI*K**2/NL2)
      CALL CMPY (IX1, IY1, IX1, IY1, ICX, ICY, NL)
      ICHAR=IC0
      RETURN
      END


      SUBROUTINE FXCV(IXO, IYO, IX2, IY2, IC2, IEXP, NEXP,
      ICO, ISW2)
C     IZO= FAST CONVOLUTION OF IZO WITH IZ2
C     IZO= (IXO, IYO) AT OUTPUT
C     IZ1=(IXO, IYO) AT INPUT
C     IZ2=(IX2, IY2) CAN BE CONTROLLED BY ISW2
C     NEXP=FFT LENGTH
C     ASSUMES IZO AND IZ2 PRESTRUCTURED(ZERO EXTENDED)
      FOR FFT
```

```
C       ISW2=.TRUE.  => IZ2 ALREADY TRANSFORMED, OTHER-
        WISE ISW2 . FALSE.
C       ICO=ICO+IC1+ IC2 IS TOTAL # OF NODES SCALED BY
C       1/2 IN THE 2 FFT'S AND THE IFFT
        DIMENSION IXO(1),  IYO(1),   IX2(1), IY2(1), IEXP(1)
        LOGICAL ISW2
        NX = 2**NEXP
C       TRANSFORM IZ1
        CALL FXCTC(IXO, IYO, IEXP, NEXP, IC1)
C       UNLESS ISW2 IS .TRUE.,  TRANSFORM IZ2
        IF (ISW2) GO TO 1
        CALL FXCTC(IX2, IY2, IEXP, NEXP, IC2)
C       IZO(F) = IX1(F) * IZ2(F)
1       CALL CMPY(IXO, IYO, IXO, IYO, IX2, IY2, NX)
C       IZO(K) = IFFT(IXO, IYO, IEXP, NEXP,ICO)
        CALL CONJZ(IYO, NX)
        CALL FXCTC(IXO, IYO, IEXP, NEXP, ICO)
        CALL CONJC(IYO, NX)
        ICO = ICO+ IC1+ IC2
        RETURN
        END



        SUBROUTINE CZT0 (ICX, ICY, IFX, IFY, IFC, IEZ, NL, N)
C       GENERATE CZT COEFS
        DIMENSION ICX(1), ICY(1), IFX(1), IFY(1), IEZ(1)
C       ICZ = CZT COEF= EXP(-I*2*PI*N**2/2*NL)
C       IFZ = FFT((ICZ+)+ (ICZ-1))
        N2 = N*2
        N2P = LOG2(N2)
        NL2 = NL*2
        PI = 3. 14159
        ARG0 = 2. *PI/ FLOAT(NL2)
        FN = N
        ARG = ARG0*FN*FN
        IX = COS(ARG)*32767.
        IY = -SIN(ARG)*32767.
        ICX(N + 1) = IX
        ICY(N + 1) = IY
        IFX(N + 1) = IX
        IFY(N + 1) = IY
        ICX(1) = 32767.
        ICY(1) = 0.
        IFX(1) = 32767.
        IFY(1) = 0.
        DO 1 J = 2, N
```

```
      FJ1 = FLOAT(J-1)
      ARG = ARG0*FJ1*FJ1
      IX = COS(ARG)*32767.
      IY = SIN(ARG)*32767.
      IY = -IY
      ICX(J) = IX
      ICY(J) = IY
      IFX(J) = IX
      IFY(J) = IY
      NP = N2 - (J-1) + 1
      ICX(NP) = IX
      ICY(NP) = IY
      IFX(NP) = IX
1     IFY(NP) = IY
      CALL CONJZ(IFY, N2)
      CALL FXCTC(IFX, IFY, IEZ, N2P, IFC)
      RETURN
      END



      SUBROUTINE CMPY(IX1, IY1, IX2, IY2, IX3, IY3, N)
      SCALED FRACTION IX1(1), IY1(1), IX2(1), IY2(1), IX3(1),
      IY3(1)
      SCALED FRACTION IAX, IAY, IEX, IEY
C     IZ1(I) = IZ2(I) * IZ3(I)   ,   (I = 1, N)
      DO 1 I = 1, N
      IAX = IX2(I)
      IAY = IY2(I)
      IEX = IX3(I)
      IEY = IY3(I)
      IX1(I) = IEX*IAX-IEY*IAY
1     IY1(I) = IEX*IAY+IEY*IAX
      RETURN
      END



      FUNCTION LOG2(N)
      DO 1 I = 0, 15, 1
      K = 2**I
      KD = K-N
      IF (KD) 1, 3, 1
3     LOG2 = I
      RETURN
1     CONTINUE
```

```
        WRITE (6. 100)
100     FORMAT (30H ERROR PAUSE IN LOG2')
        PAUSE
        END


        SUBROUTINE CONJZ (IY, N)
        DIMENSION IY (1)
        DO 1  I = 1, N
1       IY (I) = - IY (I)
        RETURN
        END


        SUBROUTINE CZERO (IX, IY, N)
        DIMENSION IX (1), IY (1)
        DO 1 I = 1, N
        IX (I) = 0
1       IY (I) = 0
        RETURN
        END
```

REFERENCES

1. Heitmeyer, R. M. , Underwater Sound Propagation in the Straits of Florida: The Preliminary Analysis of the MIMI Experiment of 1970, C. E. L. Technical Report No. 213, Cooley Electronics Laboratory, The University of Michigan, Ann Arbor, February 1972.

2. Veenkant, R. L. , Preliminary Report on CANDOR: Complete Analysis with Decision Oriented Recording, C. E. L. Technical Report No. 221, Cooley Electronics Laboratory, The University of Michigan. (To Be Published)

3. Kailath, T. , "Measurements on Time-Variant Communication Channels," IRE Trans. Information Theory IT-8, S229-S236 (Sept. 1962).

4. Tucker, D. G. , and B. K. Gazy, Applied Underwater Acoustics, Permagon Press, Oxford, 1966.

5. Steinberg, J. C. and T. G. Birdsall, "Underwater Sound Propagation in the Straits of Florida," Journal of the Acoustical Society of America, Vol. 39, No. 2, February 1966.

6. Birdsall, T. G. , Acoustic Signal Processing, (Final Report) Cooley Electronics Laboratory, The University of Michigan, Ann Arbor, June 1972.

7. Steinberg, J. C. , et al. , "Fixed-System Studies of Underwater Acoustic Propagation," JASA, Vol. 52, No. 5 (Part 2), 1972, pp. 1521-1536.

8. Birdsall, T. G. , R. M. Heitmeyer, K. Metzger, Modulation by Linear Maximal Shift Register Sequences: Amplitude, Biphase, and Complement-Phase Modulation, C. E. L. Technical Report No. 216, Cooley Electronics Laboratory, The University of Michigan, Ann Arbor, December 1971.

9. Clark, J. G. , "Multipath Signal Interference in Time-Dependent Propagation Channels," JASA, Vol. 52, No. 1 (Part 2), 1972, pp. 452-454.

REFERENCES (Cont.)

10. Clark, J. G., et al., "Refracted, Bottom-Reflected Ray Propagation in a Channel with Time-Dependent Linear Stratification," JASA, Vol. 53, No. 3, 1973, pp. 802-818.

11. Deferrari, H. A., "Time-Varying Multipath Interference of Broadband Signals Over a 7 NM Range in the Florida Straits," JASA, Vol. 53, No. 1, 1973, pp. 162-180.

12. Hatter, Norman, Triband: The Three Band Filter for the Continuing MIMI Experiment, C. E. L. Technical Report No. 201, Cooley Electronics Laboratory, The University of Michigan, Ann Arbor, February 1970.

13. Kennedy, R. M., "Phase and Amplitude Fluctuations in Propagating Through a Layered Ocean," JASA, Vol. 46, No. 3 (Part 2), 1969, pp. 737-745.

14. Metzger, K., Private Communication on MIMI Signal Design, Cooley Electronics Laboratory, The University of Michigan, Ann Arbor.

15. Unger, R., and R. Veenkant, Underwater Sound Propagation in the Straits of Florida: The MIMI Experiment of 3 and 4 February 1965, C. E. L. Technical Report No. 183, Cooley Electronics Laboratory, The University of Michigan, Ann Arbor, May 1967.

16. Unger, R., and R. Veenkant, Underwater Sound Propagation in the Straits of Florida: The MIMI Continuous and Sampled Receptions of 11, 12, and 13 August 1966, C. E. L. Technical Report No. 186, Cooley Electronics Laboratory, The University of Michigan, Ann Arbor, June 1967.

17. Veenkant, R., and E. Tury, Underwater Sound Propagation in the Straits of Florida: The MIMI Lunar-Cycle Receptions, C. E. L. Technical Report No. 219, Cooley Electronics Laboratory, The University of Michigan, Ann Arbor, January 1972.

18. Bar-David, I., "Estimation of Linear Weighting Functions in Gaussian Noise," IEEE Trans. on Information Theory, Vol. IT-14, No. 3, May 1968, pp. 395-407.

REFERENCES (Cont.)

19. Bello, P. A., "Some Techniques for the Instantaneous Real-Time Measurement of Multipath and Doppler Spread," IEEE Trans. on Comm. Tech., Vol. 13, No. 3, September 1965, pp. 285-292.

20. Bello, P. A., "Measurement of Random Time-Variant Linear Channels," IEEE Trans on Information Theory, Vol. IT-15, No. 4, July 1969, pp. 496-475.

21. Bello, P. A., "On the Measurement of a Channel Correlation Function," IEEE Trans on Information Theory, Vol. IT-10, No. 4, October 1964, pp. 381-383.

22. Bello, P. A., "Time-Frequency Duality," IEEE Trans. on Information Theory, Vol. IT-10, No. 1, January 1964, pp. 18-33.

23. Gaarder, N. T., "Scattering Function Estimation," IEEE Trans. on Information Theory, Vol. IT-14, No. 5, September 1968, pp. 684-693.

24. Root, W. L., "On the Measurement and Use of Time-Varying Communication Channels," Information and Control 8, 1965, pp. 390-422.

25. VanTrees, H. L., Detection, Estimation, and Modulation Theory, Part III, Wiley, New York, 1971.

26. Bluestein, L. I., "A Linear Filtering Approach to the Computation of the Discrete Fourier Transform," Nerem Rec., 1968, pp. 218-219.

27. Gentlemen, W. M., and G. Sande, "Fast Fourier Transforms - For Fun and Profit," in 1966 Fall Joint Computer Conference, AFIPS Conf. Proc., Washington, D.C.: Spartan, 1966, pp. 563-578.

28. Gold, B., and C. M. Rader, Digital Processing of Signals, McGraw-Hill, 1969.

29. Rabiner, L., R. Schafer, C. Rader, "The Chirp-Z Transform Algorithm," IEEE Trans. Audio and Electroacoustics, Vol. AU-17, June 1969.

REFERENCES (Cont.)

30. Singleton, R. C., "An Algorithm for Computing the Mixed Radix Fast Fourier Transform," IEEE Trans. Audio Electroacoustics, Vol. AU-17, June 1969, pp. 93-103.

31. Stockham, T. G., Jr., "High Speed Convolution and Correlation," Spring Joint Computer Conference, AFIPS Proc., 28:220-233, 1966.

32. Bello, P. A., "Characteristics of Randomly Time-Variant Linear Channels," IRE Trans. Comm. Syst. CS-11, December 1963.

DISTRIBUTION LIST

No. of Copies

Office of Naval Research (Code 468)	1
(Code 102-OS)	1
(Code 480)	1
Navy Department	
Washington, D.C. 20360	

Director, Naval Research Laboratory   6
Technical Information Division
Washington, D.C. 20390

Director   1
Office of Naval Research Branch Office
1030 East Green Street
Pasadena, California 91101

Dr. Christopher V. Kimball   1
Special Studies Group
IAR/PGI
Suite 4
9719 South Dixie Highway
Miami, Florida 33156

Director   1
Office of Naval Research Branch Office
495 Summer Street
Boston, Massachusetts 02210

Office of Naval Research   1
New York Area Office
207 West 24th Street
New York, New York 10011

Director   1
Office of Naval Research Branch Office
536 S. Clark Street
Chicago, Illinois 60605

DISTRIBUTION LIST (Cont.)

No. of Copies

Commander Naval Ordnance Laboratory
Acoustics Division
White Oak, Silver Spring, Maryland 20907
    Attn: Dr. Zaka Slawsky

1

Commanding Officer
Naval Ship Research & Development Center
Annapolis, Maryland 21401

1

Commander
Naval Undersea Research & Development Center
San Diego, California 92132
    Attn: Dr. Dan Andrews
        Mr. Henry Aurand

2

Director
Naval Research Laboratory
Attn: Library, Code 2029 (ONRL)
Washington, D.C. 20390

8

Chief Scientist
Navy Underwater Sound Reference Division
P. O. Box 8337
Orlando, Florida 32800

1

Commanding Officer and Director
Navy Underwater Systems Center
Fort Trumbull
New London, Connecticut 06321

1

Commander
Naval Air Development Center
Johnsville, Warminster, Pennsylvania 18974

1

Commanding Officer and Director
Naval Ship Research and Development Center
Washington, D.C. 20007

1

Superintendent
Naval Postgraduate School
Monterey, California 93940

1

DISTRIBUTION LIST (Cont.)

<div style="text-align: right">No. of Copies</div>

Commanding Officer & Director Naval Ship Research & Development Center* Panama City, Florida 32402	1
Naval Underwater Weapons Research & Engineering Station Newport, Rhode Island 02840	1
Superintendent Naval Academy Annapolis, Maryland 21401	1
Scientific and Technical Information Center 4301 Suitland Road Washington, D.C. 20390 Attn: Dr. T. Williams Mr. E. Bissett	2
Commander Naval Ordnance Systems Command Code ORD-03C Navy Department Washington, D.C. 20360	1
Commander Naval Ship Systems Command Code SHIPS 037 Navy Department Washington, D.C. 20360	1
Commander Naval Ship Systems Command Code SHIPS 00V1 Washington, D.C. 20360 Attn: CDR Bruce Gilchrist Mr. Carey D. Smith	2
Commanding Officer Fleet Numerical Weather Facility Monterey, California 93940	1

---

*Formerly Mine Defense Laboratory.

DISTRIBUTION LIST (Cont.)

DISTRIBUTION LIST (Cont.)

No. of Copies

Dr. Alan Winder
EDO Corporation
College Point, New York 11356

1

Dr. T. G. Birdsall
Cooley Electronics Laboratory
The University of Michigan
Ann Arbor, Michigan 48105

1

Mr. Morton Kronengold
Director, Institute for Acoustical Research
615 S.W. 2nd Avenue
Miami, Florida 33130

1

Mr. Robert Cunningham
Bendix Corporation
11600 Sherman Way
North Hollywood, California 91606

1

Dr. H. S. Hayre
University of Houston
Cullen Boulevard
Houston, Texas 77004

1

Dr. Ray Veenkant
Texas Instruments, Inc.
North Central Expressway
Dallas, Texas 75222
Mail Station 208

1

Dr. Stephen Wolff
John Hopkins University
Baltimore, Maryland 21218

1

Dr. Bruce P. Bogert
Bell Telephone Laboratories
Whippany Road
Whippany, New Jersey 07981

1

Dr. Albert Nuttall
Navy Underwater Systems Center
Fort Trumbull
New London, Connecticut 06320

1

DISTRIBUTION LIST (Cont.)

No. of Copies

Dr. Philip Stocklin   1
Raytheon Company
P. O. Box 360
Newport, Rhode Island 02841

Dr. H. W. Marsh   1
Navy Underwater Systems Center
Fort Trumbull
New London, Connecticut 06320

Dr. David Middleton   1
35 Concord Avenue, Apt. #1
Cambridge, Massachusetts 02138

Mr. Richard Vesper   1
Perkin-Elmer Corporation
Electro-Optical Division
Norwalk, Connecticut 06852

Dr. Donald W. Tufts   1
University of Rhode Island
Kingston, Rhode Island 02881

Dr. Loren W. Nolte   1
Dept. of Electrical Engineering
Duke University
Durham, North Carolina 27706

Dr. Thomas W. Ellis   1
Texas Instruments, Inc.
13500 North Central Expressway
Dallas, Texas 75231

Mr. Robert Swarts   1
Honeywell, Inc.
Marine Systems Center
5303 Shilshole Ave., N.W.
Seattle, Washington 98107

Mr. Charles Loda   1
Institute for Defense Analyses
400 Army-Navy Drive
Arlington, Virginia 22202

DISTRIBUTION LIST (Cont.)

No. of Copies

Mr. Beaumont Buck   1
General Motors Corporation
Defense Research Division
6767 Holister Avenue
Goleta, California 93017

Professor Richard A. Roberts   1
Department of Electrical Engineering
University of Colorado
Boulder, Colorado 80302

Capt. Jurgen O. Gobien   1
AFIT - ENE
Air Force Institute of Technology
Wright-Patterson AFB, Ohio 45433

Dr. John Steinberg   1
Institute for Acoustical Research
615 South West 2nd Avenue
Miami, Florida 33130

Dr. M. Weinstein   1
Underwater Systems, Inc.
8121 Georgia Avenue
Silver Spring, Maryland 20910

Dr. Harold Saxton   1
1601 Research Blvd.
TRACOR, Inc.
Rockville, Maryland 20850

Dr. Thomas G. Kincaid   1
General Electric Company
P. O. Box 1088
Schenectady, New York 12305

Applied Research Laboratories   2
The University of Texas at Austin
Austin, Texas 78712
          Attn: Dr. Lloyd Hampton
                Dr. Charles Wood

DISTRIBUTION LIST (Cont.)

No. of Copies

Dr. Paul McElroy
Woods Hole Oceanographic Institution
Woods Hole, Massachusetts 02543

1

Dr. John Bouyoucos
Hydroacoustics, Inc.
P. O. Box 3818
Rochester, New York 14610

1

Dr. Joseph Lapointe
Systems Control, Inc.
260 Sheridan Avenue
Palo Alto, California 94306

1

Cooley Electronics Laboratory
University of Michigan
Ann Arbor, Michigan 48105

22

REPORT DOCUMENTATION PAGE		READ INSTRUCTIONS BEFORE COMPLETING FORM
1. REPORT NUMBER TR 226	2. GOVT ACCESSION NO.	3. RECIPIENT'S CATALOG NUMBER
4. TITLE (and Subtitle) INVESTIGATION OF THE PROPAGATION STABILITY OF A TIME SPREAD UNDERWATER ACOUSTIC CHANNEL		5. TYPE OF REPORT & PERIOD COVERED Technical Report
		6. PERFORMING ORG. REPORT NUMBER 004860-4-T
7. AUTHOR(s) Raymond L. Veenkant		8. CONTRACT OR GRANT NUMBER(s) N00014-67-A-0181-0035
9. PERFORMING ORGANIZATION NAME AND ADDRESS Cooley Electronics Laboratory The University of Michigan Ann Arbor, Michigan 48105		10. PROGRAM ELEMENT, PROJECT, TASK AREA & WORK UNIT NUMBERS
11. CONTROLLING OFFICE NAME AND ADDRESS Office of Naval Research Department of the Navy Arlington, Virginia 22217		12. REPORT DATE May 1974
		13. NUMBER OF PAGES 186
14. MONITORING AGENCY NAME & ADDRESS(if different from Controlling Office)		15. SECURITY CLASS. (of this report) Unclassified
		15a. DECLASSIFICATION/DOWNGRADING SCHEDULE

16. DISTRIBUTION STATEMENT (of this Report)

Approved for public release; distribution unlimited.

17. DISTRIBUTION STATEMENT (of the abstract entered in Block 20, if different from Report)

18. SUPPLEMENTARY NOTES

19. KEY WORDS (Continue on reverse side if necessary and identify by block number)

Underwater Acoustic propagation
Acoustic Signal processing
Research Display
Time Spread Channel

Channel Digit Response
Coherent Display

20. ABSTRACT (Continue on reverse side if necessary and identify by block number)

An experimental investigation of analysis and display techniques for extracting stability information from underwater acoustic propagation data has shown the feasibility and usefulness of a specific display format, called the Channel Digit Response. All of the complex nature of the channel reception is retained in the display, but the format compresses the data and enhances the extraction of qualitative stability information. The investigation

DD FORM 1473 EDITION OF 1 NOV 65 IS OBSOLETE
S/N 0102-014-6601 |

Block 20:

and conclusions are limited to propagation tests using periodic transmissions, as periodic transmissions are the usual type used for studying varying multipath propagation.

The investigation data base spanned 133 hours, from a 43 n. mile range across the Straits of Florida. The effective time resolution of the data was .02 seconds. Crosscorrelation, autocorrelation, and power spectrum analysis, and several threshold techniques based on time-lag crosscorrelation were investigated, and their effectiveness compared to the Channel Digit Response.